16 State House Station
Augusta, Maine 04333

MaineDOT

# Transportation Research Division

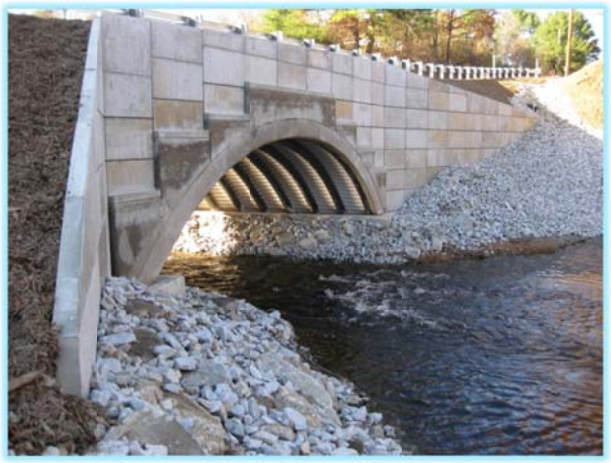

## Technical Report 14-04

*Bridge-in-a-Backpack™*

*Task 3: Investigation of Durability Enhancements Relative to Abrasion from Ice and other Sources*

*Final Report – Task 3, February 2013*

Technical Report Documentation Page

| 1. Report No.<br>ME 14-04 | 2. | 3. Recipient's Accession No. | |
|---|---|---|---|
| 4. Title and Subtitle<br>Bridge-in-a-Backpack™<br>Task 3: Investigation of Durability Enhancements Relative to Abrasion from Ice and Other Sources | | 5. Report Date<br>February 2013<br>6. | |
| 7. Author(s)<br>Mackenzie Demkowicz<br>Bill Davids Ph.D P.E.<br>Heather Parry<br>Keenan Goslin P.E.<br>Roberto Lopez-Anido Ph.D, P.E. | | 8. Performing Organization Report No.<br>AEWC Report Number 13-32.815 | |
| 9. Performing Organization Name and Address<br>University of Maine – Advanced Structures and Composites Center | | 10. Project/Task/Work Unit No.<br>Project 17681.00 - Task 3<br>11. Contract © or Grant (G) No.<br>Contract # 2010*3692 | |
| 12. Sponsoring Organization Name and Address<br>Maine Department of Transportation | | 13. Type of Report and Period Covered<br>14. Sponsoring Agency Code | |
| 15. Supplementary Notes | | | |

16. Abstract (Limit 200 words)

The arch-shaped concrete filled fiber reinforced polymer tube bridges are being constructed throughout New England and elsewhere. The composite system durability and maintenance requirements need to be evaluated. For this study, an asymmetric hybrid carbon and E-glass fiber braided reinforced composite laminate was selected. This material is representative of that used to fabricate the arches. The laminates were subjected to different environmental conditions to assess durability. The factors investigated include resistance to: water, saltwater, dry heat, alkali, freeze thaw, UV and gasoline. After exposure to these conditions coupons are tested in tension to determine tensile strength and elastic properties. Most tensile properties retained at least 90% of the control values. Water, saltwater, alkali and dry heat exposure are evaluated based on criteria set forth by AASHTO. It is found that most conditions passed the acceptance criteria. Studies were also done on abrasion resistance and ignition resistance. Tests for abrasion conclude that an additional abrasion protection layer would provide a significant increase in performance.

| 17. Document Analysis/Descriptors<br>Arch bridges, concrete filled FRP tubes, durability testing, Bridge-in-a-Backpack | | 18. Availability Statement | |
|---|---|---|---|
| 19. Security Class (this report) | 20. Security Class (this page) | 21. No. of Pages<br>170 | 22. Price |

**Bridge-in-a-Backpack**
**Task 3: Investigation of Durability Enhancements Relative to Abrasion from Ice and Other Sources**
**PIN 017681.00**

**Prepared for:**
**Dale Peabody**
**Maine Department of Transportation**
**Office of Safety, Training, and Research**
**16 State House Station**
**Augusta, ME 04333**
**(207) 624-3305**

**Advanced Structures and Composites Center**
Report Number 13-32.815

February 6, 2013

**Prepared by:**
Mackenzie Demkowicz
Roberto Lopez-Anido Ph.D. P.E.
Bill Davids Ph.D. P.E.
Keenan Goslin P.E.
Heather Parry



*An ISO 17025 accredited testing laboratory*
*Accredited by International Accreditation Service*

Advanced Structures and Composites Center
35 Flagstaff Rd
University of Maine
Orono, ME 04469

Telephone: 207-581-2123
FAX: 207-581-2074
composites@umit.maine.edu
www.composites.umaine.edu

# ENVIRONMENTAL DURABILITY OF HYBRID BRAIDED POLYMER MATRIX COMPOSITES FOR INFRASTRUCTURE APPLICATIONS

By

Mackenzie Demkowicz

B.S. University of Maine, 2009

A THESIS

Submitted in Partial Fulfillment of the

Requirements for the Degree of

Master of Science

(in Civil Engineering)

The Graduate School

The University of Maine

August, 2011

Advisory Committee:

Roberto A. Lopez-Anido, Professor of Civil Engineering, Advisor

William Davids, Professor of Civil Engineering

Edwin Nagy, Instructor of Civil Engineering

# ENVIRONMENTAL DURABILITY OF HYBRID BRAIDED POLYMER MATRIX COMPOSITES FOR INFRASTRUCTURE APPLICATIONS

By Mackenzie Demkowicz

Thesis Advisor: Dr. Roberto A. Lopez-Anido

An Abstract of the Thesis Presented
in Partial Fulfillment of the Requirements for the
Degree of Master of Science
(in Civil Engineering)
August, 2011

The composite arch technology developed by researchers at the University of Maine is being implemented in several bridges throughout New England. These bridges use concrete-filled structurally integrated stay-in-place fiber reinforced polymer (FRP) composite forms. The FRP composite arch form confines the concrete and provides tensile strength traditionally gained with steel rebar. The composite system durability and maintenance requirements need to be evaluated and compared to that of traditional bridge structures.

An asymmetric hybrid carbon and E-glass fiber braided reinforced composite laminate was selected. This hybrid composite laminate is representative of the material used to fabricate the composite arch forms. The hybrid composite laminate was adopted for evaluation of the effect of various environmental conditions on the material properties. First, the proposed asymmetric hybrid composite laminate was investigated to determine if the experimental procedure would produce accurate and consistent measurements of material properties. A rectangular

composite coupon reinforced with one layer of braided carbon fibers and one layer of braided E-glass fibers embedded in vinyl ester epoxy resin was used to determine the elastic properties. A notched composite coupon, made of the same materials, was adopted to produce a fiber rupture failure mode in order to determine the ultimate tensile strength in the longitudinal direction of the arch. First a model was implemented using micromechanics equations and classical lamination theory to predict the elastic properties of the composite under a tensile load. Second, a phenomenological damage model was proposed to predict the strength of the hybrid composite based on the properties of individual carbon and E-glass fiber reinforced layers. The model is bilinear to account for damage in the layer that fails at the lower tensile strain. After the initial failure the model can consider either a brittle or a yielding response of the damaged layer. Furthermore, the model considers the efficiency of the carbon fiber tows in the notch specimen to determine the ultimate tensile strength.

The asymmetric hybrid composite laminates were subjected to different environmental conditions to assess the durability of the composite arch forms. The environmental factors investigated include: water resistance, saltwater resistance, dry heat resistance, alkali resistance, freeze thaw resistance, UV resistance, and gasoline fuel resistance.

After being exposed to a particular environmental condition coupons were cut from the laminate sheets and tested in tension to determine their tensile strength and elastic properties. Selected environmental conditions had coupons tested for multiple exposure durations to determine the rate of change of material

properties over time. The change of elastic properties over 1000 hours was less than 10% and the corresponding change of tensile strength was less than 15% when comparing mean values.

The environmental durability studies showed that after exposure to seven separate environmental conditions, most tensile material properties retained at least 90% of the control values. Water, saltwater, alkali, and dry heat exposure was also evaluated based on Acceptance Criteria 125 (ICC Evaluation Service) as recommended by AASHTO (2009). It was found that most conditions passed the acceptance criteria after the initial round of testing as described in this study.

Studies were also done on the abrasion resistance and ignition resistance of the composite system. A test for ignition resistance showed that a small flame was not able to ignite the outer surface of the arch material after a 10 min exposure time. Furthermore, tests for abrasion resistance lead to the conclusion that an additional abrasion protection layer would provide a significant increase in abrasion resistance.

**ACKNOWLEDGEMENTS**

I would like to thank my graduate committee for all their time and effort spent helping throughout my research. I would especially like to thank my advisor, Dr. Roberto Lopez-Anido for his continuous assistance and support. I would also like to thank the AEWC Advanced Structures and Composites Center staff for all of their assistance during my time here.

I am grateful for all of the undergraduate employees who helped me with testing as well as my fellow graduate students who offered support and encouragement. Finally a special thanks to Heather Parry for her dedication to the project and immense support during her time here.

I would like to acknowledge the Maine Department of Transportation and Advanced Infrastructure Technologies who funded the research associated with this thesis.

## TABLE OF CONTENTS

## LIST OF TABLES

## LIST OF FIGURES

# Chapter 1. EXECUTIVE SUMMARY

## 1.1 Background

The composite arch technology developed at the AEWC Advanced Structures and Composites Center is being implemented as part of a commercially available bridge system. The bridge system is supported by concrete-filled structurally integrated stay-in-place fiber reinforced polymer (FRP) composite forms. The FRP composite arch form confines the concrete and provides tensile strength traditionally gained with steel rebar.

The composite materials used in the arch forms consist of braided carbon fiber, braided glass fiber and a vinyl ester epoxy resin. Composite materials are becoming more popular for strengthening bridge structures; due to their light weight, corrosion resistance, and ease of constructability, FRP composites have become a attractive material for structural reinforcement (Balazs and Borosnyoi 2001; Tan et al. 1997). Carbon fibers can exhibit a very high ultimate strength, up to ten times higher than the yield of steel (Wu et al. 2010), a modulus of elasticity that is comparable to steel and can exhibit more corrosion resistance than steel, which is traditionally used as bridge reinforcement. The composite system durability and maintenance requirements need to be evaluated and compared to that of traditional bridge structures.

## 1.2 Significance of Research and Objectives

In order to verify that the composite system is durable enough to be used for bridges, a full environmental durability study needed to be performed. Coupons that were representative of the composite material used in the arches were fabricated for tensile testing. Using coupons cut from an asymmetric hybrid braided composite laminate, an experimental test program was carried out to determine how various environmental conditions affected the tensile material properties of the composite. Three main objectives were accomplished through this research.

The first objective was to develop a composite coupon that is representative of the composite arches and can be tested in tension to measure the elastic material properties. Elastic material properties include the elastic modulus in the longitudinal and transverse direction as well as Poisson's ratio. The second objective was to develop a composite coupon that is representative of the composite arches and can be tested in tension to measure the strength in the longitudinal direction of the material. The third objective was to carry out a full environmental durability study by exposing the composite coupons to various environmental conditions and testing them in tension to determine the material properties retained.

## 1.3 Chapter Summaries

This thesis is organized into three main chapters. Chapters 2, 3, and 4 represent individual segments of research as outlined in the thesis objectives. Conclusions and future recommendations for each segment of research are addressed at the end of each chapter.

### 1.3.1. Chapter 2- Characterization of Hybrid Braided Composite Tensile Properties

Chapter 2 focuses on the development of a composite coupon used for material level tension tests to determine the elastic properties. The composite arches consist of a hybrid carbon fiber and E-glass fiber reinforced composite with an asymmetric layup. Experimental work was performed on coupons cut from laminates with carbon fiber, E-glass fiber and a hybrid of carbon and E-glass fiber reinforced composite. This study served to determine if coupons with an asymmetric layup were acceptable to use for durability testing.

A variability study was also executed to determine if improvements in the coupon manufacturing process could be made. It was determined that coupons cut from an asymmetric hybrid composite laminate, which would be representative of the composite arch material, was acceptable to use for measuring elastic properties.

In addition to experimental work, a model was implemented to predict the elastic properties. The model used micromechanics and classical lamination theory to determine the elastic properties for composites made from a single layer of braided carbon fiber, a single layer of braided E-glass fiber, or a hybrid of braided carbon fiber and E-glass fiber reinforced composite. The model was verified experimentally.

The experimental and modeling work discussed in the chapter resulted in validating the use of coupons cut from an asymmetric hybrid composite laminate, which was used in the durability experimental study to determine the elastic

properties of the material. Future recommendations include additional studies to determine the material variability due to manufacturing and the development of a finite element model for more precise material predictions.

### 1.3.2. Chapter 3- Notched Tensile Test Method for Braided Composites

Chapter 3 focuses on the development of a composite coupon used for material level tension tests to determine the ultimate longitudinal strength. Due to the fibers in the composite being braided, conventional tension tests fail to capture the ultimate tensile strength of the composite. In order to produce a fiber rupture failure through tension testing a notched coupon was used. Experimental work was performed on notched coupons made from carbon fiber, E-glass fiber and a hybrid of carbon and E-glass fiber reinforced composite to determine if coupons cut from braided composite laminates were acceptable to use for future durability experimental studies to determine the material strength.

A variability study was again executed to determine if improvements in the manufacturing process could be made. It was determined that notched coupons cut from an asymmetric hybrid composite laminate, which are representative of the composite arch material, were acceptable to measure the tensile strength of the braided composite.

In addition to testing, a model was investigated to predict the ultimate strength. A phenomenological damage model was proposed to predict the strength of the hybrid composite based on the properties of individual carbon fiber and E-glass fiber reinforced layers. The model is bilinear to account for damage in the layer that fails at the lower tensile strain. After the initial failure the model can

consider either a brittle or a yielding response of the damage layer. Furthermore, the model considers the efficiency of the carbon fiber tows in the notch specimen to determine the ultimate tensile strength.

The experimental testing and modeling discussed in the chapter resulted in the validation of a notched coupon cut from asymmetric hybrid composite laminates, which was used in the durability experimental study to determine the longitudinal strength of the braided composite. Future recommendations include the development of a finite element model for material strength and failure mode predictions.

### 1.3.3. Chapter 4- Implementation of Durability Test Protocol to Braided Composites

The environmental durability test program is presented in Chapter 4. An environmental durability test matrix was followed that outlined exposures to water, saltwater, alkali, dry heat, UV, freeze thaw, and fuel. The test matrix was proposed by AASHTO (AASHTO 2009) for qualifying composite material used in bridge structures. Composite coupons were exposed to the listed conditions for various durations before being tested in tension to determine the percentage of material properties retained after exposure. Experimental work was performed on the composite coupons and the relationship between the FRP composite and the concrete in the arch was not investigated.

Material properties measured experimentally for comparison purposes included the elastic modulus in the longitudinal and transverse directions, tensile strength in the longitudinal and transverse directions and the shear stress at failure.

Mean values and calculated B-Basis values were compared to determine the percentage of material properties that was retained. Coupons that were exposed to water, saltwater, alkali and dry heat for 1000 hours were also evaluated using Acceptance Criteria 125 (AC125) (ICC Evaluation Service 2007). This criteria states that after 1000 hours of exposure the composite material should retain at least 90% of the original material properties. Both mean values and calculated B-Basis values were evaluated.

In addition to the environmental conditions listed in the durability test matrix, studies were performed to investigate the ignition resistance and abrasion resistance of the composite material. The material did not ignite after being exposed to a small flame for 10 min. Also it was found that the use of an additional abrasion layer could increase the abrasion resistance.

Overall it was found that most environmental conditions did not result in a loss of material properties greater than 90%. Samples that were exposed to one environmental condition for multiple durations did not show any significant trend in the change of material properties. Also, AC 125 was met in most cases, and those that did not meet the criteria in the initial round of testing are recommended to undergo additional experimental testing to determine if the loss in material properties was partially due to material variability or variability in test conditions.

Future recommendations include additional experimental testing to study the variability in the change of material properties for unconditioned samples over time, to generate B-Basis values that meet the Composite Material Handbook (Department of Defense 2002), and to observe the effects of environmental conditioning over longer exposure durations.

# Chapter 2. CHARACTERIZATION OF HYBRID BRAIDED COMPOSITE TENSILE PROPERTIES

## 2.1 Introduction

Textile composites are widely used for advanced structures in the field of aerospace, automobile and marine industries (Tan et al. 1997). In the past several years researchers and industrial companies have been showing an increased interest in alternative fabric architectures due to advantages over conventional unidirectional pre-impregnated fiber reinforced polymers (FRP) (Donadon et al. 2007). Braiding has been used since the 1800's to produce textile fabrics; a braided fabric is produced by a machine that has fiber carriers moving in a circular pattern. Fibers are carried half in a clockwise direction and the other half in a counter clockwise direction and intertwined to create a braided tube (Ayranci and Carey 2008). Some of the advantages of a braided composite include improved damage tolerance and impact resistance, low fabrication cost and easy handling (Donadon et al. 2007).

One current application of braided composites are concrete filled fiber reinforced polymer arch members developed at the AEWC Advanced Structures and Composites center (Bannon 2009; El-Chiti 2004; Tomblin 2006). Previous tensile testing has been performed on the composite bridge material, which is made from braided carbon and E-glass fibers. Initial tests were performed on braided carbon

only coupons, which resulted in verification of the material properties model implemented by Bannon (2009). This model was used to calculate predicted values for material properties of a braided carbon fiber composite.

## 2.2 Material Description

All coupons used for testing were fabricated at the University of Maine's AEWC Advanced Structures and Composites Center (AEWC) or at Kenway Corporation facilities in Augusta, Maine. The coupons were cut from sheets of single layer carbon fiber or E-glass fiber reinforced composites or multilayer hybrid carbon and E-glass fiber braided reinforced composites. The braided reinforcement is a 2 X 2 bias braid, which is a braid of only off axis fibers at angle θ where each tow passes over and under two consecutive tows.

The typical inner layer of an arch consists of a layer reinforced with braided E-glass with fibers arranged close to the transverse or hoop direction (approximately ±81 degrees relative to the longitudinal arch axis). The E-glass braid was made with single end rovings. The typical outer layer of an arch, which provides longitudinal strength, consists of carbon fibers arranged closer to the longitudinal direction (measured as approximately ±22 or ±20 degrees from the longitudinal arch axis for the tested specimens made from UM6447 and AIT2011 respectively). The UM6447 carbon fiber braid was made with 15,000 filaments per tow while the AIT2011 carbon fiber braid was made with 24,000 filaments per tow. Detailed information on the braided fiber product information, tow description, and fiber mechanical and physical properties can be found in Table 2.1 through Table 2.3 respectively.

Table 2.1 Braided Fiber Product Information

| Product Number | Fiber Material | Material Name | Calculated Nominal Expanded Condition Properties | | |
|---|---|---|---|---|---|
| | | | Braid Angle | Inner Diameter (mm) | Grams/ Square Meter |
| UM6447 (A&P Technology 2009a) | E-glass | FG 450 Hybon 2022 Roving | +/-81° | 294.6 | 2142 |
| UM6448 (A&P Technology 2009b) | Carbon | Carbon PYROFIL TR50S 15K | +/-20° | 294.6 | 698 |
| AIT2011 (A&P Technology 2011) | Carbon | Carbon Torayca T700S | +/18.4° | 294.6 | 748 |

Table 2.2 Tow Description

| Fiber Type | Fiber ID | Supplier | Yield (yd/lb) | Tex (g/km) | Filament Diameter (µm) |
|---|---|---|---|---|---|
| E-Glass | FG450 (PPG Fiber Glass 2008) | PPG Industries | 450 | 1100 | 17 |
| Carbon | TR50S (Grafil Inc 2008) | Grafil Inc. | 496 | 1000 | 7 |
| Carbon | T700S (Torayca 2009) | Torayca | 301 | 1650 | 7 |

Table 2.3 Fiber Mechanical and Physical Properties

| Fiber Type | Fiber ID | Strength (MPa) | Modulus (GPa) | Density ($g/cm^3$) | Elongation (%) |
|---|---|---|---|---|---|
| E-Glass | FG450 (Daniel and Ishai 2006) | 3450 | 73 | 2.54 | 4-5 |
| Carbon | TR50S (Grafil Inc 2008) | 4,900 | 240 | 1.82 | 2 |
| Carbon | T700S (Torayca 2009) | 4,900 | 230 | 1.80 | 2.1 |

All tubes were infused with DERAKANE 8084 or DERAKANE 610C, both provided by Ashland, which is a rubber toughened vinyl ester resin, and did not undergo a post cure. The mechanical properties of both resins are summarized in Table 2.4.

Table 2.4 Mechanical Properties of DERAKANE Resin

| **Resin** | **DERAKANE 8084** | **DERAKANE 610C** |
|---|---|---|
| Tensile Strength* | 76 MPa | 71 MPa |
| Tensile Modulus* | 2900 MPa | 3530 MPa |
| Compressive Strength** | 127 MPa | 127 MPa |
| Poisson's Ratio** | .35 | .35 |
| Shear Modulus** | 1.1-1.5 GPa | 1.1-1.5 GPa |
| Shear Strength** | 53 MPa | 53 MPa |
| Ultimate tensile strain* | 8-10% | 1-5% |
| *(Ashland 2006) & (Ashland 2010)<br>**Vinylester (Derakane) resin (Daniel and Ishai 2006) | | |

The mean measured thickness as well as the coefficient of variation for each material used is listed in Table 2.5. The thickness of the E-glass and TR50S were measured from single layer infused sheets. These thicknesses were verified by comparing the sum of the thicknesses to the thickness of hybrid composite coupons reinforced with one layer of E-glass and one layer of TR50S carbon fiber braids. No single layer of T700S carbon fiber reinforced composites were infused so the thickness of the T700S carbon was calculated by subtracting the thickness of the E-glass fiber reinforced layer from the thickness of hybrid coupons reinforced with one layer of E-glass and one layer of T700S carbon fiber braids. All thicknesses were measured with calipers to the closest 0.01mm.

The fiber volume fraction was then estimated using the areal weight, *AW,* and fiber densities, $\rho$ given by supplies, listed in Table 2.1 and Table 2.3 respectively, and the mean measured thicknesses, *t*. The resulting estimated fiber volume fraction, $V_f$, for each material is listed in Table 2.5. Equation 2-1 and Equation 2-2 show the equations used to estimate the fiber volume fraction. Also included in Table 2.5 for comparison purposes are the thicknesses and fiber volume fraction of braided carbon and E-glass used to create tubes for compression testing in testing performed by Walton (2011).

$$W = \frac{AW}{t} \qquad \text{Equation 2-1}$$

$$V_f = \frac{W}{\rho} \qquad \text{Equation 2-2}$$

Table 2.5 Consolidated Part Properties

| **Fiber Type** | **Fiber ID** | **Thickness** | | **Fiber Volume Fraction** |
|---|---|---|---|---|
| | | **Mean (mm)** | **COV (%)** | |
| E-Glass | UM6447 | 1.29 | 4.8 | 0.65 |
| Carbon | UM6448 | 0.74 | 5.5 | 0.52 |
| Carbon | AIT2011 | 1.00 | 5.0 | 0.42 |
| E-Glass | UM5595 | 0.89* | 8.0 | NA |
| Carbon | UM6448sub | 0.69* | 5.0 | 0.56 |
| *Thickness measured with micrometer not calipers | | | | |

In some circumstances a bleeder mat used for resin distribution during the infusion process remained with the consolidated sheets (i.e., a peel ply was not used to remove the bleeder mat). The bleeder mat was a thin (the consolidated thickness

was approximately 0.7 mm) polyester random-orientation batting material. The stay-in-place bleeder layer served as an abrasion resistant layer for bridge structures.

## 2.3 Prediction of Elastic Properties

Braided composites have been found to be advantageous in many applications, however the analytical tools to evaluate the properties of the material are still being developed and reliable databases of fundamental properties are incomplete (Masters et al. 1993). Several types of models have been developed to predict the elastic properties of braided composites; two common types of models include finite element models and theoretical models based on classical lamination theory.

### 2.3.1. Classical Lamination Theory

Classical lamination theory can be used to predict the material properties of a laminate where the overall behavior of the multidirectional laminate is a function of the properties and stacking sequence of the individual layers (Daniel and Ishai 2006). One of the assumptions required for the classical lamination theory is that each of the layers, or lamina, of the laminate is quasi-homogenous and orthotropic. The material properties of each lamina can be determined using micromechanics models, which are then are transformed based on their orientation in the laminate to determine the laminate properties. Classical lamination theory can be applied to predict the material properties of textiles, however general assumptions are typically made to account for the effect of the fiber architecture.

This method of analysis works best for multidirectional laminates that consist of unidirectional stacked lamina; however this is not the case for a braided material, where the fibers are going in several directions over the same layer thickness. One commonly used analysis technique used for braided material is to model each set of tows that travel in the same direction (0 or ±θ) as if they were a unidirectional ply, or lamina, in a (0/±θ) symmetric laminate (Masters et al. 1993). The braid angle, ± θ, is taken as the angle off of the longitudinal direction of the braid as depicted in Figure 2.1. The thickness of each ply is taken as half the total thickness of the braided layer; a model of this can be seen in Figure 2.2. This technique ignores the tow undulations completely, however a tow waviness knockdown factor (Cox and Flanagan 1997) can be applied to account for the fiber architecture. In a comparison of analysis models performed by Masters two models based on classical lamination theory were compared to experimental data. The two models compared were the same except for one of the models had a correction factor applied to the material properties (similar to the tow waviness knockdown factor) to account for the tow undulations. It was found that the correction for braid undulations only improved the correlation slightly and that both correlated well with experimental data (Masters et al. 1993).

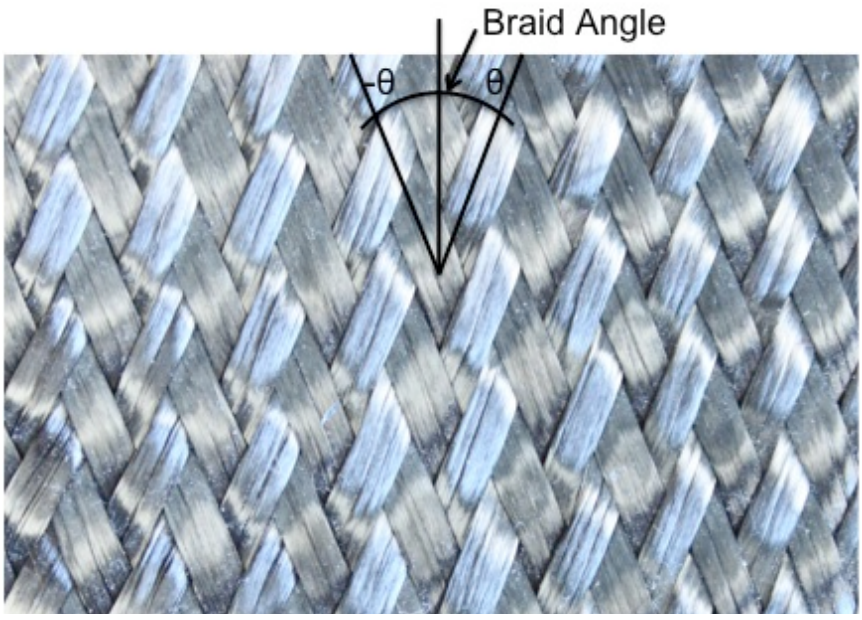


Figure 2.1 Braid Angle of a Biaxial Braid

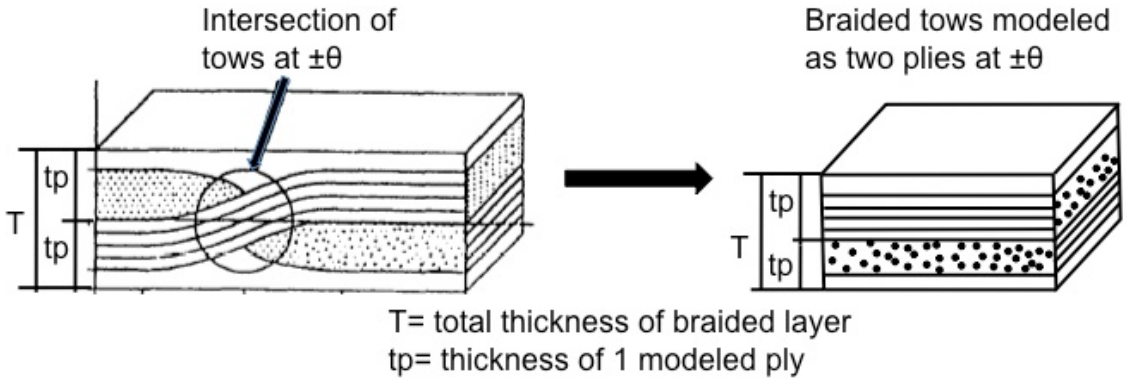


Figure 2.2 Ply Thickness for Braided material (adapted from (Tan et al. 1997))

One of the biggest benefits of the theoretical model based on classical lamination theory is that it is simpler and can be much faster to implement than a more complex finite element model. Also detailed parameters about the fiber architecture are not needed since general knockdown factors can be generated from a few easily attainable parameters.

### 2.3.2. Finite Element Analysis

Finite element analyses (FEA) became popular due to their ability to incorporate the effects of various fiber architecture parameters on the material properties of a braided composite (Tan et al. 1997). The general approach taken for a FEA model starts by modeling the fiber architecture of the unit cell. The unit cell is a repeatable unit of fabric geometry; Figure 2.3 shows a graphical rendering of the fiber architecture of triaxial braid, the picture on the right outlines the smallest unit cell contained in the generated rhombic unit cell. It is important that the unit cell is modeled accurately since the geometry and parameters of the unit cell are repeated to represent the full laminate and effect the final predictions from the FEA model (Donadon et al. 2007). Figure 2.4.a depicts a finite element model of the unit cell of a triaxial braid using beam elements; while Figure 2.4.b shows how the unit cell is repeated to form to form a finite element mesh representative of a typical composite coupon to be tested in tension.

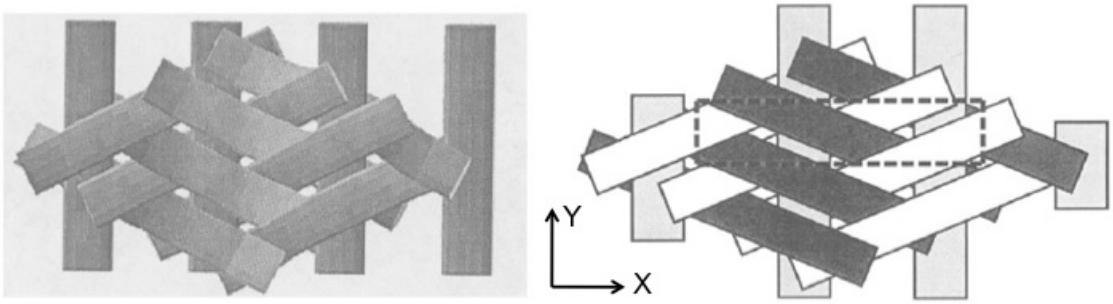


Figure 2.3 Rendering of Fiber Architecture for a Triaxial Braid (Masters et al. 1993)

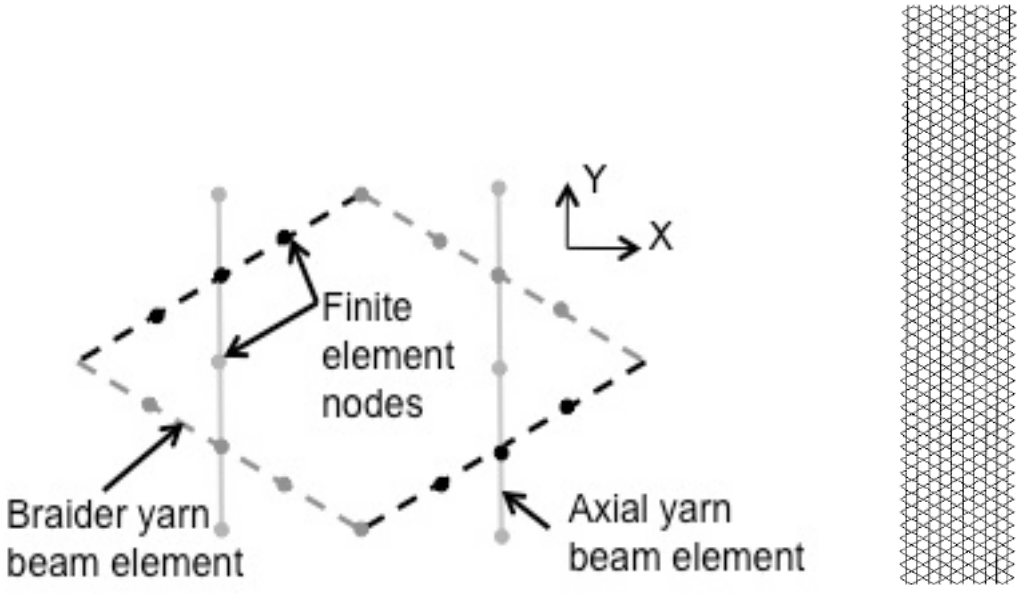


Figure 2.4 Finite Element Modeling of the Unit Cell (a.) and Composite Coupon (b.) (Dano et al. 2000)

Different fiber architectures may require different types of models for accurate predictions. Masters et al. (1993) compared various predictive models including FEA models and theoretical models based on CLT for a triaxial braided laminate; generally it was found that a FEA model provided the closest overall agreement to experimental tension tests. However it was also noted that the while the FEA model had the closest agreement it was not a dramatic improvement over other models. A downfall of FEA models is that they involve complicated geometric modeling that can take a lot of computation time. This can also become tedious because the finite element geometry should be remodeled for any changes in fiber architecture or material properties (Byun 2000).

Overall a theoretical model based on classical lamination theory and rule of mixtures was chosen for our predictions. While FEA models provide the most accurate prediction, theoretical models have also been shown to correlate well with experimental data. Theoretical models are also more simple and less time consuming since the model does not include complex fiber architecture details.

### 2.3.3. Prediction of Elastic Properties for the Arch Braided Material

In the past the elastic properties for the braided arch material were predicted by Bannon (2009) by implementing a model based on micromechanics and classical lamination theory approach described in a composite engineering textbook (Daniel and Ishai 2006). To apply this approach to a laminate composed of layers of braided fiber material, each braided layer was modeled as two symmetric off axis unidirectional plies with fibers oriented in ±θ, where θ is the specified braid angle. The reference plane for each ply is half of the total thickness of the braided material layer as described in Figure 2.2.

The model input parameters include the number of braided fiber layers, the braid angle, θ, of each layer, the braided material layer thickness, braid fiber volume and fiber and matrix properties. The material properties needed for both the fibers and matrix include, the elastic modulus in the longitudinal and transverse direction, the shear modulus and the major Poisson's ratio. The layer thickness and fiber volume can be measured from sample coupons. Fiber and matrix properties can be determined through technical data sheets from suppliers, composite textbooks, or through material testing of neat resin or unidirectional fibers.

In addition to input parameters, several assumptions are made to account for the braided composite material. The first assumption is that the composite material is linearly elastic. This is a common assumption for composite materials where the elastic modulus of the composite is dominated by the fiber elastic modulus, which is typically linear until failure. During testing the braided composite does not remain linear until failure due to the possible shifts in the braided material, however, it is linear over the range of strain values from which the elastic modulus is measured for the composite material.

Another assumptions made is an assumed fiber volume of .5, this input parameter can be measured through acid digestion of a coupon, however it was assumed for initial prediction purposes. The model implemented by Bannon also assumed a balanced and symmetric laminate, which was a reasonable assumption for his one layer of carbon braided composite, but is not valid for an asymmetric layup. Bannon also used a tow waviness knockdown factor of 20% to 30% reduction of the elastic modulus to account for the undulations of the braided material based on the tow waviness factor developed by Cox and Flanagan (1997). This factor is described in full later on in this section.

To predict the elastic properties (longitudinal elastic modulus, transverse elastic modulus and the major Poisson's ratio) the in-plane input properties are transformed according to the specified fiber orientation and assembled according to the laminate stacking sequence. Micromechanics equations and classical lamination theory were used to predict the elastic properties of each ply and the full laminate.

The longitudinal elastic modulus, $E_1$, for each ply can be predicted using the rule of mixtures as:

$$E_1 = E_f V_f + E_f(1 - V_f)$$

Equation 2-3

where $E$ is the elastic modulus of the fiber or matrix, denoted by subscripts $f$ and $m$ respectively, and $V_f$ is the fiber volume fraction of the lamina. The transverse elastic modulus, $E_2$, is predicted using the semi-empirical Halpin-Tsai equation as:

$$E_2 = E_m\left(\frac{1+2\eta_t V_f}{1-2\eta_t V_f}\right)$$

Equation 2-4

where:

$$\eta_t = \frac{\frac{E_f}{E_m} - 1}{\frac{E_f}{E_m} + 2}$$

Equation 2-5

Poisson's ratio in the longitudinal, $\upsilon_{12}$, and transverse, $\upsilon_{21}$, directions for a single ply can also be predicted using the rule of mixtures and elasticity equations as:

$$\nu_{12} = \nu_f V_f + \nu_m\left(1 - V_f\right)$$

Equation 2-6

$$\nu_{21} = \nu_{12}\frac{E_2}{E_1}$$ Equation 2-7

Where υ is the Poisson's ratio of the fiber and matrix, as denoted by the subscript. The in-plane shear modulus, $G_{12}$, can be predicted using the Halpin-Tsai equation as:

$$G_{12} = G_m\left(\frac{1+\eta_g V_f}{1-\eta_g V_f}\right)$$ Equation 2-8

where:

$$\eta_g = \frac{\frac{G_f}{G_m}-1}{\frac{G_f}{G_m}+1}$$ Equation 2-9

Where G is the shear modulus of the fiber and matrix, as denoted by the subscript.

To account for tow undulations in the braided material a knockdown factor, $\eta$, given by Cox and Flanagan (Cox and Flanagan 1997) is applied to the longitudinal elastic modulus.

$$E'_1 = \eta \cdot E_1$$ Equation 2-10

$$\eta = \left[1 + 2\left(\frac{\pi d}{\lambda}\right)^2 \cdot \left(\frac{E_1}{G_{12}} - 2(1+\nu_{12})\right)\right]^{-1}$$ Equation 2-11

Where $\eta$ is the tow waviness knockdown factor and $E'_1$ is the reduced longitudinal elastic modulus. Each tow is assumed to form a sine wave with the amplitude $d$, and wavelength $\lambda$ where $d$ is the measured layer thickness and the $\lambda$ is the measured distance between tow peaks. This reduction factor is dependant upon the ply stiffness and the fiber architecture. Bannon implemented this knockdown factor for the braided arch material and found that it decreased the longitudinal elastic modulus by 30% (Bannon 2009).

From the material properties of a single ply, the reduced stiffness matrix, $Q$, can be assembled as:

$$Q = \begin{bmatrix} \frac{E'_1}{1-\nu_{12}\nu_{21}} & \frac{\nu_{12}E_2}{1-\nu_{12}\nu_{21}} & 0 \\ \frac{\nu_{12}E_2}{1-\nu_{12}\nu_{21}} & \frac{E_2}{1-\nu_{12}\nu_{21}} & 0 \\ 0 & 0 & G_{12} \end{bmatrix}$$ Equation 2-12

The reduced stiffness matrix, $Q$, is transformed from local coordinates (1, 2) to laminate coordinate (x, y) using the transformation matrix, $T$, where *mc* and *ns* are computed from the given braid angle, θ.

$$mc = \cos(\theta)$$

Equation 2-13

$$ns = \sin(\theta)$$

Equation 2-14

$$T = \begin{bmatrix} mc^2 & ns^2 & 2 \cdot mc \cdot ns \\ ns^2 & mc^2 & -2 \cdot mc \cdot ns \\ -mc \cdot ns & mc \cdot ns & mc^2 - ns^2 \end{bmatrix}$$

Equation 2-15

The transformation matrix is applied to the reduced stiffness matrix to create the transformed stiffness matrix, $Q_{xy}$.

$$Q_{xy} = T^{-1} \cdot Q \cdot R \cdot T \cdot R^{-1}$$

Equation 2-16

Where $R$ is:

$$R = \begin{bmatrix} 1 & 0 & 0 \\ 0 & 1 & 0 \\ 0 & 0 & 2 \end{bmatrix}$$

Equation 2-17

The laminate extensional stiffness matrix, $A$, is calculated as the summation of the product of the transformed stiffness matrix, $Q_{xy}$, and the ply thickness, $t$, for each ply in the total laminate.

$$A = \sum Q_{xy} \cdot t$$

Equation 2-18

The laminate coupling stiffness matrix and the bending stiffness matrix are not included in this analysis because an experimental coupon would be fixed in the testing grips during loading, therefore restraining the coupon from any bending or twisting. The laminate extensional compliance matrix, $a$, is the inverse of the stiffness matrix.

$$a = A^{-1}$$

Equation 2-19

The laminate compliance matrix relates the stresses to the strains.

$$\varepsilon = a \cdot \sigma$$

Equation 2-20

From the laminate compliance matrix elastic properties of the laminate can be determined. The main properties of interest include $E_x$, $E_y$, and $\nu_{xy}$, where $E_x$ and $E_y$ have units of kN/mm and $\nu_{xy}$ is unitless.

$$E_x = \frac{1}{a_{xx}}$$

Equation 2-21

$$E_y = \frac{1}{a_{yy}}$$ Equation 2-22

$$\nu_{xy} = -\frac{a_{yx}}{a_{xx}}$$ Equation 2-23

Where h is the total thickness of the laminate. Finally the general load-deformation relationship for the laminate is:

$$\begin{bmatrix} N_x \\ N_y \\ N_s \end{bmatrix} = \begin{bmatrix} A_{xx} & A_{xy} & A_{xs} \\ A_{yx} & A_{yy} & A_{ys} \\ A_{sx} & A_{sy} & A_{ss} \end{bmatrix} \cdot \begin{bmatrix} \varepsilon_x^o \\ \varepsilon_y^o \\ \gamma_s^o \end{bmatrix}$$ Equation 2-24

Where $N$ is the applied load and $\varepsilon$ is a strain, both of which can be in the x, y, or s directions.

The output properties of $E_x$, $E_y$, and $\nu_{xy}$ from the model described above can be used to predict the elastic properties of the braided material used in the arches. This model and the output properties were verified to accurately predict the elastic properties of a laminate composed of a single layer of a carbon biaxial 2 x 2 braid (Bannon 2009).

## 2.4 Review of Previous Experimental Results at the University of Maine

Following the testing of carbon only coupons to determine elastic and strength properties of the arch laminate, coupons were manufactured as a symmetric sandwich laminate of two layers of UM6448 carbon and one layer of UM6447 E-glass with a laminate stacking sequence of carbon-E-glass-carbon. Product details of the braided material can be seen in Table 2.1 through Table 2.3. The resin used for infusion was DERAKANE 8084 epoxy vinyl ester resin, mechanical properties of the resin can be seen in Table 2.4. Before infusion the resin is promoted with a mix of styrene, cobalt naphthenate and dimethylaniline. To initiate the curing reaction the chemical trigonox is added to the promoted mix. While this layup is representative of the elastic and strength properties of the arch materials, it does not provide a similar material layup and number of layers used in the arches. This difference may skew the effect of environmental conditioning by protecting the E-glass on both sides when in reality the E-glass in the composite arch would be exposed to concrete and possibly degraded by alkali contained in the concrete (Balazs and Borosnyoi 2001).

In order to better represent the material used for the rigidified composite arches, a coupon with an asymmetric layup of one layer of braided carbon and one layer of braided E-glass was adopted. The following sections discuss the development of the asymmetric coupon.

## 2.5 Asymmetric layup

The objective of using an asymmetric layup was to fabricate a layup that is representative of the number of layers and how they are arranged in the rigidified composite arches, while also making sure that the coupon could be appropriately tested and produce reasonable experimental values for material properties.

Some of the problems with testing an asymmetric layup include the creation of an eccentric load when testing tension coupons and the introduction of internal stresses in the material possibly due to unequal coefficients of thermal expansion between the carbon and the E-glass. The carbon layer of the composite is oriented in the longitudinal direction to provide tensile strength to the arch, while the E-glass is oriented in the transverse direction to confine the concrete. Since the carbon fibers are carrying the majority of the tensile load in the arch structure, it is ideal for the tensile load applied during coupon testing to be in line with the carbon layer of the composite. The layer of E-glass (which is slightly thicker than the layer of carbon) creates an eccentric load applied to the carbon layer. Figure 2.5 shows a cross section of the coupon layup.

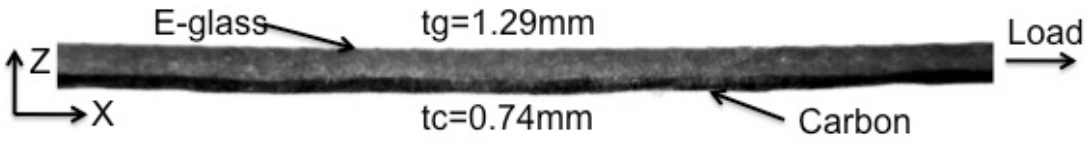


Figure 2.5 Composite Coupon Cross-section

The second problem with an asymmetric layup is that the sheets exhibit a curvature after infusion. This could possibly be due to the difference in the coefficient of thermal expansion. The E-glass layer has a higher coefficient of

thermal expansion, 5.0 $\cdot 10^{-6}$/°C, in the longitudinal direction of the arch; as opposed to the coefficient of thermal expansion for carbon which is -0.5 $\cdot 10^{-6}$/°C in the same direction. During curing the resin experiences an exothermic reaction, and when the infused composite sheet cools the difference in the coefficient of thermal expansion could result as a curve in the composite sheet. Another possible explanation for the observed curvature is the difference in stiffnesses between the two layers. Figure 2.6 shows the visible curvature in a sheet after infusion where the carbon layer is the visible top layer.

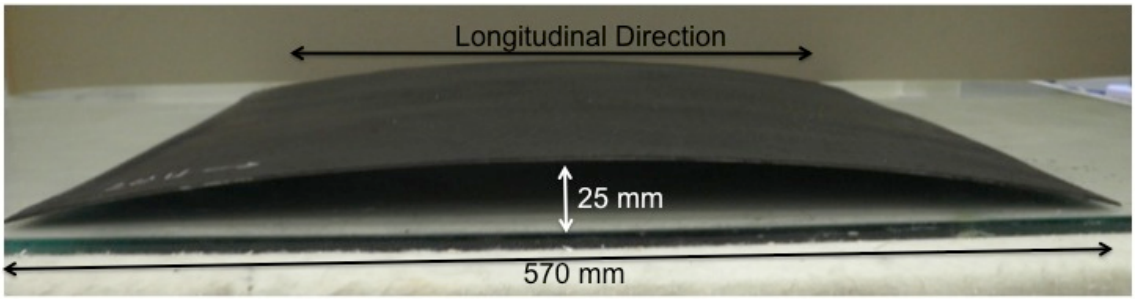


Figure 2.6 Observed Curvature in an Asymmetric Sheet

This curvature can be problematic during experimental testing where placing the sample coupon in the test apparatus straightens out the composite coupon. The act of straightening the coupon before testing can damage the composite by cracking the matrix or create uneven strains in the composite layers. The issues associated with testing an asymmetric layup are addressed through laminate testing in the following chapters.

### 2.5.1. Literature Review of Asymmetric Laminates

Fiber reinforced composites have been studied and used in many different applications, however hybrid composites, particularly those with an asymmetric layup, are less commonly researched. Typically one type of fiber is used as reinforcement, with both carbon and E-glass, along with aramid fibers being the most common type of fibers used in composite materials. The fiber used in a composite may be selected for various reasons such as strength, durability, or cost. Carbon fiber may be chosen for a specific application over E-glass fiber because it is stronger and more durable (Balazs and Borosnyoi 2001); however it is also more expensive so in applications where cost is important E-glass fibers may be selected over carbon fibers.

The composite arches use an asymmetric hybrid of carbon and E-glass, which takes advantage of both fibers' best qualities. The E-glass fibers are in the hoop direction of the arch tube, where their strength and stiffness are needed to confine the concrete and help carry shear. Since a high strength fiber isn't needed to confine the concrete it is economical to use E-glass fibers, which are less expensive than carbon fibers. The cost of braided carbon fiber initially used was 75$/kg compared to the cost of braided E-glass fiber which was 30$/kg (A&P Technology 2010). However the layer of carbon fiber is necessary to provide tensile strength for the arch under loading. Having the carbon fiber as the outside layer of the arch also provides more protection to the E-glass fibers and concrete inside the tube since carbon fibers are generally more resistant to environmental degradation (Waldron et al. 2001).

This unique hybrid composite allows for the needed strength and durability while also keeping down costs, however a downside is that there is much less established research on hybrid composites than on FRP composites in general. Areas of particular interest include the effects on material properties such as strength and stiffness and the effects on the overall durability of the composite.

Asymmetric laminates are known to have an anisotropic response to elevated temperatures such as those experienced during manufacturing (Betts et al. 2010). Residual stresses upon cooling can cause a curved deformation, which was seen during experimental testing. Betts implemented an experimental investigation to create a predicted map of the surface geometry of an asymmetric thin laminate. This tool is useful in predicting the shape of an asymmetric layup, however there is less information on how the surface geometry affects the material properties under tensile loading. Some research has been done regarding the prediction of material properties for a hybrid composite. A study done by Wu found that a hybrid one layer carbon, one layer glass tension coupon "showed favorable material properties when compared to the value predicted by the rule of hybridization." (Wu et al. 2010)

Some types of hybrid laminates have been tested in tension to observe the changes in elastic properties. Wu et al. (2010) studied the fatigue behavior of hybrid composites by comparing the fatigue life and failure mode of carbon fiber or glass fiber composites with hybrid carbon and glass fiber composites. In respect to the failure mode Wu noted that the smooth surface of the glass fibers resulted in a delamination failure mode in the hybrid coupons and a lower fatigue resistance,

however fibers with a rough surface allowed for a better bond and increased fatigue resistance. He also found that the tensile modulus of the fibers contributed to the failure mode where high modulus fibers, like carbon, developed longitudinal cracks along the test coupon as opposed to low modulus fibers, like glass, which developed transverse cracks. Under fatigue loading, carbon only coupons developed progressive cracks in the resin that affected the "simultaneous stressing of the carbon fibers" (Wu et al. 2010); this led to fibers surrounding a fractured fiber to also fail in succession and the premature failure of the coupon. In a hybrid coupon it was observed that the low modulus glass fibers helped prevent the continuous fracture of high modulus carbon fibers after resin cracking had occurred resulting in a "steadier fatigue life" (Wu et al. 2010).

### 2.5.2. Asymmetric Laminate Experimental Characterization

An experimental plan was designed to compare different composite laminates used in tension tests to determine material properties. One type of composite arch currently used in bridges is a composite laminate of one layer of carbon and one layer of E-glass. As previously mentioned, in the past coupons were fabricated of a single layer of carbon, or a symmetric layup of two pieces of carbon with a piece of E-glass in between.

Experimental characterization in accordance with ASTM D 3039- Standard Test Method for Tensile Properties of Polymer Matrix Composite Materials (ASTM 2008b) was performed to determine if a composite layup more similar to the actual arch layup could produce accurate elastic properties. Previous testing by Bannon (2009) showed that single layer carbon coupons could produce appropriate and

consistent failures. Samples tested consisted of only one layer of E-glass, only one layer of carbon, and a combination of 1 layer of E-glass, and 1 layer of carbon in order to compare elastic properties individually and combined as one composite.

Tension coupons were cut from larger sheets of infused carbon and E-glass fiber braids. Each sample layup was fabricated separately with individual batches of resin. These sheets consisted of a flattened braided tube of fibers, with a spacer in the center of the tube and were infused as a flat panel on a smooth table surface. From each infusion two sheets were produced (from either side of the spacer) from which coupons could be cut.

Three different coupon lay-ups were manufactured; these included only one layer of E-glass, only one layer of carbon, and a combination of 1 layer of E-glass, and 1 layer of carbon. All three coupon types were tested for elastic properties in accordance with ASTM D 3039 (ASTM 2008b). Table 2.6 below shows the number of samples per layup tested.

Table 2.6 Number of Samples for Each Test Set

| **Sample Lay-Up** | **Longitudinal Direction** | **Transverse Direction** |
|---|---|---|
| 1 Layer E-glass | 12 | 12 |
| 1 Layer Carbon | 12 | 12 |
| 1 Layer E-glass & 1 Layer Carbon | 12 | 12 |

Samples were all made from UM6447 E-glass and UM6448 carbon from A&P Technology (A&P Technology 2009a; A&P Technology 2009b) and infused with DERAKANE 8084 epoxy vinyl ester resin (Ashland 2006). The same VARTM/SCRIMP manufacturing technique was used for all three types of plates.

The carbon braid was oriented with tows measured at ±22 degrees, while the E-glass tows were oriented at ±81 degrees, both braid angles were measured off of the longitudinal X axis. Samples were cut using a computer controlled water-abrasive cutting machine to be 254 mm by 25.4 mm (10 in by 1 in). Coupons were cut and tested according to ASTM D3039 in both the longitudinal and transverse direction of the material. For each specimen lay up, twenty-four samples were cut, twelve in the longitudinal direction and twelve in the transverse direction. For all samples the longitudinal direction was defined as the longitudinal direction of the carbon (since the E-glass braid is considered perpendicular to the carbon braid). Figure 2.7 shows the coordinate system used for the longitudinal and transverse samples.

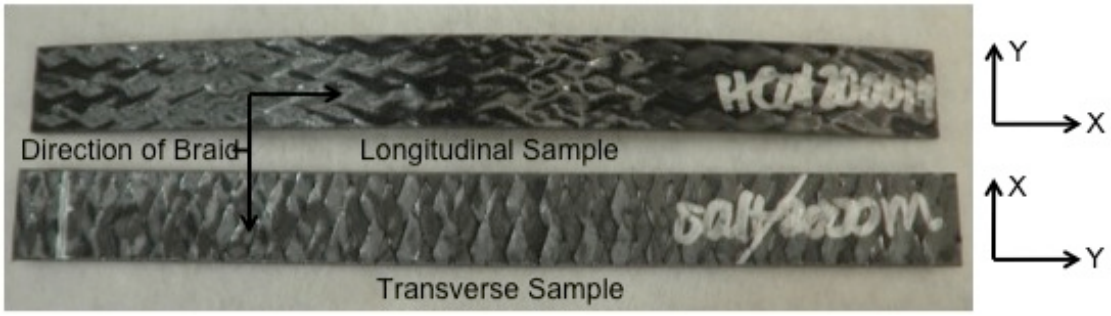


Figure 2.7 Coordinate System for Braided Coupons

After cutting each coupon, the gage width, thickness and braid angle was measured for quality control and analysis purposes. Dimensions were taken to the nearest .01 mm at three locations using a digital caliper. The coupon braid angle was measured to the nearest degree using a clear protractor. The carbon face of the samples was painted with a black and white high contrast speckle pattern throughout the gage section for non-contact strain measurement, which is shown in Figure 2.8.

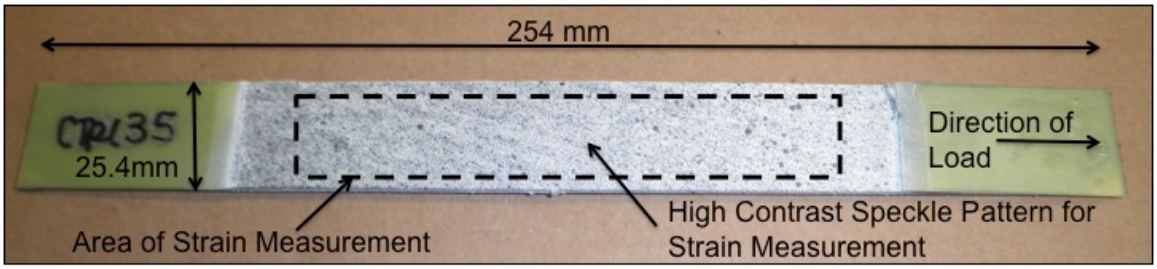


Figure 2.8 Painted Sample for Non-Contact Strain Measurement

Samples were tested using an Instron servo-hydraulic actuator with a load capacity of 98kN (22 kip). Each sample was gripped approximately 50.8 mm (2 in) on each end. Load was applied at a rate of 1.27 mm (0.05 in) per minute and samples were tested until failure. The stress in the sample was calculated as the load divided by the width of the sample and reported as a load per unit width.

Strain data was collected using ARAMIS, a non-contact digital image correlation (DIC) system, in X and Y directions on the sample for both the longitudinal and transverse samples. The DIC system continually measures full field strain by tracking the relative movement of the contrasting speckle pattern on the face of the sample. Strain data was calculated by the DIC system as an average strain collected over roughly 60% of the gage area. Figure 2.9 shows the distribution of strains seen by the DIC system in a longitudinal (bottom) and transverse (top) sample during testing. The darker areas are where the greatest amount of strain is being measured.

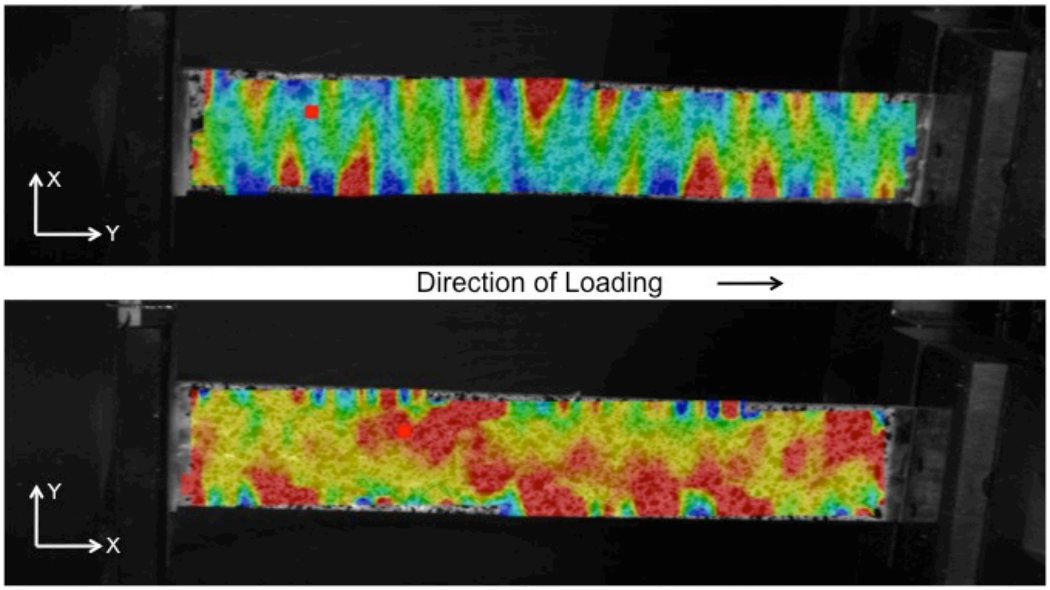


Figure 2.9 Strain Measurements Taken by ARAMIS while Loading

When reporting material property results, the elastic modulus ($E_x$) is taken from the longitudinal samples, while the transverse elastic modulus ($E_y$) is taken from the transverse samples. The major Poisson's ratio is calculated according to ASTM E132 Stand Test Method for Poisson's Ratio at Room Temperature (ASTM 2004) using strain data in both directions from only the longitudinal samples. A target coefficient of variation of 15% was used to determine if the results were consistent. To aid with sample comparison the micromechanics model implemented by Bannon (2009) was used to produce predicted values of the longitudinal elastic modulus, transverse elastic modulus and Poisson's ratio for the carbon only and glass only samples.

The composite material initially indicates a linear elastic response, which allows for the elastic modulus to be calculated as the slope of the stress strain curve. The slope of the stress strain curve is calculated over the range of 1000 to 3000

microstrains, also reported as 0.1% to 0.3% strain. The range of strain data used to determine the elastic modulus was selected by consulting prior experimental work and the literature (Tate et al. 2004) and (Masters 1996).

#### 2.5.2.1 Asymmetric Layup Results: Longitudinal Elastic Modulus

The carbon only samples have an elastic modulus that is close and slightly higher to a predicted value of 42.5 kN/mm. The predicted elastic modulus for the carbon only samples was calculated using the theoretical model implemented by Bannon, which assumes a symmetric layup. The results from the carbon only and glass only samples are shown in Table 2.7. The elastic modulus in the longitudinal direction ($E_x$) for the hybrid carbon and E-glass samples resulted in a coefficient of variation of nearly 40% and was deemed unacceptable. The high coefficient of variation is likely due to manufacturing or testing error.

Table 2.7 ASTM D3039 Test Results: Longitudinal Elastic Modulus

| **Longitudinal Elastic Modulus (kN/mm)** | | | |
|---|---|---|---|
| **Fiber reinforcement** | **Hybrid** | **Carbon** | **E-glass** |
| Mean | 43.9 | 45.1 | 7.6 |
| STD | 17.5 | 6.3 | 1.3 |
| COV(%) | 39.8 | 14.1 | 16.6 |

During manufacturing the samples of carbon and E-glass need to have the carbon tensioned over the E-glass, or for the carbon only samples, over the plastic spacer. If the carbon was not properly tensioned the difference in braid angle or any waviness in the braid could greatly affect the elastic modulus. An example of a sheet that exhibits a wavy braid and imprecise braid angle can be seen in Figure 2.10, the

gray lines in the figure show how the braid pattern is not straight as it should be. Figure 2.11 shows the change in elastic modulus vs. the braid angle of the carbon fiber for a composite coupon made of carbon and E-glass (the E-glass had a constant fiber angle of +/-81 degrees for the analysis) based on the theoretical model discussed in section 2.3.3. The target angle of the carbon fiber layer corresponds to the angle of the carbon fibers in the composite arches. This fiber angle is on the steep part of the curve, where slight variations of braid angle have a large effect on the elastic modulus.

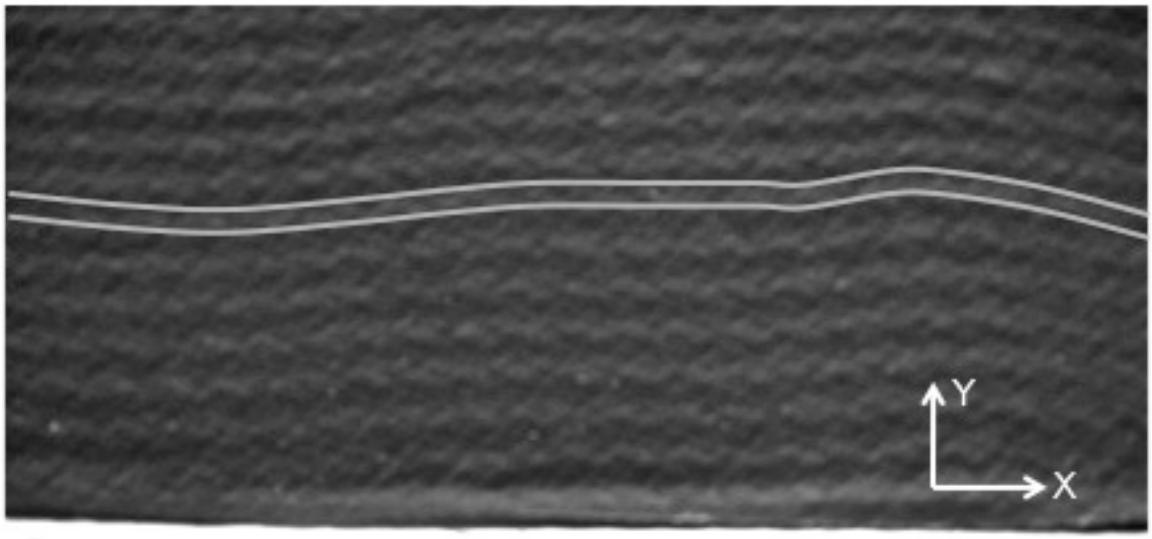


Figure 2.10 Example of a Wavy Braid in an Infused Sheet

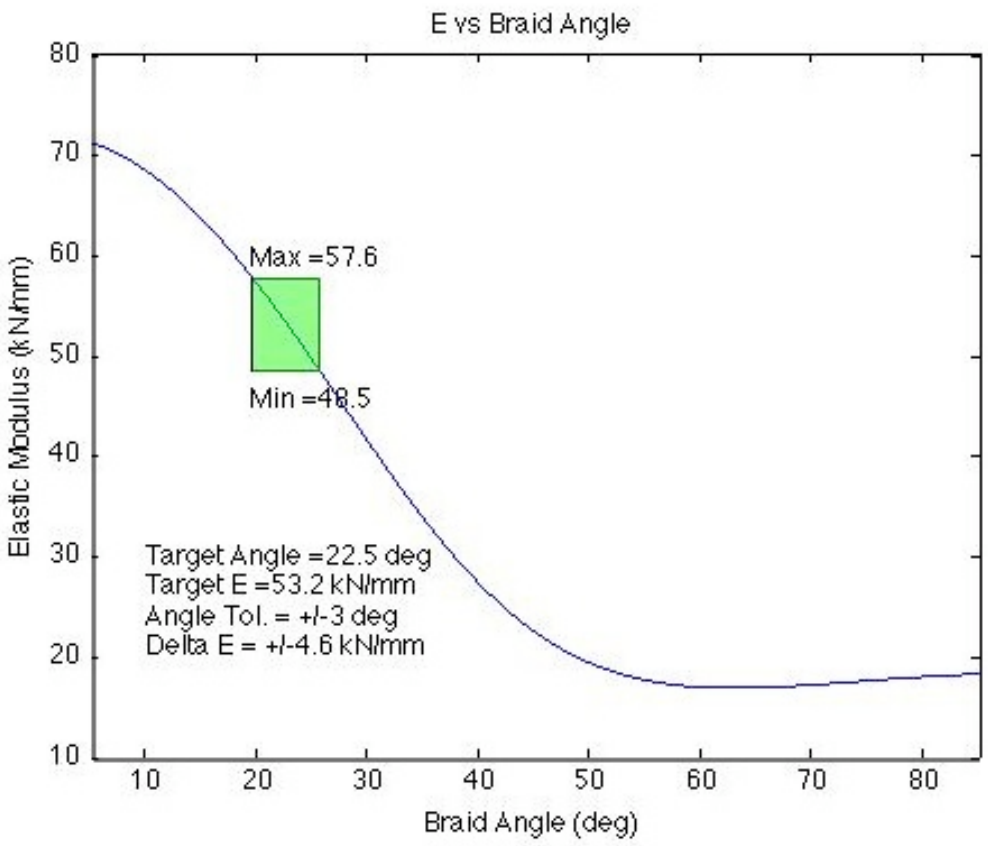


Figure 2.11 Longitudinal Elastic Modulus vs Braid Angle

Since the first round of testing was performed, quality control measures were implemented to ensure that all samples have a braid angle within a ± 3 degree tolerance, which should limit the difference in elastic modulus to ± 4.6 kN/mm. The resulting elastic modulus allowable range is less than a third of the standard deviation of the test samples. By implementing more stringent quality control measures, such as a braid angle tolerance, future testing resulted in a lower coefficient of variation for the samples composed of carbon and E-glass.

#### 2.5.2.2 Asymmetric Layup Results: Transverse Elastic Modulus

The results for elastic modulus in the transverse direction, shown in Table 2.8 are much better for the hybrid carbon and E-glass samples. The coefficient of variation is acceptable at 4.51%. The results of the E-glass reinforced specimens are also reasonable with a low coefficient of variation and less than 2% difference from a predicted value of 30.9kN/mm. Again, the predicted elastic modulus for the E-glass only samples was calculated using the theoretical model implemented by Bannon (2009), which assumes a symmetric layup. The results of the carbon only sample are not as reasonable due to a high coefficient of variation. From looking at the stress-strain plots it has been determined that the data collected from those samples are not accurate due to a small number of data points combined with noise from testing equipment which led to a nonlinear slope.

Table 2.8 ASTM D3039 Test Results: Transverse Elastic Modulus

| **Transverse Elastic Modulus (kN/mm)** | | |
|---|---|---|
| **Fiber reinforcement** | **Hybrid** | **E-glass** |
| Mean | 37.57 | 31.4 |
| STD | 1.7 | 1.4 |
| COV(%) | 4.5 | 4.5 |

#### 2.5.2.3 Asymmetric Layup Results: Poisson's Ratio

Experimental results for the major Poisson's ratio of the carbon and E-glass, and carbon only samples, shown in Table 2.9 give reasonable coefficient of variations. The E-glass samples resulted in a high coefficient of variation but this is

most likely due to a lack of data points and noisy data collection in the longitudinal samples (similar to the issues with the data from the carbon only samples in the transverse direction).

Table 2.9 ASTM D3039 Test Results: Poisson's Ratio

| **Poisson's Ratio** | | |
|---|---|---|
| **Fiber reinforcement** | **Hybrid** | **Carbon** |
| Mean | 1.18 | 1.34 |
| STD | 0.07 | 0.11 |
| COV(%) | 5.8 | 8.2 |

While the data appears consistent, only the carbon results are close to the predicted amount of 1.18. It was also noted that the carbon and E-glass results were not close to the predicted value of 0.33, but was the same as the predicted value of 1.18 for just the carbon. The difference was speculated to be an issue with the way Poisson's ratio is measured. Since the strain is measured off of the carbon side of the coupon, it was hypothesized that Poisson's ratio changed throughout the thickness of the asymmetric coupon and that DIC system was actually only capturing the Poisson's ratio for the carbon layer.

This hypothesis was investigated during testing control samples for the durability studies. Longitudinal samples of carbon and E-glass were tested in tension and strain was monitored on the E-glass side of the sample to determine if the Poisson's ratio measured from the E-glass side was different from that measured

on the carbon side. It was found that the Poisson's ratio measured from the E-glass side was in fact significantly smaller than what was measured from the carbon side. Details of this test can be found in section 4.3.3.2.

#### 2.5.2.4 Conclusions from Layup Testing

Overall it was decided to fabricate future samples using the combined carbon and E-glass layup for environmental durability testing. The experimental results yielded a large COV and under predicted the elastic modulus in the longitudinal direction, however it is thought this could be due to manufacturing error. The transverse direction had much more accurate results than the longitudinal, which would make sense if the manufacturing issues only effected the carbon, since the E-glass, which is easier to keep at a constant braid angle, contains fibers closer to the direction of loading. The samples composed of carbon and E-glass are also more representative of the layup used in the arches and therefore would allow exposure conditions to different environments to be more accurate.

### 2.5.3. Tabbing

In the composite arch structure, the layer of carbon braided reinforcement provides the majority of tensile strength, while the E-glass layer is oriented in the hoop direction to primarily confine the concrete. Since an asymmetric layup was chosen for coupon, testing tabs were added to the carbon side to help center the applied load on the carbon layer. The tabs also protected the carbon fibers from being cut or damaged by the grips. Tabs were manufactured by DESS Machine (DESS Machine 2007) and were made out of a 0,90 degree E-glass laminate. The

tabs were 50.8 mm (2 in) by 25.4 mm (1 in) with a 7 degree taper at the end and a thickness of 0.813 mm (0.032 in), which is close to the thickness of the E-glass layer in the coupons when bonded to the sample. Tabs were bonded using the high shear strength adhesive Pliogrip 7779 (Ashland 2005).

## 2.6 Verification of Strain Measurement

All strain measurements during the asymmetric coupon testing were taken using ARAMIS, a non-contact Digital Image Correlation (DIC) system. This system was chosen due to its ability to monitor strain over the entire 152.4mm (6 in) gage length of the sample. Other typical ways of measuring strain for tensile coupons include mounted strain gages or extensometers, however both of those methods may not be able to monitor the strain over the full gage length.

The in house extensometer has the ability to measure strain over a 50.8mm (2 in) gage length and only in the direction of loading. Since the coupons do not always break in the same position it would be difficult to get any data on the strain at failure or be able to observe stress concentrations in the full gage length. The extensometer also may slip as the matrix or fibers start to break.

The use of strain gages allow for strain to be measured in more than one direction, provided multiple strain gages are applied to the coupon. While strain gages allow for strain measurements in multiple directions, the area of measurement is still limited by the size of the gage. Small strain gages, around 6.35mm (0.25in), are not long enough to bridge several tows. Using small strain gages would not give accurate strain data for the composite braid, since it might only be measuring the strain in one fiber tow. In order to measure the strain in the

composite a larger strain gage was needed; 25.4mm (1 in) strain gage was long enough to contact more than one tow, therefore providing a better strain measurement in the braided material.

Even with a larger strain gage there are still issues similar to that of the extensometer. A strain gage cannot cover the entire gage length of the sample, and therefore may not necessarily capture the strain at failure or discern stress concentrations. Also, strain gages take additional time and effort to apply to each coupon and are not re-usable. The use of strain gages in this application is not cost effective when compared to extensometers or a DIC system.

The ARAMIS DIC system provides for full field strain measurement and records strain at failure as well as observed stress concentrations. The preparation of samples to be measured with ARAMIS is also much faster and easier than applying strain gages. Samples are painted with a black and white speckle pattern so that the ARAMIS cameras can follow the relative change in pattern during loading. One drawback with ARAMIS is that strain measurement is only taken on the front face of the sample. Since the composite material is an asymmetric layup of carbon and E-glass, the samples have a slight curve to them prior to being clamped in the grips. Carbon and E-glass fibers also have different modulus of elasticity. These coupon characteristics led to concerns that the front face (carbon) and the back face (E-glass) may not experience the same strain during loading.

To verify that the strain data taken from the front face was representative of the strain experienced by the entire coupon, several coupons were tested with strain gages mounted on both sides of the coupon. The elastic modulus was

calculated from the strain data on the front and back of the sample during loading and compared to verify that the strain observed on the front of the coupon was similar to the strain on the back of the coupon. Due to the initial straightening of the coupon an offset in the stress strain curves was observed, which can be seen in Figure 2.12. Even with the offset of some stress strain curves, the elastic modulus for the front and back of the coupon was similar for both the longitudinal samples and the transverse samples, shown in Figure 2.13.

The results of the strain gage testing, shown in Table 2.10, validated the use of ARAMIS for future strain measurement. The strain gages showed that the strain measurements on the back of each coupon were similar to the strain measurements on the front of the coupon; therefore using a DIC system to measure strain off of the front face of the coupon was considered adequate. While some samples had a higher difference than desirable between the front and back calculated elastic modulus, the results were still deemed acceptable due to the difficulty in precisely aligning strain gages on the front and back off the sample. All future strain measurement was measured using the ARAMIS DIC system.

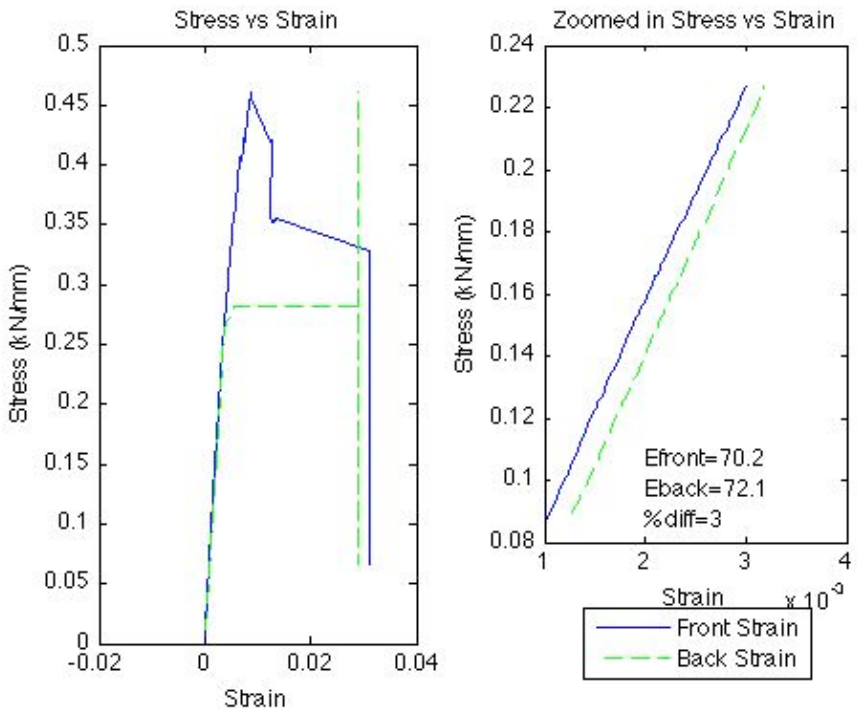


Figure 2.12 Longitudinal Sample 4 Strains Comparison

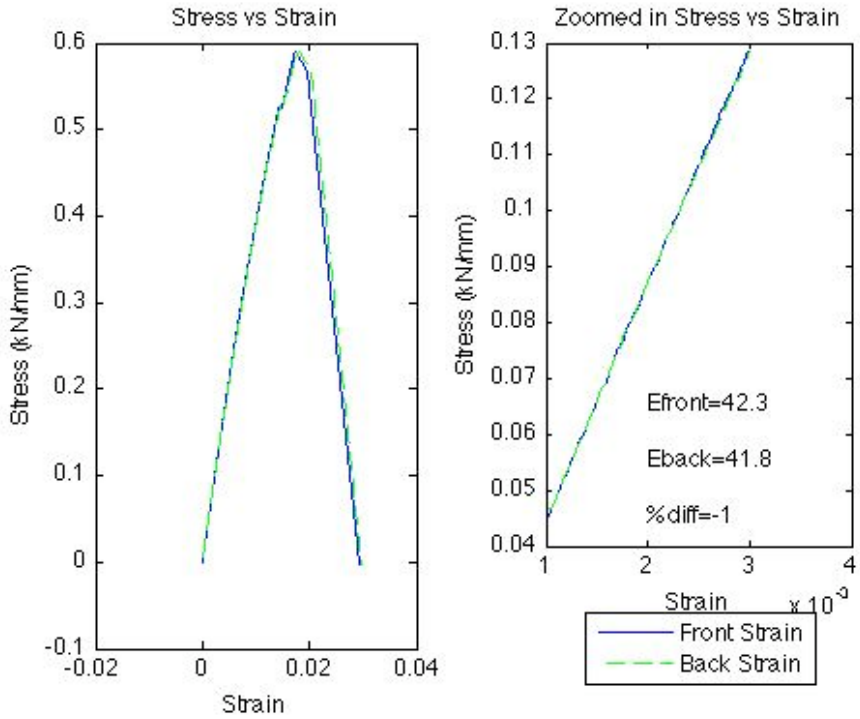


Figure 2.13 Transverse Sample A Strains Comparison

Table 2.10 Strain Gage Comparison Data

| Sample | E Front (kN/mm) | E Back (kN/mm) | % Difference |
|---|---|---|---|
| **Longitudinal** | | | |
| 1 | 73.5 | 71.1 | 3.3 |
| 2 | 75.9 | 88.4 | 14.1 |
| 3 | 59.7 | 66.5 | 10.2 |
| 4 | 70.2 | 72.1 | 2.7 |
| **Transverse** | | | |
| A | 42.3 | 41.8 | 1.1 |
| B | 48.6 | 43.5 | 11.6 |
| C | 39.6 | 37.3 | 6.0 |
| D | 43.8 | 37.3 | 17.5 |

## 2.7 Asymmetric Coupon Development Triaxial Braid

After selecting a coupon layup and an appropriate system for measuring strain the next step taken was to verify that the asymmetric coupon would provide consistent results from batch to batch. The first set of asymmetric coupons tested had relatively low coefficients of variation for the transverse elastic modulus (4.5%) and Poisson's ratio (5.8%), however the coefficient of variation for the elastic modulus in the longitudinal direction was 39.8%, which is considered high for a composite material. As discussed in section 2.2.1, the high coefficient of variation was assumed to due to the laminate manufacturing process and the difficulty in keeping a consistent braid angle during infusion. To reduce the coefficient of variation, quality control measures were taken to insure that the coupons tested had a braid angle within ± 3 degrees of the target angle.

Using the new quality control measures, six sheets were manufactured from three different infusions (each infusion produces two sheets from either side of the spacer in the mold). All infusions used the same resin cure packages, materials,

layups and manufacturing methods. All six sheets had both longitudinal and transverse coupons cut from them and evaluated using the predetermined quality control measures. From the coupons that were deemed acceptable, four longitudinal and four transverse coupons were randomly selected from each of the three infusion sets for a total of twelve longitudinal and twelve transverse coupons. By selecting samples from several infusion sets, the variability between infusions sets could be observed. The results of each batch, as well as the combined batches are shown in Table 2.11, the coefficient of variation is shown in parenthesis. For the elastic modulus in the longitudinal direction each batch and the combined batches have a higher coefficient of variation than the target value of 15%. The elastic modulus in the transverse direction and Poisson's ratio show acceptable and consistent coefficients of variation for all of the batches.

Table 2.11 Asymmetric Variability Test Results

| **Batch** | **$E_x$ (kN/mm)** | **$E_y$ (kN/mm)** | **$\upsilon_{xy}$** |
|---|---|---|---|
| 1 | 65.6 (18) | 41.1 (2) | 1.12 (5) |
| 2 | 64.4 (24) | 40.0 (4) | 1.21 (10) |
| 3 | 44.8 (23) | 40.2 (7) | 1.16 (8) |
| All | 58.3 (26) | 40.42 (5) | 1.16 (8) |

The results from the asymmetric variability tests confirm that the quality control measures did help reduce the coefficient of variation from approximately 40% to 26% for the elastic modulus in the longitudinal direction, however this was still higher than the target coefficient of variation of 15%. The elastic modulus also was about 3% higher than a predicted value of 56.6 kN/mm. The predicted value

was calculated using the theoretical model described in section 2.3.3 where the asymmetric layup was modeled as a two ply laminate (one ply of carbon and one ply or E-glass) and the experimental results from the layup testing of one layer of carbon and one layer of E-glass were used as inputs for $E_1$ and $E_2$. The data for the transverse elastic modulus and Poisson's ratio have acceptable coefficients of variation, and the transverse modulus was about 8% higher than the predicted value of 37.0 kN/mm.

While the 26% coefficient of variation was an improvement on the first batch of samples tested, it is still considered relatively high. It was decided that further improvements should be made to reach a target coefficient of variation of 15% or less. The stress strain curves for the variability test set were plotted to see if there were any patterns or grouping in the data. It was observed that out of the four samples from set 1, three of the samples were grouped together and had a higher elastic modulus. Also three of the samples from set 3 were grouped together and at the lower end of the range of elastic modulus. The samples from set 2 were not grouped and ranged from the lower end to the higher end of elastic modulus spectrum. Figure 2.14 shows the overall spread of data. From this plot it was determined that the variability was not only seen as a product of separate infusions, but there was also variability within one infusion set, seen from the variation in the samples from set 2.

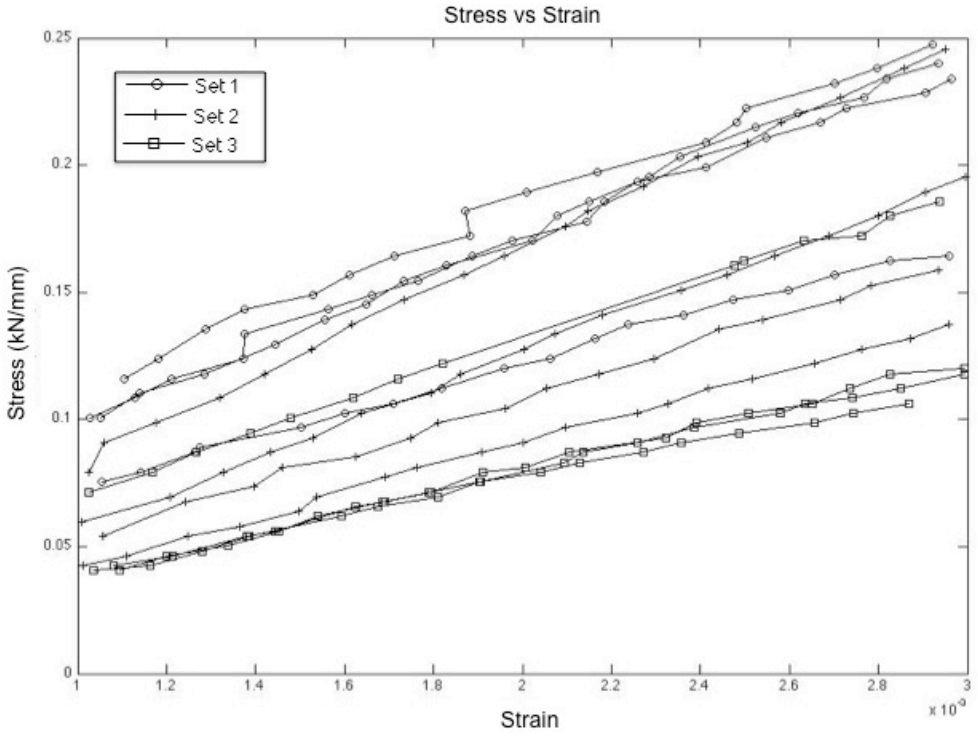


Figure 2.14 Variability Test Longitudinal Stress Strain Plots

The variability in the longitudinal elastic modulus was still believed to be from the variability in the angle of the carbon fiber braid caused during coupon sheet manufacturing and infusion. The first attempt at mitigating the problem was by implementing a quality control procedure into the infusion process; the next step taken was to modify the braided material to produce a more consistent braid. Throughout previous testing it was observed that the coefficient of variation for the elastic modulus in the transverse direction was much lower than the longitudinal direction, and an acceptable value of 4.62%. Figure 2.15 also shows that the stress strain curves are much closer to each other, as opposed to the spread in curves seen for the longitudinal samples.

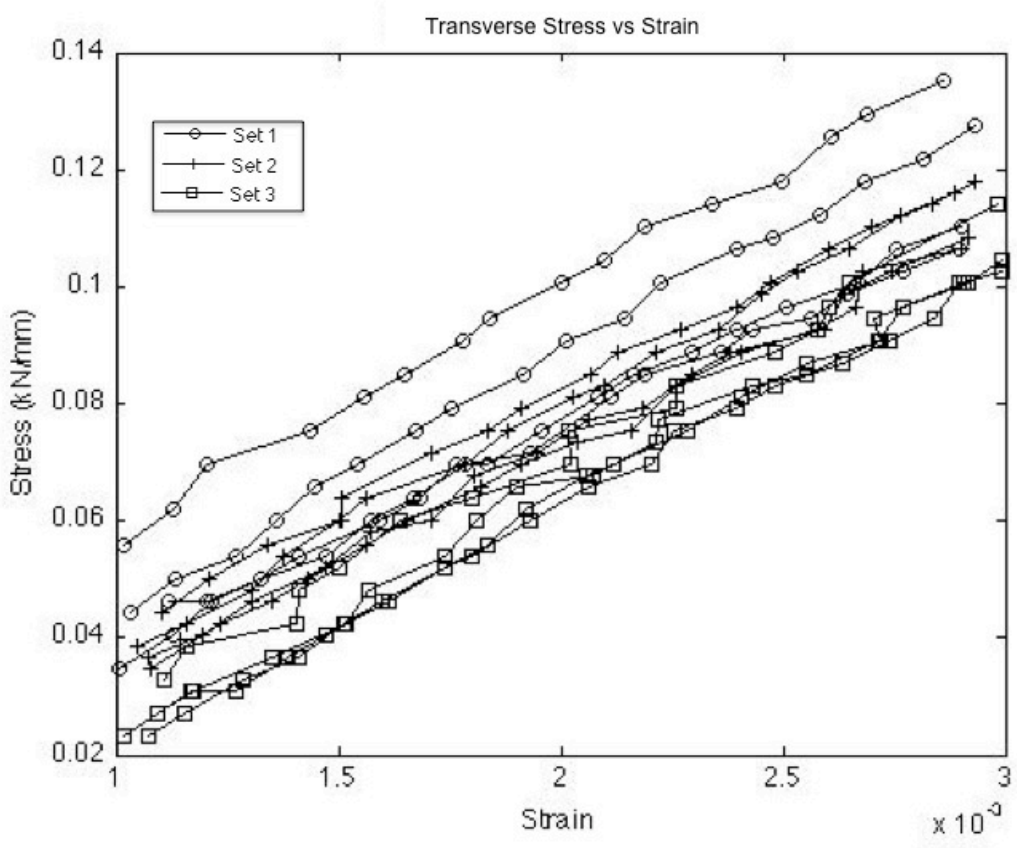


Figure 2.15 Variability Test Transverse Stress Strain Plots

The E-glass layer controls the elastic modulus in the transverse direction. The braided E-glass tube has glass fibers at an angle of ± 81 degrees, it also has elastics in the 0 degree direction that help hold the material together. The elastics seemed to minimize the variability in braid angle for the E-glass braided layer. It was proposed to modify the carbon braid to have a similar constraint. The new carbon fiber braid consisted of carbon fiber tows with a measured braid angle of ±20° and new hot melt plastic strands in the 0 degree direction to lock the carbon fiber braid angle into place, creating a triaxial braid. The hot melt plastic was also added to the E-glass braid in replace of the elastics for the first set of samples tested.

Twelve longitudinal and twelve transverse samples were tested using the new triaxial carbon layer and triaxial E-glass layer; the results from these tests can be seen in Table 2.12. The triaxial braided material successfully lowered the coefficient of variation to under 3% for both the longitudinal and the transverse elastic modulus.

Table 2.12 Triaxial Test Results

| **Sample Composition** | **$E_x$ (kN/mm)** | **$E_y$ (kN/mm)** | **$\upsilon_{xy}$** |
|---|---|---|---|
| Mean | 63.78 | 34.19 | 1.30 |
| STD | 1.79 | 0.71 | 0.09 |
| COV(%) | 2.81 | 2.08 | 7.16 |

## 2.8 Conclusions and Recommendations for Future Work

Overall, the asymmetric coupon development studies produced a type of coupon to be used for future durability studies. Coupons for measuring elastic modulus would have an asymmetric layup of one layer of a triaxial carbon fiber braid measured at ± 20 degrees with hot melt plastic strands at 0 degree and one layer of an E-glass braid at ± 81 degrees and elastic strands in the 0 degree direction. The E-glass braid used in future testing was not the triaxial hot melt braid since the E-glass braid with elastic axial strands also produced an acceptable coefficient of variation in previous tests and there was more initial material on hand. The asymmetric coupons were also tabbed with a 0/90 degree E-glass

tapered tab on the carbon side of the coupon to align the carbon layer with the center of applied load during testing. Also all future strain measurements were recorded using the ARAMIS DIC system.

Recommendations for future work include additional experimental testing to observe product variability and the development of an FEA model. The use of a triaxial hot melt braid greatly reduced the variability in the experimental elastic properties, however since the hot melt plastic is not present in the braided carbon used in the composite arches, further studies should be done to reduce product variability without the additional hot melt plastic axials. The model based on classical lamination theory adequately predicts the elastic modulus of the composite, however the use of an FEA model should be investigated to help eliminate assumptions and knockdown factors that currently account for the fiber architecture in the theoretical model.

It is also recommended that more research be done to determine the effects of the curvature seen in the coupons. While the coefficient of thermal expansion for carbon and glass fibers are known, the coefficient of thermal expansion for the hybrid carbon and E-glass composite and the individual lamina of carbon and E-glass are not currently known. It is recommended that the coefficient of thermal expansion for the individual layers and the hybrid composite be measured to determine if the residual curvature is due to the difference in the coefficient of thermal expansion between the two materials.

# Chapter 3. NOTCHED TENSILE TEST METHOD FOR BRAIDED COMPOSITES

## 3.1 Introduction

One of the unique things about the rigidified composite arches is that the composite fibers are braided to form the hollow arch tube. While the braided material is an advantage in some aspects, it also produces a new type of laminate. Current standardized test methods used for determining material properties do not consider the difference between testing a braided composite and a unidirectional composite.

ASTM D 3039-Standard Test Method for Tensile Properties of Polymer Matrix Composite Materials (ASTM 2008b) is typically used to measure both elastic and strength properties of a composite material, however it has been observed that the type of specimen suggested in ASTM D 3039 misrepresents the longitudinal tensile strength of the laminate (Bannon 2009). To represent the full tensile strength of the braided composite tube the coupon must fail due to fiber rupture. FIGURE shows the fiber rupture failure of the carbon fibers in an arch that was loaded until failure at the AEWC Advanced Structures and Composites Center.

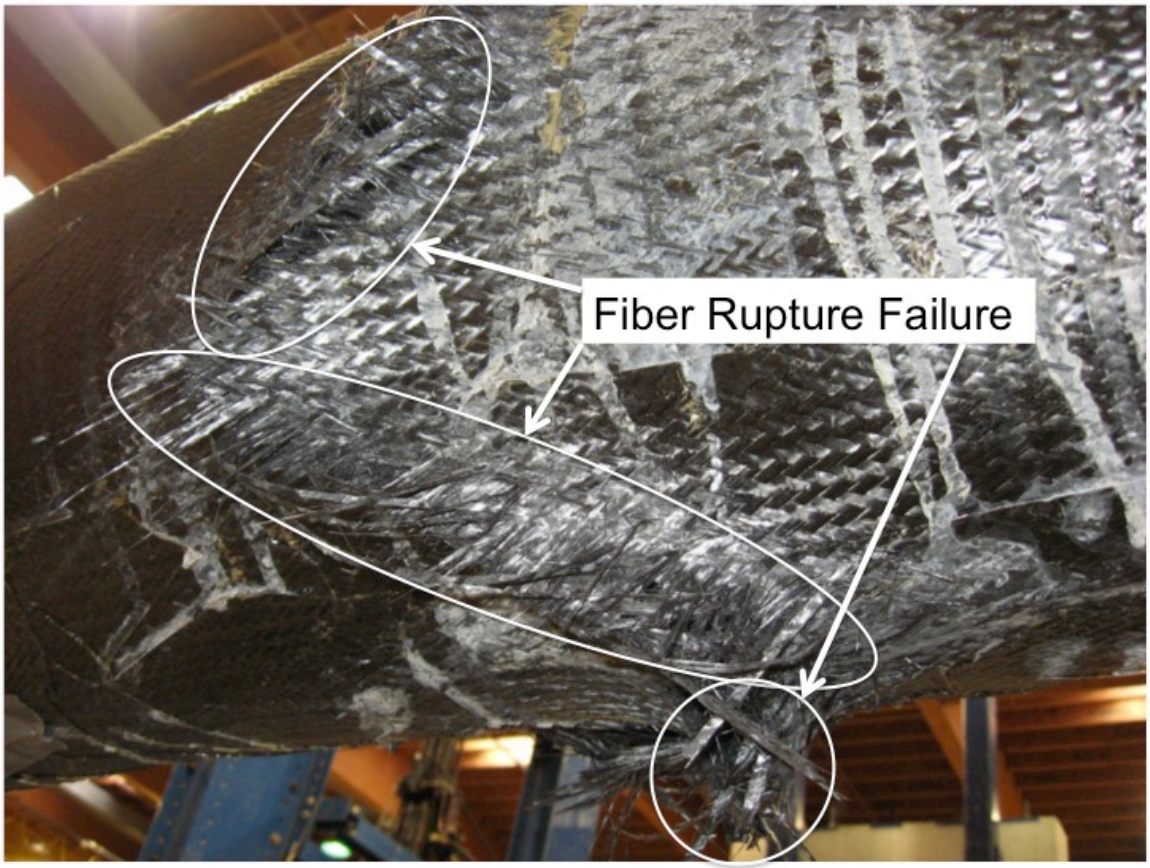


Figure 3.1 Fiber Rupture Failure of an Arch

The geometry of the standard ASTM D 3039 coupon causes the coupon to fail due to shear or interfiber failure when loaded in the longitudinal direction since there are no continuous fibers that are gripped at both ends of the coupon. In order to develop the full tensile strength of the composite Bannon designed a new notched coupon geometry that would produce fiber rupture failures (Bannon 2009). Bannon also implemented a model to predict the tensile strength of a single braided layer of carbon that was verified through tensile tests preformed on notched coupons.

## 3.2 Notched Coupon Geometry

The notched coupon was based on a bowtie shaped coupon developed by Bowman; the bowtie shaped coupon had a shorter gage length than a typical tension specimen (Bowman et al. 2003). The shape of the coupon allowed for continuous tows to be gripped at both ends, therefore making a fiber rupture failure possible. Bannon used the bowtie coupon shape and optimized the gage section length, width and overall geometry to create a notched coupon that would produce fiber rupture failures in coupons made from the composite arch material. Figure 3.2 shows several coupon geometries studied by Bannon. The N2 notched coupon geometry was ultimately chosen because it produced fiber rupture failures, with a high mean strength and a low coefficient of variation and was simple to manufacture.

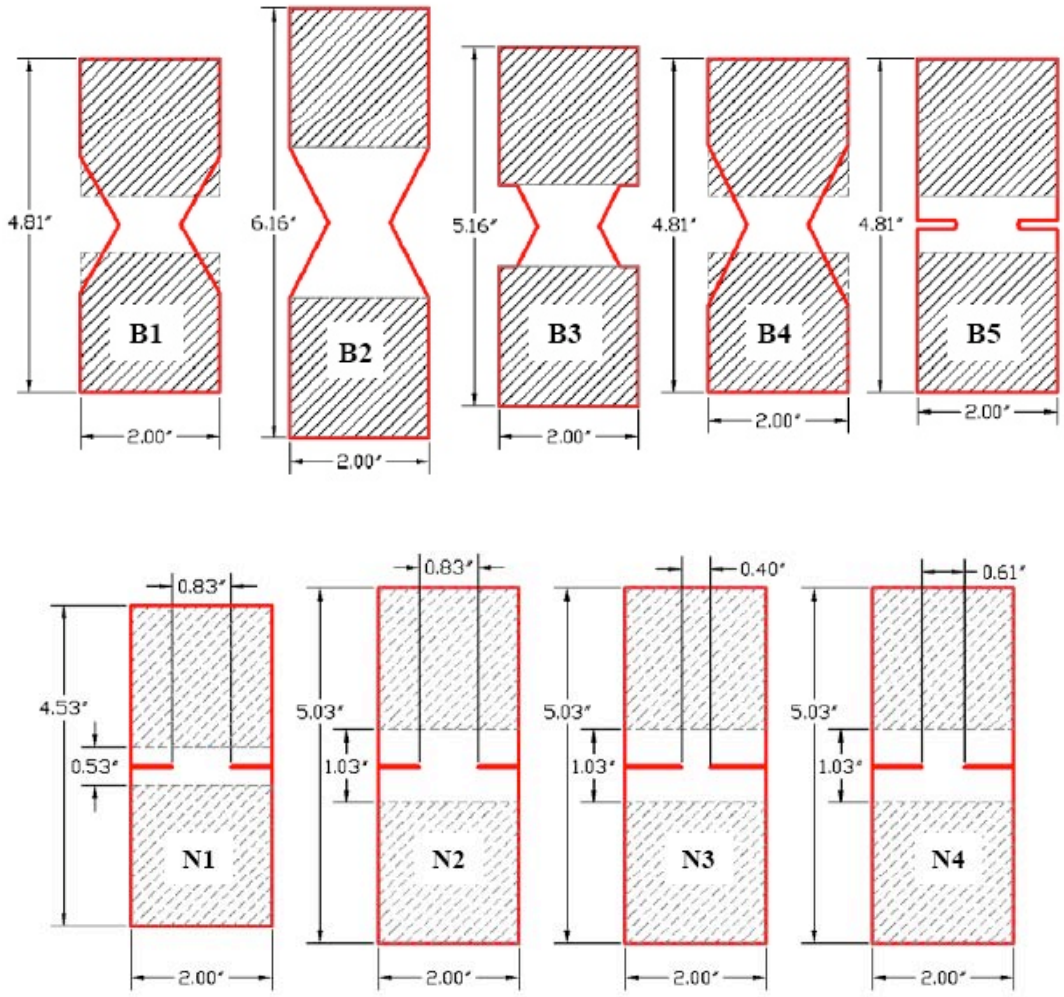


Figure 3.2 Tensile Coupon Geometry Alternatives (Bannon 2009)

One of the most important features of the notched coupon geometry is that it has continuous fibers from grip to grip which allows for the full fiber dominated tensile strength of the laminate to be represented. Another important feature is the size of the gage section, which is specified such that only continuous fibers that contribute to the coupon strength are considered in the calculation of the gage section area.

## 3.3 Prediction of Strength Properties

The prediction of strength properties build on the predicted elastic properties as discussed in section 2.3. The two common types of models discussed for the prediction of elastic properties were finite element analysis (FEA) models and theoretical models based on classical lamination theory. These two models may also be used to predict the tensile strength properties of a composite.

### 3.3.1. Classical Lamination Theory

The model implemented by Bannon to predict strength properties was an extension of the theoretical model used to predict the elastic properties, which was based on micromechanics and classical lamination theory approach described in a composite engineering textbook (Daniel and Ishai 2006). The material inputs and calculated elastic properties are used in conjunction with a selected failure theory to determine the laminate strength properties. There are several common stress and strain based failure theories know as the maximum stress theory, maximum strain theory, Tsai-Hill theory, and Tsai-Wu theory.

The maximum stress theory states that failure occurs when at least one stress component along one of the principal material axes exceeds the corresponding strength in that direction. Similar to the maximum stress theory, is the maximum strain theory, which states that failure occurs when at least one strain component along one of the principal material axes exceeds the corresponding strain limit in that direction.

Both theories account for three different modes of failure, fiber failure in tension or compression, interfiber failure in tension or compression, and in-plane shear failure. The maximum stress theory works best for brittle modes of failure in the longitudinal or transverse direction and does not consider any stress interaction in biaxial stress states (Daniel and Ishai 2006). The maximum strain failure theory does allow for some interaction of stress components due to Poisson's ratio effects; it also considers the principle strains in tension, compression and shear separately.

The Tsai-Hill and Tsai-Wu failure theories both allow for an interaction of stresses however the Tsai-Hill theory does not differentiate between tension and compression and neither theories clearly show the source of failure (Daniel and Ishai 2006). Tsai-Hill theory, or the Strain Energy Based Interaction Theory is based off of the Von Mises yield criteria for metals. Tsai-Hill theory uses all the applied stresses in one equation to determine if the laminate has reached failure.

The Tsai-Wu theory, also know as the Interactive Tensor Polynomial Theory differentiates between tension and compression and produces an interactive failure theory for a laminate under a multi axial stress state. One drawback of the Tsai-Wu theory is that it requires biaxial experimental testing to produce an interaction coefficient.

### 3.3.2. Finite Element Analysis

A FEA model, which predicts elastic properties, as discussed in Section 2.3.2, can also be extended for strength predictions. Strength prediction models that use classical lamination theory failure criteria are based on critical strength parameters measured from unidirectional composites. Since the fibers in the fabric are braided,

the critical strength parameters measured from unidirectional composites may be even less applicable (Huang and Ramakrishna 2003).

The Handbook of Analytical Methods for Textile Composites (Cox and Flanagan 1997) lists some of the documented available codes for predicting material properties of composites. Not all of the codes on that list have been experimentally validated, however there is a FEA code that is able to predict strength and has been experimentally validated. The authors of the code were able to use it to simulate a variety of complex failure phenomena (Cox and Flanagan 1997).

The advantages and disadvantages between using a theoretical model and a FEA model for strength prediction are similar to those for the prediction of elastic properties. FEA models can better capture the effect of the fiber architecture on the failure of the composite, however the model is more detailed and requires more time to implement. While both models have been shown to be able to predict strength values, neither was able to be used in this study to produce strength predictions for the hybrid material.

### 3.3.3. Previous Correlation of Experimental Results & Model Predictions

Testing was preformed by Bannon to validate the predicted strength using a theoretical model. Carbon only braided laminates with various braid angles were tested in tension using the notched geometry. With a measured braid angle of ± 22 degrees the failure theory that correlated best with the experimental results was the maximum strain failure theory with a predicted strength less than 3% different from the experimental. All of the other theories under predicted the ultimate tensile strength at that braid angle by at least 36% (Bannon 2009).

## 3.4 Asymmetric Notched Coupon

Similar to the rectangular tension coupons used to measure elastic properties, there were concerns with testing and modeling an asymmetric notched coupon. Again there was a slight curvature in the coupons, however it was not as severe since the notched coupons were half the length of the rectangular coupons. Also there was the problem of an eccentric load applied to the carbon layer due to the layer of E-glass. The problem of an asymmetric load was managed by using extra tabs to center the carbon layer in the grips. The details of the tabbing are further discussed in section 3.4.3.

### 3.4.1. Literature Review of Asymmetric Strength Coupons

As previously mentioned there is less established research on the material properties, such as tensile strength, of hybrid composites than there is on carbon fiber or E-glass fiber composites. Carbon and E-glass have different tensile strengths and values of strain to failure; it is important to understand how these differences affect the ultimate tensile strength and strain of a hybrid composite.

Carbon fiber, when compared to E-glass, has a higher tensile strength but a lower rupture strain. Based on the "crack-constrain theory of hybrid composites" (the breakage of low elongation fibers will be restrained by high elongation fibers) when loading hybrid composites, carbon fibers will begin to fracture before E-glass fibers (Cao et al. 2009). A study showed a decrease of 35% in the rupture strains in the hybrid coupon as compared to glass only coupons; this is attributed to the fact that the rupture strain of the hybrid composites was governed by the carbon fibers (Wu et al. 2010).

Hybrid coupons can also experience different failure modes, as discussed in 2.5.1. Tensile coupons can experience delamination between the E-glass and carbon layers leading to premature failure. However the E-glass can also allow for more consistent and possibly higher failure strengths by helping to distribute the load to the carbon fibers, and redistribute the load to undamaged carbon fibers when the first carbon fibers fail.

### 3.4.2. Notched Asymmetric Laminate Experimental Characterization

A test study was done to compare an asymmetric notched coupon with notched coupons made of only one layer of carbon, or only one layer of E-glass. The notched test study was implemented in the same manner as the rectangular coupon test study for asymmetric coupons. The samples were made from UM6447 E-glass and UM6448 carbon from A&P Technology (A&P Technology 2009a; A&P Technology 2009b) and infused with DERAKANE 8084 epoxy vinyl ester resin (Ashland 2006). Coupons were infused using the same process as the rectangular samples. A water-abrasive cutting machine was used to cut the notched samples to be 127mm (5 in) by 50.8mm (2 in) with 0.76mm (0.03in) wide notches at midspan that cut in 15.4mm (.61 in) on each side of the coupon leaving a 20mm (0.79in) gage width. The dimensions can also be seen on Figure 3.3.

All samples were cut to be loaded in the longitudinal direction only to determine the tensile strength in the carbon fiber dominated X direction. Figure 3.4 shows the fiber orientation of the glass and carbon fibers across the gage section for all of the notched coupons. Dimensions of each coupon were measured after cutting to insure proper manufacturing and for analysis purposes.

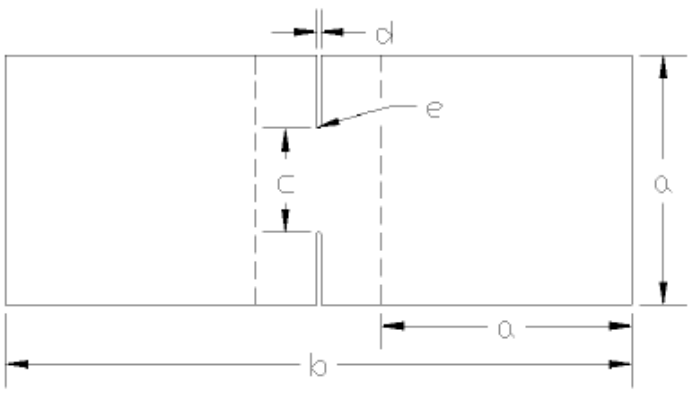


| Dimension | |
|---|---|
| A | 50.8 mm |
| B | 127 mm |
| C | 20 mm |
| D | 0.76 mm |
| E | 0.40 mm |

Figure 3.3. Notched Coupon Geometry (Bannon 2009)

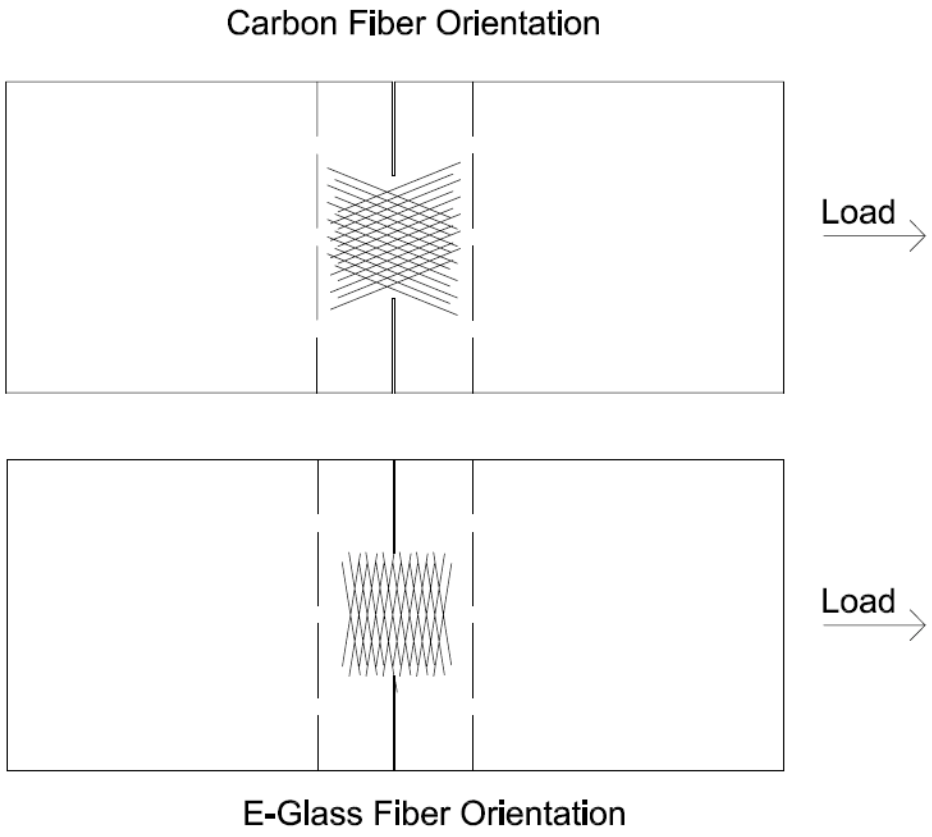


Figure 3.4 Fiber Orientation of Carbon and E-Glass Fibers in Notched Coupons

The notched coupons were tested using an Instron servo-hydraulic actuator in accordance with ASTM D 3039 with an applied load rate of 1.27 mm (0.05 in) per minute and loaded until failure. Each coupon was gripped 50.8mm (2 in) on both ends as show by the dashed line in Figure 3.3. Load and displacement data was recorded for each test. The maximum load divided by the notched width of the sample was reported as the ultimate tension failure strength in the X direction as a stress per unit width. Only samples that failed due to fiber rupture were included in the test results. Also, a target coefficient of variation of 15% was used to determine if the results were consistent.

For each type of coupon (carbon only, E-glass only, and an asymmetric layup of one layer of carbon and one layer of E-glass) twelve samples were tested. From the notched coupon tensile strength tests it was found that samples composed of a layer of E-glass and a layer of carbon had a higher kN/mm tensile strength, 1.19 kN/mm, than the samples composed of only carbon, 0.88 kN/mm, or only E-glass, 0.03 kN/mm. Also the asymmetric coupons had a lower coefficient of variation than the samples of carbon only. A table summarizing the notched results can be seen in Table 3.1.

Table 3.1 Asymmetric Notched Tensile Test Results

| **Ultimate Tensile Strength** | | | |
|---|---|---|---|
| **Sample Composition** | **Mean (kN/mm)** | **STD (kN/mm)** | **COV (%)** |
| Carbon and Glass | 1.19 | 0.14 | 11.8 |
| Carbon Only | 0.88 | 0.11 | 12.2 |
| Glass Only | 0.03 | 0.004 | 11.3 |

Since the E-glass braid was oriented in the transverse direction of the sample, it was expected that the E-glass would have a very low ultimate tensile strength on its own. Coinciding with that assumption, it was also expected that the layer of E-glass in the samples composed of carbon and E-glass, would not provide a significant increase in ultimate tensile strength in comparison to samples of carbon only. However when reviewing the test results the asymmetric coupons had a 35% higher mean strength than the mean strength of the carbon only and E-glass only samples combined.

The asymmetric samples of carbon and E-glass produced a more consistent failure mode of tensile fiber rupture that appeared to be evenly distributed throughout the gage section, this is shown in Figure 3.5 a and b. The samples of only carbon had a predominant failure mode of fiber rupture, however in some samples it seems only some of the fiber bundles carried the load through the gage section, Figure 3.5. c, and a toe pullout failure mode was also seen in one sample, Figure 3.5. d. It appears that the E-glass may help distribute the load through the gage section of the sample, allowing the load to be carried by more fiber bundles and increasing the overall tensile strength.

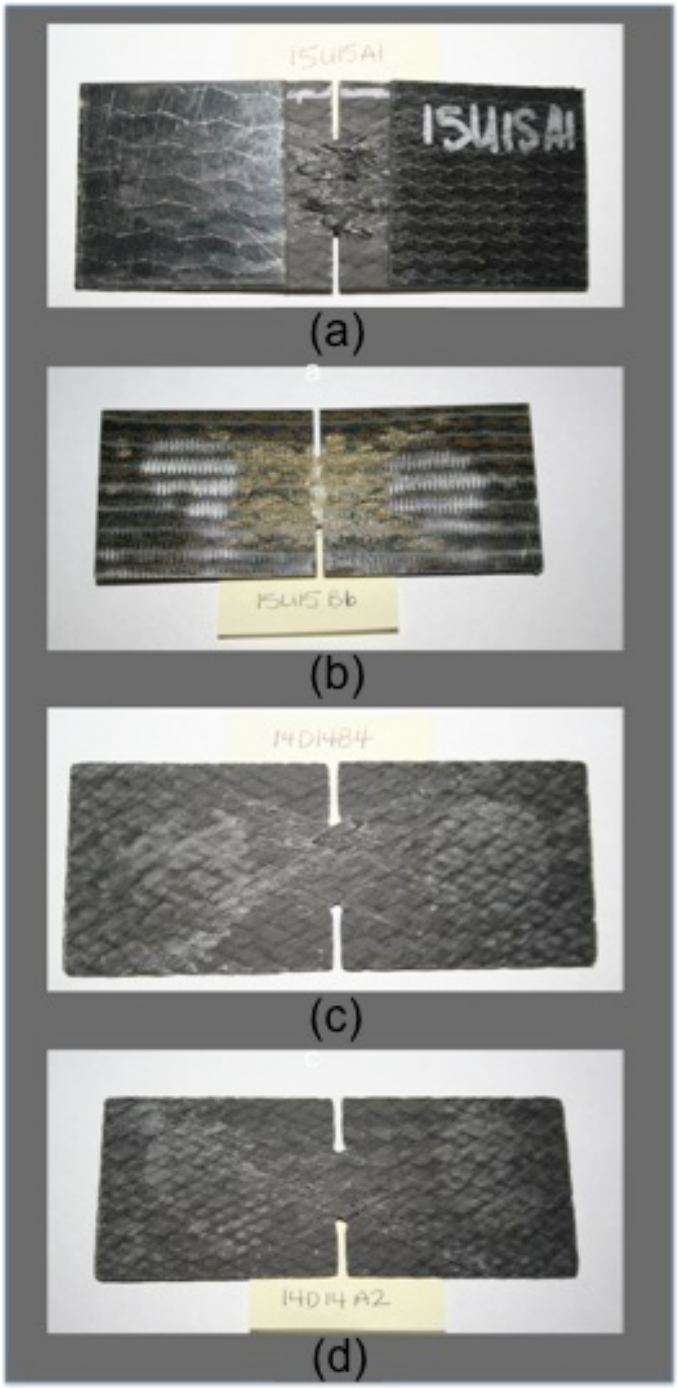


Figure 3.5 Notched Tensile Coupons After Testing

The relationship between the strength of the carbon only coupons and the strength of the carbon layer in the hybrid coupons is shown in Equation 3-1; where $\varphi$ represents the strength efficiency factor, $F_{xt}^{C*}$ is the experimental strength of the carbon only samples and $F_{xt}^{C}$ is the predicted full strength of the carbon layer.

$$F_{xt}^{C} = \frac{1}{\varphi} \cdot F_{xt}^{C*} \qquad \text{Equation 3-1}$$

$$\varphi = \frac{number\ of\ tows\ failed\ in\ carbon\ coupons}{number\ of\ tows\ failed\ in\ hybrid\ coupons} \qquad \text{Equation 3-2}$$

When reviewing the failures seen in the tested coupons it was observed that the hybrid coupons had all or most of the tows rupture at failure in the gage section, while the carbon only samples had about three quarters of the tows rupture at failure. An initial efficiency factor was based on the assumption that all of the tows in the gage section for the hybrid coupons failed due to fiber rupture, and the efficiency factor would be the ratio of the average number of tows which failed in the carbon only coupons over the number of tows in the gage section. However it was also observed that while more tows failed in the gage section for the hybrid coupons, not every coupon had every fiber in the gage section fail. After that observation was made, the ratio was changed to be calculated based on the average amount of ruptured tows seen in the carbon coupons over the average amount of ruptured tows seen in the hybrid coupons; this ratio was approximately 0.78. The ratio was then used as the strength efficiency factor in Equation 3-1.

To help explain the difference of strength between the carbon only and the asymmetric hybrid carbon and E-glass coupons a phenomenological damage model was created. The model is bilinear to account for the damage in the layer of E-glass that fails at the lower tensile strain. After the initial failure, the model can consider either a brittle or a yielding response of the damaged E-glass layer. In addition the model considers the efficiency of the carbon fiber tows, where the full failure strength of the carbon layer is represented by $F_{xt}^{C}$ and the experimental partial failure strength is denoted as $F_{xt}^{C*}$. The damage model assumes that all of the fibers that pass through the gage section behave the same and have the same response. Figure 3.6 shows of the general stress strain diagram for the brittle response. The solid Xs show were the E-glass layer would fail and where the carbon layer would fail prematurely, while the outlined X shows the full strength of the carbon layer as seen in the hybrid coupons.

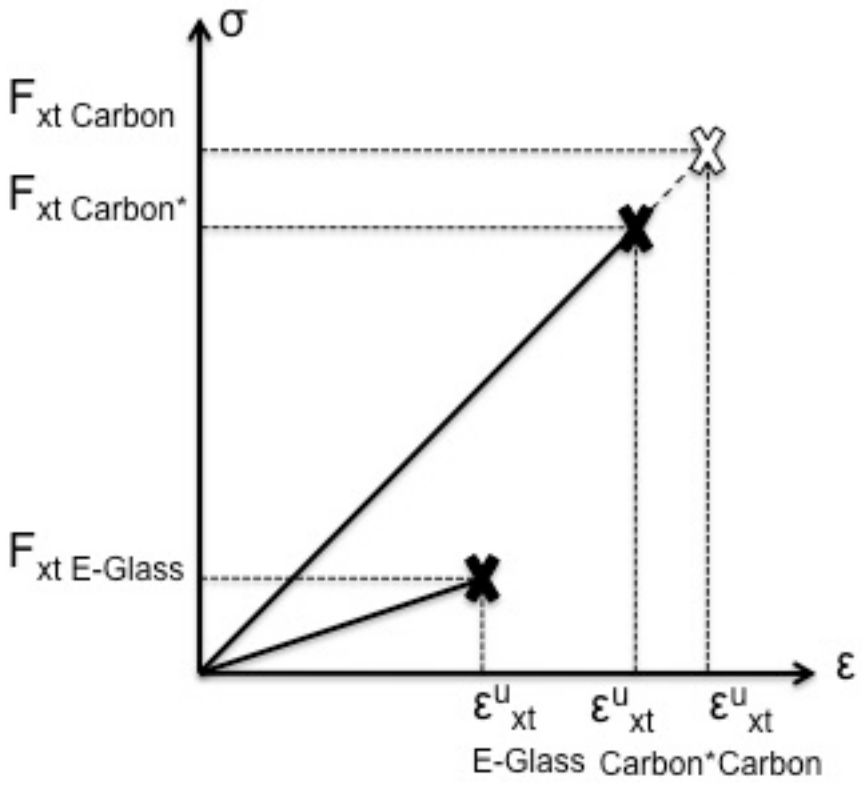


Figure 3.6 Composite Stress Strain Relationship Brittle Response

Figure 3.7 shows of the general stress strain diagram for the yielding response. The solid X shows were carbon layer would fail prematurely, while the outlined X shows the full strength of the carbon layer as seen in the hybrid coupons. The horizontal line represents the E-glass yielding and the residual strength is modeled as a plateau where the yield strength is equal to the ultimate strength of a E-glass only sample and contributes to the strength of the hybrid coupons.

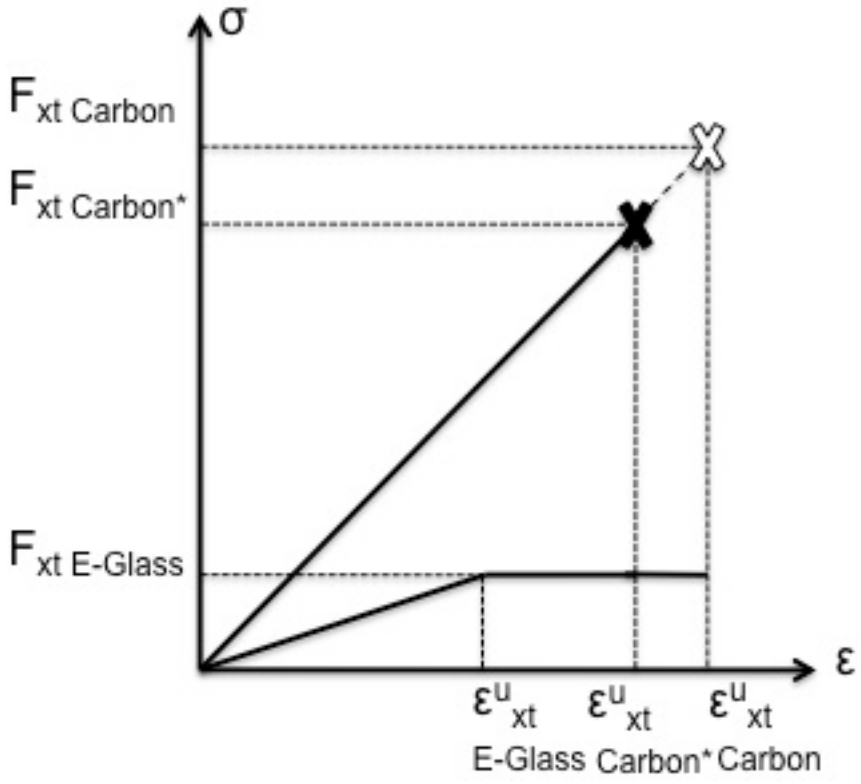


Figure 3.7 Composite Stress Strain Relationship Yielding Response

The ultimate tensile strength of the hybrid coupons can be shown using the efficiency factor with either the brittle response or the yielding response. Equation 3-3 shows the predicted value for a hybrid composite based on the brittle response, while Equation 3-4 shows the predicted value for a hybrid composite based on the yielding response, where $F_{xt}^{C}$ is the full strength of the carbon layer as given in Equation 3-1 in units of GPa, $t$ is the total thickness of the hybrid composite, and $tc$ and $tg$ are the thickness of carbon and E-glass layers respectively.

$$F_{xt}^{HB} = F_{xt}^{C} \cdot \frac{t_C}{t} \qquad \text{Equation 3-3}$$

$$F_{xt}^{HB} = F_{xt}^{C} \cdot \frac{t_C}{t} + F_{xt}^{G} \cdot \frac{t_G}{t}$$ Equation 3-4

Since the brittle response is more conservative it was recommended that that response be used for future predictions. When applying experimental values to the damage model with a brittle response a hybrid strength of 1.13 kN/mm is predicted which is about 5% less than the experimental mean value for the strength of the hybrid coupons.

Overall, from the layup development testing, it was decided to create future tensile strength notched samples using the combined carbon and glass layup for environmental durability testing. The samples produced a higher mean ultimate tensile strength and lower coefficient of variation and consistently exhibited the intended failure mode of fiber rupture in the gage section. The samples composed of carbon and glass are also more representative of the layup used in the arches and therefore will create exposure conditions to different environments to be more accurate.

### 3.4.3. Notched Coupon Tabbing

During the original notched coupon optimization done by Bannon, a batch of coupons was tested with tabs bonded to the grip area. The tabs consisted of 50.8 mm (2 in) by 50.8 mm (2 in) squares cut from an infused braided carbon sheet. It was found that the use of tabs effectively distributed the stresses over all the active tows and practically eliminated the undesirable failure modes (Bannon 2009).

Due to the benefits of using tabs, they were implemented in the asymmetric coupons with several adjustments. Instead of using tabs cut from an infused layer of braided carbon, tabs were made from a fine mesh of 0/90 degree glass to minimize any additional effects of using of a composite material. Tabs were bonded to each end of the coupon on both sides. The carbon side of the coupon had an additional tab bonded to each end for the purpose of aligning the carbon fibers in the center of the grips.

## 3.5 Asymmetric Notched Coupon Development: Traxial Braid

Following the asymmetric layup selection a variability study was preformed on the notched samples. The notched samples did not exhibit the high coefficient of variation seen in the longitudinal rectangular samples, however there is the change for variation between infusions. For the notched variability testing the quality control measures of specifying a braid angle tolerance were implemented.

The notched samples were cut from the same sheets of material infused for the variability study on the rectangular samples. Six sheets were manufactured from three different infusions (each infusion produced two sheets from either side of the spacer in the mold). All infusions used the same resin cure packages, materials, lay ups and manufacturing methods. All six sheets had notched samples cut from them and evaluated using the predetermined quality control measures. From the coupons that were deemed acceptable, four notched coupons were randomly selected from each of the three infusion sets for a total of twelve notched coupons. By selecting samples from several infusion sets, the variability between infusions could be observed. The results for each batch and the combined results

are shown in Table 3.2. All of the batches showed acceptable coefficients of variation that were consistent when compared to the coefficient of variation of the combined batches.

Table 3.2 Asymmetric Variability Tensile Strength Test Results

| Batch | Mean (kN/mm) | STD (kN/mm) | COV (%) |
|---|---|---|---|
| 1 | 1.25 | 0.07 | 5.7 |
| 2 | 1.04 | 0.10 | 10.1 |
| 3 | 1.16 | 0.09 | 8.1 |
| All | 1.15 | 0.12 | 10.8 |

The results of the variability study, also shown in Table 3.3, were very similar to that of the initial set of asymmetric coupons. The mean strength was slightly lower that the initial asymmetric coupons, as was the coefficient of variation. The results were so close that the difference is considered statistically insignificant when compared statistically with a T-test with a 95% confidence level. This comparison and the coefficient of variation of 10.8% show that there isn't a considerable batch to batch variation for the notched coupons as seen in the rectangular longitudinal coupons.

Table 3.3 Comparison of Asymmetric Notched Tensile Test Results

| Ultimate Tensile Strength | | | |
|---|---|---|---|
| Sample Set | Mean (kN/mm) | STD (kN/mm) | COV (%) |
| Initial Asymmetric Testing | 1.19 | 0.14 | 11.8 |
| Variability Study | 1.15 | 0.12 | 10.8 |
| Triaxial Braid | 1.30 | 0.13 | 9.77 |

The results from both the initial asymmetric testing and the variability study were deemed acceptable with appropriate failure modes observed and a coefficient of variation less than 12%. However, since the rectangular samples saw a significant improvement in the data through the use of a triaxial braid, a set of notch samples created with a triaxial braid were also tested. The triaxial notched samples were cut from the same sheets as the rectangular samples. The results from the triaxial set of coupons are also listed in Table 3.3. The mean strength of the notched coupons went up 13% and the coefficient of variation lowered 10%.

## 3.6 Conclusions and Recommendations for Future Work

The asymmetric notched coupon with a triaxial carbon fiber braid was used for all future testing. Coupons for ultimate tensile strength in the longitudinal direction had an asymmetric layup of one layer of a triaxial carbon fiber braid measured at ± 20 degrees with hot melt plastic strands at 0 degrees and one layer of an E-glass braid at ± 81 degrees and elastic strands in the 0 degree direction. Again, the E-glass braid used in future testing was not the triaxial hot melt braid since the E-glass braid with elastic axial strands also produced an acceptable coefficient of variation in previous tests and there was more initial material on hand. The asymmetric coupons were also tabbed with a 0/90 degree E-glass tapered tab with two tabs bonded on the carbon side, and one on the E-glass side of the coupon to align the carbon layer with the center of applied load during testing.

The strength prediction model implemented by Bannon worked well for coupons made of a single layer of braided carbon. However the model did not do a good job predicting the strength of the asymmetric carbon and E-glass coupons. The model significantly under predicts the ultimate tensile strength of the coupons. This may be due to the fact that the simplified model does not capture the complex fiber architecture and the hybrid effects of the distribution of load near failure.

The strength of a hybrid coupon can be determined from the individual experimental failure strengths of the carbon and E-glass plies. A strength correction factor is also implemented to account for the increase of tensile strength seen in hybrid coupons due to the E-glass layer distributing the load over the entire gage section.

Future recommendations for the notched tensile strength coupons include the development of a finite element model to predict the ultimate strength and additional experimental testing with strain measurements. By measuring the strain during loading the notched coupons, more knowledge can be gained about load distribution, potential stress concentrations, and how failure is initiated. A model to predict tensile strength using a finite element analysis would be able to better capture the complex fiber architecture and the load distribution to provide a more accurate tensile strength prediction. A finite element model would also allow for strength predictions determined from fiber and matrix properties as opposed to experimental testing of the hybrid components.

# Chapter 4. IMPLEMENTATION OF DURABILITY TEST PROTOCOL TO BRAIDED COMPOSITES

## 4.1 Introduction

FRP composites are used in many fields including corrosion equipment, automotive, marine, and aerospace (Karbhari 2005). All of these applications require the FRP material used to withstand different environmental conditions. Typical building materials can have a limited service lifespan when used in harsh environments, which can result in material degradation including concrete cracking and spalling, steel corrosion and marine borer attack on timber. FRP composites could offer advantages such as improved durability and cost savings in terms of life cycle analysis (Pando et al. 2002). Carbon fiber is well known for its excellent durability in different environmental conditions; in a study performed by Steckel it was found that any limitations in a carbon/epoxy composite were due to the epoxy matrix (Steckel et al. 1999).

Accelerated testing is useful in determining the effects that different environmental conditions have on certain materials. It is important to note that accelerated exposure data and real time performance are unlikely to follow a simple linear relationship, and that the relationships have yet to be confidently determined (Waldron et al. 2001). Accelerated testing is most useful when a comparison between materials, previous testing standards or environmental conditions can be made, where the latter was explored in this study. It has been proposed that

"appropriately designed and fabricated FRP systems can provide longer lifetimes and lower maintenance than equivalent structures fabricated from conventional materials" (Karbhari 2005).

The durability of a material or structure has been defined as "its ability to resist cracking, oxidation, chemical degradation, delamination, wear, and/or the effects of foreign object damage for a specified period of time, under the appropriate load conditions, under specified environmental conditions" (Karbhari et al. 2003). The objective of this section is to determine how durable the composite material used in the rigidified composite arches is under various environmental conditions that a typical bridge may experience. While the material was exposed to various environmental conditions the coupons were only loaded in tension after being exposed. This test does not cover all appropriate load conditions; other conditions that could be explored include fatigue loading or testing the material while being exposed to a particular environmental condition.

It is important to note that the experimental work done to determine the durability of the composite is for the FRP material only and the relationship between the FRP composite and the confined concrete in the arches is not investigated in this study. Previous studies on FRP wrapped cylinders have shown that different environmental conditioning does effect the composite action of FRP and concrete.

The environmental aging of E-glass fiber composites and concrete was studied by Kshirsagar et al (2000). It was found that in the stress-strain response of the FRP-concrete cylinders, there is coupling between the residual hygrothermal

strains in the FRP material, which lead to a reduction in confinement, and the environmental damage in the E-glass fibers, which leads to a reduction in tensile strength of the FRP material.

In addition there are several bridges in the U.S. have had columns wrapped in FRP material and are being monitored to observe their durability. A study done by Teng et al. (2003) included up to two years of field monitoring of a bridge in Indiana with glass FRP wrapped columns and laboratory durability testing. Overall all it was found that the glass FRP provided "excellent protection against aggressive environmental conditions" (Teng et al. 2003). Another study by Pantelides et al. (2006) discusses the durability monitoring of a bridge in Utah that had been retrofitted with carbon FRP for seismic protection. The report states that the carbon FRP retrofit prolonged the useful life of the bridge for the six years it was monitored and was "expected to continue protecting the bridge from the environment for the foreseeable future" (Pantelides et al. 2006). It was also noted that one environmental condition that was found to affect the composite used on the bridge the most was UV radiation.

## 4.2 Previous Environmental Testing on Arch Material

A study was done by researchers at the Advanced Structures and Composites Center (Goslin et al. 2009) to determine whether dry and wet thermal cycling of concrete filled FRP tubes affects the shear strength at the interface of the concrete and FRP shell. Eight different conditions were evaluated including the control where the specimen was cured, conditioned, and tested in ambient indoor conditions. The other specimens were conditioned in wet or dry environments, held

at a constant hot (71° C), ambient (23° C), or cold (-17° C) temperatures, or cycled between -17° C and 25° C. Specimens were also tested at elevated temperatures and frozen conditions as well as room temperatures. Structural testing and visual inspection were used to evaluate the effect of environmental conditioning of samples. To determine the shear strength of the bond, shear transfer tests were performed by pushing the concrete core through a section of FRP shell. The shear strength was calculated as the maximum load before slippage at the bond over the shear area of the specimen.

Overall it was found that there was no evidence of degradation of shear strength in the bond between the concrete core and outer FRP shell due to thermal cycling. The test results showed that mean value seen for each condition fell within one standard deviation from the mean value of the control samples, which had a coefficient of variation of approximately 14%. The results from the shear tests are summarized in Table 4.1

Table 4.1 Summary of Results from Push though Testing (Goslin et al. 2009)

| **Condition** | **Test Condition** | **# Tested** | **Mean Peak Load (kN)** | **Mean Shear Strength (MPa)** | **COV %** | **% Diff.** |
|---|---|---|---|---|---|---|
| Control | Room Temp | 3 | 88.7 | 1.51 | 14.1 | 0.00 |
| Hot Dry | Hot | 3 | 84.1 | 1.39 | 12.0 | 8.63 |
| Frozen Dry | Room Temp | 3 | 87.9 | 1.46 | 12.6 | 3.42 |
| Cycled Wet | Room Temp | 5 | 86.4 | 1.48 | 4.49 | 2.03 |
| Cycled Dry | Room Temp | 5 | 89.1 | 1.50 | 7.92 | 0.67 |
| Frozen Wet | Room Temp | 3 | 94.7 | 1.57 | 10.9 | -3.82 |
| Dry Cycled Cold | Frozen | 3 | 92.3 | 1.58 | 4.97 | -4.43 |
| Frozen Dry | Frozen | 3 | 101.8 | 1.65 | 17.4 | -8.48 |

## 4.3 Environmental Conditions

The FRP composite arches are exposed to numerous environmental conditions, which they must withstand as the external reinforcement for the bridge substructure. While FRP is believed to be more durable than other conventional building materials, actual data on durability is sparse, not well documented, and not easily accessible to the civil engineer (Karbhari 2005). Typical environmental conditions include exposure to water, saltwater, alkalis, heat, fuel, ultraviolet light, freeze thaw cycles, and abrasion.

Various studies have been performed on the durability of FRP after exposure to the previously listed environmental conditions, however there are currently no specific standards for the durability of FRP, therefore the current research may not be comparable due to different test methods and exposure times. To quantify the durability of the FRP composite arches, a referenced environmental durability test matrix was followed. The environmental durability test matrix was developed through collaboration between the California Department of Transportation (Caltrans) and the Aerospace Corporation (Karbhari 2005). This test matrix is referenced in an AASHTO draft for durability requirements of composite materials used as external reinforcement in bridge structures (AASHTO 2009). The test matrix is given in Table 4.2 and describes the test conditions and duration of exposure.

Table 4.2 Environmental Durability Test Matrix (Karbhari 2005)

| Environment | Test Condition | Duration |
|---|---|---|
| Water resistance | 100% humidity at 38°C | 1000, 3000, and 10000 hours |
| Salt water resistance | Immersion at 23 °C | 1000, 3000, and 10000 hours |
| Alkali resistance | Immersion in $CaCO_3$ at pH 9.5 and 23 °C | 1000, 3000, and 10000 hours |
| Dry heat resistance | Furnace at 60°C | 1000 and 3000 hours |
| Fuel resistance | Immersion at 23°C | 4 hours |
| UV resistance | Cycle between UV at 60°C and condensate at 38°C | 4 hours per condition with 100 cycles |
| Freeze/Thaw resistance | Cycle between 100% humidity at 38°C and freezer at -18°C | 12 hr per condition for 20 cycles |

The test conditions listed in the test matrix had been previously implemented by Steckel on various combinations of E-glass or carbon and different types of matrices (none of the combinations had composites made of both E-glass and carbon fiber). The results from that round of testing found that for most systems and environments the reduction was "less than 20% after 417 day exposures" (Steckel et al. 1999). In addition it was found that there was "no significant reduction in Young's modulus [and] no reductions in Young's modulus exceeding 5% were measured."

The purpose of this study is to determine the environmental effects on the tensile properties of the FRP composite arches. Coupons representative of the composite arch were exposed to each condition and tested to measure any degradation in tensile strength or elastic modulus. The duration of exposure for water, saltwater, alkali and dry heat resistance were modified due to time

constraints. The water exposure duration was modified to 500, 750, 1000 hours, while saltwater, alkali and dry heat resistance exposure durations were modified to 500, 1000, and 2000 hours.

In conjunction with the environmental durability test matrix the acceptance criteria, AC125 (ICC Evaluation Service 2007), was implemented as a reference for acceptable material properties after exposure. AC125 states a criterion of samples retaining at least 90% of the tensile properties after 1000 hours and at least 85% retention after 3000 hours of exposure. This criterion was directly applicable to the samples exposed to water, saltwater, alkali solution and heat since the test matrix calls for exposure duration of 1000 and 3000 hours. For the environmental conditions with shorter exposure times, exposure to ultraviolet light, freeze thaw cycles, and fuel, the acceptance criteria for after 1000 hours of exposure was used for comparison purposes.

### 4.3.1. Test Protocol for Durability Testing

After being conditioned, coupons were cut from sheets at least 25 mm from all edges and 6mm from another coupon. Coupons were cut using a water jet abrasive cutting machine and labeled so that they could be matched back to the location they were cut from. Each set of durability testing consisted of 36 coupons, 12 longitudinal rectangular samples, 12 transverse rectangular samples and 12 notched samples. Each coupon was then tabbed, which is described in sections 2.5.3 and 3.4.3. Samples were then tested in tension following ASTM D 3039 as described in 2.5.2. Each set of samples was tested within 4 days of removal from conditioning unless otherwise specified.

### 4.3.2. Sample Manufacturing

For all of the durability testing coupons were cut from flat panels. The carbon used was AIT2011, the same as used in the triaxial braid testing. The E-glass used was UM6447, product details can be found in Table 2.1 through Table 2.3. A new resin, DERAKANE 610C, was used and is similar to the DERAKANE 8084, resin properties can be found in Table 2.4. This new resin was selected because it was more likely to be used in future arches.

Kenway Corporation infused all of the sheets for durability testing over a period of 6 days. The braided carbon was delivered as a roll of a 340mm wide flat braid with stitched edges (as opposed to a braided tube). Since the carbon was not a braided tube, spacers were not needed to separate the carbon into two sheets; this allowed for an easier set up for infusion and less fabric for the resin to wet out in one infusion.

The E-glass used was a braided tube due to the on hand availability of it. In order to use the E-glass tube with the single layer of braided carbon the E-glass braided tube needed to be cut open, and in half, to efficiently use all of the material. One potential problem with cutting open the E-glass braided tube is the risk of the braid unraveling or changing the braid angle. To prevent the braided material from shifting during cutting the tube was laid flat and a 50mm strip of resin was painted along the long edges as seen in Figure 4.1. This was done as an open molding process and the resin was allowed to cure before flipping the E-glass tube over and repeating the process on the other side. After both sides had cured the E-glass was cut with a grinder in the middle of the infused strips. The diameter of the E-glass

tube when laid flat was approximately 432mm wide, compared to the carbon which was about 340mm wide, so trimming the edges did not effect the useable area of the final infused sheet. When cutting was completed the end product was two flat sheets of braided E-glass with infused edges to keep the braid from shifting. The carbon and E-glass un-infused sheets can be seen in Figure 4.2.

Figure 4.1 E-glass Edge Infusion

Figure 4.2 Carbon and E-glass Sheets for Durability Testing

The durability sheets were infused in 2.4 m lengths on a heated table that was warmed to 40°C to assist with the curing process. The first sheet was 4.9 meters long which is shown in the figures, but all following sheets were 2.4 m. Flow media were laid on the table surface, followed by release film to keep the flow media from infusing to the panel. On top of the release film was the E-glass braided sheet then the carbon braided sheet which was aligned with the center of the E-glass sheet. A resin line was run along the length of the part on one side and a vacuum line was run along the length of the other side of the part. The entire part was then

covered with a plastic film and sealed along the edges using tacky tape, the part can be seen in Figure 4.3. The infusion time took approximately 30 min from initiating the resin until the resin gelled.

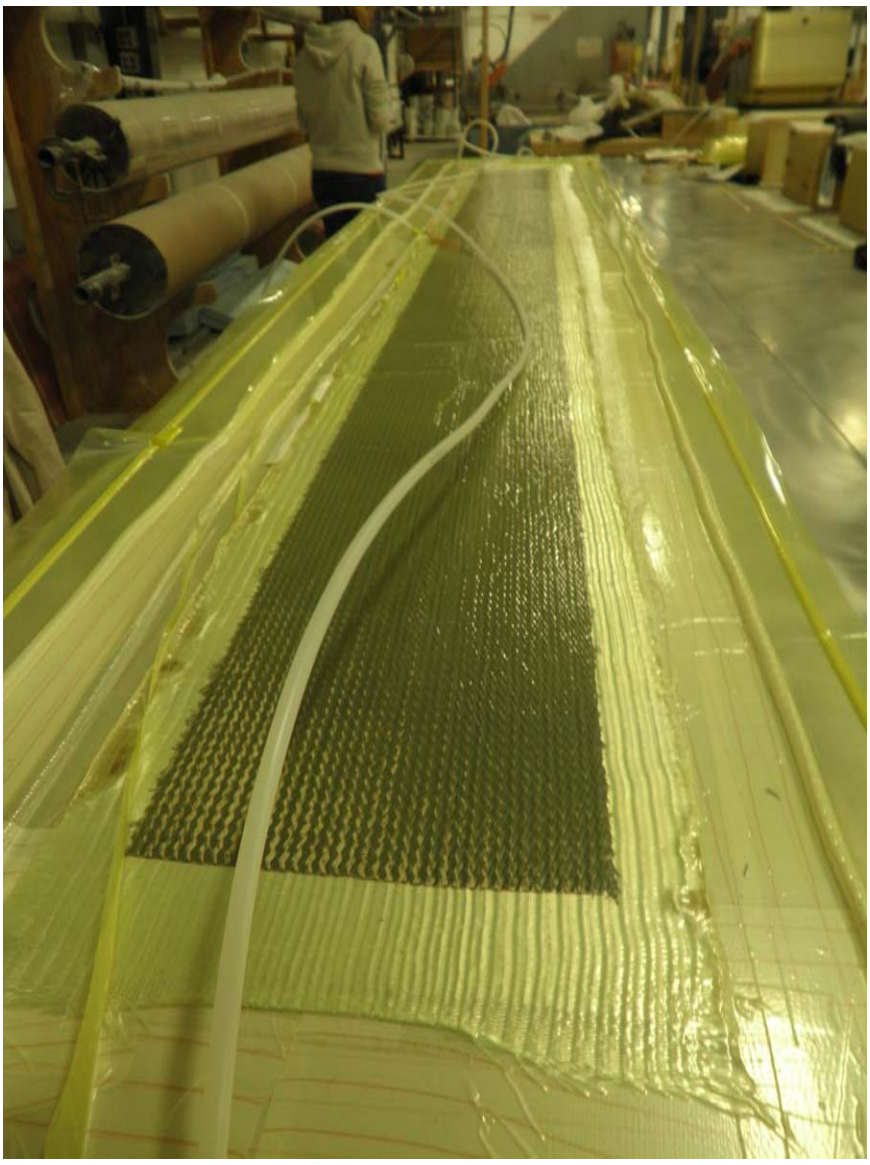

Figure 4.3. Infusion Layup for Durability Sheets

A total of 36 m of braided material was infused as 2.4 m sections (except for the first 4.9 m which was cut in half for transporting) resulting in 15 infused sheets. The table used for infusions was large enough to infuse up to 6 sheets at a time, and

all of the sheets were infused after 4 separate infusions. The cure package used for each infusion was the same and consisted of DERAKANE 610C, cobalt naphthanate, 24P, and methyl ethyl ketone peroxide (MEKP) as the catalyst. The sheets were not post cured since the arches used in the field are not post cured. It should be noted that the ambient cure process may leave the sheet more susceptible to moisture induced degradation since resins cured under ambient conditions typically do not fully cure (Rivera and Karbhari 2001). Rivera also comments that the incomplete conversion of resin can lead to changes in resin properties over time, as the resin may additionally cure slowly over time, and "induce lower heat stability, lower resistance to hydrolysis and a greater degree of susceptibility of swelling in solvents." After all sheets were infused they were stored at Kenway Corporation for about at week before being transported to the AEWC Advanced Structures and Composites Center where they were stored in a climate controlled room at ambient temperature of 23°C and 25% relative humidity.

To prepare sheets to be conditioned they were labeled and cut into smaller sheets that would fit their respective conditioning chambers. All sheets were trimmed of excess E-glass on the wet saw, resulting in a 340mm width while the lengths of the sheet varied from 230mm to 540mm. The edges of all the samples were sealed with resin to prevent moisture from being absorbed through the exposed edges. Sheets were dipped into a trough of DERAKANE 8084 resin with a typical cure package of cobalt, DMA, and trigonox, and placed on a drying rack to cure. Figure 4.4 shows the process of edge sealing and an example of the final product used for conditioning. Finally, samples that were not immediately put into

conditioning chambers were stored in a cabinet in a temperature and humidity controlled room to keep the samples at an ambient atmosphere of about 23°C and 25% relative humidity.

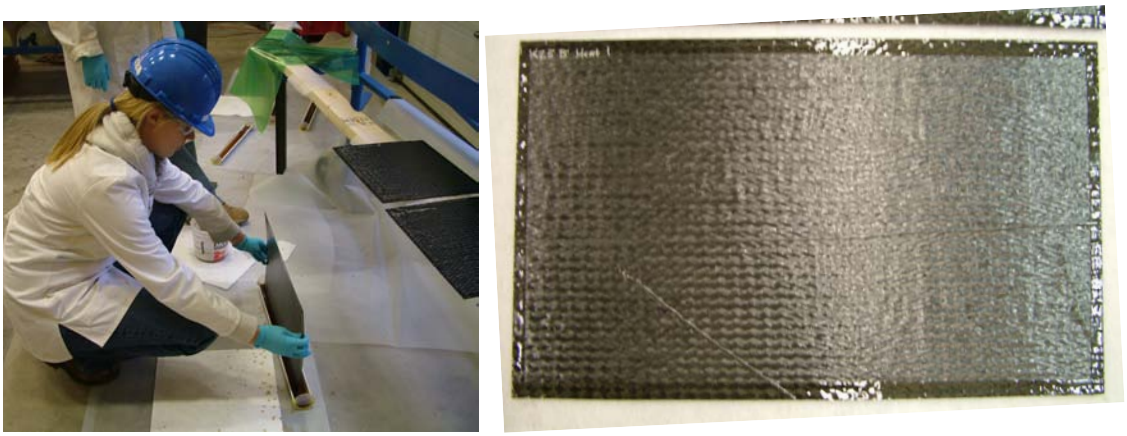

Figure 4.4 Edge Sealing and Sheet with Edges Sealed

### 4.3.3. Control Samples

From the set of sheets manufactured for durability testing, 3 groups of control samples were set aside to be tested at certain times during the full course of durability testing. The first set of control samples were tested approximately 3 weeks after infusion, a week and a half before the first 500 hour conditioned samples were tested. The next set of control samples were tested after the 1000 hour samples had been tested, and the third set of control samples were tested at the end of the durability testing approximately 3 and a half months since they had been infused. The notched coupons in the third set of control samples did not all show appropriate failure modes, and those that did had a lower mean strength than

the first two sets of control samples. Due to the failure modes and low mean strength of the notched samples, two additional batches of notched samples were tested to further investigate the drop in strength.

For the control samples and all conditioned samples, the ultimate tensile strength, longitudinal elastic modulus and transverse elastic modulus were recorded to compare between conditions and against AC 125. Poisson's ratio, ultimate tensile strength in the transverse direction and ultimate shear stress was recorded for comparison purposes.

The transverse rectangular samples exhibit an E-glass fiber rupture failure since the E-glass fibers are close to 90 degrees. Figure 4.5 shows a close up of the E-glass side of a coupon after failure. The ultimate tensile strength in the transverse direction, $F_{yt}$, was recorded as the maximum load capacity of the transverse samples divided by the mean sample width.

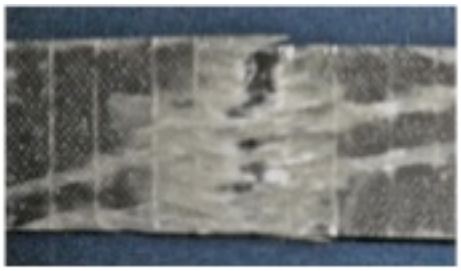

Figure 4.5 E-Glass Fiber Rupture Failure

The longitudinal rectangular samples exhibit a shear failure, which is shown in Figure 4.6. The ultimate strength in the longitudinal direction due to shear failure, $F_{xt\_R}$, was recorded as the maximum load capacity of the longitudinal rectangular samples divided by the mean sample width. Table 4.3 shows a comparison between the longitudinal tensile strength recorded from the notched coupons, $F_{xt}$, to the

longitudinal strength recorded from the rectangular samples, the coefficient of variation is reported as a percentage next to the mean value in parenthesis. As shown in the table, the strength measured from the longitudinal rectangular samples under predicts the full tensile strength developed by the notched samples.

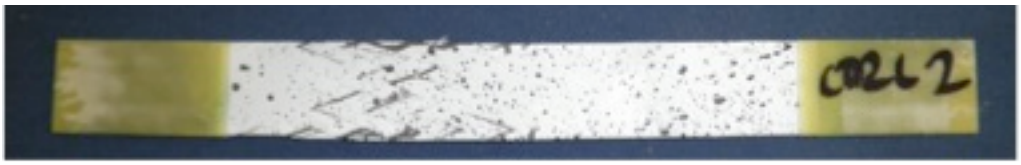

Figure 4.6 Longitudinal Shear Failure

Table 4.3 Longitudinal Strength Comparison

| **Control Batch #** | **$F_{xt}$ kN/mm** | **$F_{xt\_R}$ kN/mm** |
|---|---|---|
| 1 | 1.44 (8) | 0.52 (4) |
| 2 | 1.50 (7) | 0.44 (9) |
| 3 | 1.25 (8) | 0.44 (4) |

Since the longitudinal rectangular samples fail due to shear along the edge of the carbon fiber tows at an angle of ±20°, the ultimate shear stress along that plane can be calculated through a transformation of stresses. The applied stress, $\sigma_x$, was the maximum load per unit width experienced by the rectangular longitudinal samples. This stress was then transformed using Equation 4-1, the transformation matrix, *T,* shown in Equation 2-15 and a braid angle, $\theta$, of 20°.

$$\begin{bmatrix} \sigma_1 \\ \sigma_2 \\ \tau_6 \end{bmatrix} = T \cdot \begin{bmatrix} \sigma_x \\ 0 \\ 0 \end{bmatrix} \qquad \text{Equation 4-1}$$

The resulting transformed stresses for the three sets of control samples can be seen in Table 4.4. The shear stress, $\tau_{20}$, for all samples was then reported as the absolute value of the transformed shear stress, $\tau_6$.

Table 4.4 Transformed Stresses

| Control Batch # | $\sigma_1$ kN/mm | $\sigma_2$ kN/mm | $\tau_6$ kN/mm |
|---|---|---|---|
| 1 | 0.46 | 0.06 | -0.17 |
| 2 | 0.39 | 0.05 | -0.14 |
| 3 | 0.39 | 0.05 | -0.14 |

Overall the control samples did not show any obvious trend in the change of material properties over time. The results from the 3 full sets of control samples can be seen in Table 4.5, the coefficient of variation is reported as a percentage next to the mean value in parenthesis.

Table 4.5 Control Test Results

| Control Batch # | $E_x$ kN/mm | $E_y$ kN/mm | $\nu_{xy}$ | $F_{xt}$ kN/mm | $F_{yt}$ kN/mm | $\tau_{20}$ kN/mm |
|---|---|---|---|---|---|---|
| 1 | 69.9 (7) | 38.8 (11) | 1.16 (9) | 1.44 (8) | 0.57 (10) | 0.17 (4) |
| 2 | 66.2 (4) | 40.7 (5) | 1.21 (7) | 1.50 (7) | 0.56 (13) | 0.14 (9) |
| 3 | 67.2(5) | 40.9 (4) | 1.20 (3) | 1.25 (8) | 0.54 (9) | 0.14 (4) |

Most of the material properties did not vary much from batch to batch, the exception being the experimental results for tensile strength, $F_{1t}$, which did vary quite a bit. Table 4.6 shows the results of testing five batches of control coupons for tensile strength. Batches 4 and 5 were tested because batch 3 seemed to result in a low mean strength and several coupons did not have the appropriate failure mode (those coupons that did not have the appropriate failure mode were not included in

the mean strength). Batch 4 also had a low mean strength similar to that of batch 3, however more samples failed due to fiber rupture and the batch overall had a low coefficient of variation. Batch 5 also had a low coefficient of variation and a mean strength higher than batch 3 and 4, but lower than batch 1 and 2. The variations in tensile strength could be due to variability in manufacturing.

Table 4.6 Control Test Results for Tensile Strength

| **Control Batch #** | **1** | **2** | **3** | **4** | **5** |
|---|---|---|---|---|---|
| Mean (kN/mm) | 1.44 | 1.50 | 1.25 | 1.27 | 1.37 |
| STD (kN/mm) | 0.11 | 0.11 | 0.10 | 0.07 | 0.08 |
| COV % | 7.60 | 7.29 | 8.40 | 5.88 | 5.74 |

#### 4.3.3.1 Statistical Analysis

To determine if two batches of samples were comparable a t-test was performed to determine if the data was statistically different. The general equation for calculating the t value of two sets of data is show in Equation 4-2, where $X$ is the mean of the data set, *var* is the variance of the data set and $n$ is the number of samples in the data set; subscripts *1* and *2* denote the which set of data.

$$t = \frac{\overline{X_1} - \overline{X_2}}{\sqrt{\frac{\mathrm{var}_1}{n_1} + \frac{\mathrm{var}_2}{n_2}}}$$ Equation 4-2

After a t value is determined it can be compared with the given $t_{\alpha,\nu}$ value based on a t distribution. The $\nu$ value is the degrees of freedom, which is the sum of the number of samples for each set minus two. The alpha level, $\alpha$, was selected as 0.05, which means that 90% of the time the data will be statistically different if the calculated t value is greater than the t value listed in the table.

The results of the t-test for the control samples tested at different time periods showed that some of the results were statistically the same. Since the data appeared similar a further statistical study was preformed to determine if all of the control batches could be pooled into one set. An analysis following "Chapter 8: Statistical Methods" in the Composite Materials Handbook (CMH) (Department of Defense 2002) was implemented to determine if the data could be pooled.

The Composite Materials Handbook states that "in many ways, it is easier to analyze data which are unstructured," meaning that the data from several batches is able to be pooled, and that "it is often desirable to be able to show that a natural grouping of data has no significant effect" (Department of Defense 2002). The k-sample Anderson-Darling test can be used to show if the subpopulations of a condition are compatible. In general for composite materials, the Composite Materials Handbook recommends that different batches of samples be treated as natural groupings and tested for compatibility. The k-sample Anderson-Darling test is a nonparametric statistical procedure, where the purpose of the test is to determine if the populations from two or more groups of data are identical (Department of Defense 2002).

The k-sample Anderson-Darling statistic is shown in Equation 4-3. The data is denoted by $x_{ij}$ for i=1, …, k and j=1, …, $n_i$, where I is the group and j is the observation with in that group. The total number of observations is n and the distinct values in the combined data set from smallest to larges is denoted as $z_{(1)}$, $z_{(2)}$, …, $z_{(L)}$, where L can be less than n if there are tied observations.

$$ADK = \frac{n-1}{n^2(k-1)} \cdot \sum_{i=1}^{k}\left[\frac{1}{n_i}\sum_{j=1}^{L} h_j \frac{\left(nF_{ij} - n_i H_i\right)^2}{H_j\left(n - H_j\right) - nh_j/4}\right] \qquad \text{Equation 4-3}$$

In the equation above, $h_j$ is the number of values in the combined samples equal to $z_{(j)}$; $H_j$ is the number of values in the combined samples less than $z_{(j)}$ plus one half the number of values in the combined samples equal to $z_{(j)}$; and $F_{ij}$ is the number of values in the ith group which are less than $z_{(j)}$ plus one half the number of values in this group which are equal to $z_{(j)}$.

The calculated *ADK* value is then compared to the critical value, *ADC*, which can be calculated using Equation 4-4. The Composite Materials Handbook specifics that the critical value determined by Equation 4-4 should be based on an alpha value of .025, meaning there is a 2.5 percent risk of being in error. With an alpha value of 0.025 the corresponding interpolation coefficients, $b_0$, $b_1$, $b_2$, would be 1.960, 1.149, and -.391 respectively. More detail on the k-sample Anderson-Darling statistic, including interpolation coefficients for different alpha levels, can be found in the paper "K-Sample Anderson-Darling Tests of Fit, for Continuous and Discrete Cases" (Scholz and Stephens 1986).

$$ADC = 1 + \sigma_n \left( b_0 + \frac{b_1}{\sqrt{k-1}} - \frac{b_2}{k-1} \right)$$ Equation 4-4

In addition to pooling several batches of data, the Composite Materials Handbook also describes how a B-Basis allowable value can be determined. A B-Basis allowable value indicates that at least 90% of the population of material values is expected to equal or exceed the B-Basis value with 95% confidence. The Composite Material Handbook (2002) includes a flow chart that outlines how to pool multiple batches of data following the k-sample Anderson-Darling test and to calculate the B-Basis value for that data set.

The criteria for pooling data and calculating a B-Basis value is that there must be at least 3 batches of samples and at least 18 samples between all of the batches, all of which have consistent and appropriate failure modes. B-Basis values can be calculated for data that do not meet the sample size criteria, however the results are not acceptable to be included in the Composite Material Handbook database and should just be used as a reference.

All batches should then be reviewed to determine if there are any outliers that can be removed from the data. Data can then be tested for between batch variability using the k-sample Anderson Darling test. If the data cannot be pooled a B-Basis value can still be calculated if there are 5 or more batches using the analysis of variation (ANOVA) method. If the data can be pooled, an observed significance

level (OSL) is calculated to determine which distribution, normal, lognormal, or Weibull, the data fits best. The B-Basis value is then calculated from the best fit distribution.

A statistical analysis was performed on the control samples to determine if the data could be pooled and what the mean and B-Basis value was for each material property (excluding Poisson's ratio). Table 4.7 shows the mean, B-Basis value, best-fit distribution and if the data can be pooled for each material property. Both the mean and B-Basis values will be used as base values for comparison of material properties after environmental exposure.

Table 4.7 Statistical Analysis of Control Samples

| | $E_x$ (kN/mm) | $E_y$ (kN/mm) | $F_{xt}$ (kN/mm) | $F_{yt}$ (kN/mm) | $\tau_{20}$ (kN/mm) |
|---|---|---|---|---|---|
| Can be Pooled? | Yes | Yes | No | Yes | No |
| Mean | 67.7 | 40.2 | 1.38 | 0.56 | 0.15 |
| B-Basis | 61.6 | 35.1 | 1.01 | 0.45 | 0.06 |
| Distribution | Lognormal | Normal | ANOVA | Normal | ANOVA |

The longitudinal tensile strength and ultimate shear stress B-Basis values are calculated using the ANOVA method since the data cannot be pooled, however the Composite Material Handbook does not recommend using the ANOVA method when there are less than five batches of data. As a result of testing only three batches the B-Basis value for the shear strength is only 40% of the mean.

#### 4.3.3.2 Poisson's Ratio

Throughout the previous testing it was observed that the measured Poisson's ratio was not close to the predicted value. During the asymmetric layup testing it was observed that the Poisson's ratio of the carbon and E-glass samples was very close to the predicted value of a carbon only sample. It was then hypothesized that the value of Poisson's ratio was not the same through the thickness of the sample. Furthermore, the way Poisson's ratio was measured was only capturing the movement of the carbon layer. The predicted value for Poisson's ratio for the control samples was 0.32, while the predicted Poisson's ratio for only the layer of carbon of the control samples was 0.96. The measured Poisson's ratio from testing the control samples was 1.2. The experimental value is much closer to the predicted value for only one layer of carbon, which was also observed in the asymmetric lay up testing.

To verify the hypothesis that the measured Poisson's ratio was only representative of the carbon layer, additional samples were tested with Poisson's ratio measured from the E-glass side of the sample. An extra sheet from the control material was used to cut 10 longitudinal samples; the E-glass side was then painted with the high contrast speckle pattern for strain measurement. The results from the tested samples showed a measured Poisson's ratio of 0.28, with a coefficient of variation of 12%.

The tests confirmed that the value of Poisson's ratio varies throughout the thickness of the asymmetric coupons. The predicted value of an E-glass only sample was 0.13, which is closer to the experimental results of 0.28 than the measured

Possion's ratio of 1.2 from the carbon side. In general it seems that the measured Poisson's ratio is dependent and representative only of the surface fiber layer and is slightly under predicted by the model.

One possible explanation for the measured difference in Poisson's ratio could be due a slight cupping of the material under load. Cupping could be caused by the unequal stiffness in both the longitudinal and transverse direction. Figure 4.7 shows the displacement of two coupons in the Z direction. The top picture shows the displacement measured from the carbon side of a coupon, while the bottom picture shows the displacement measured from the E-glass side of a different coupon (since the DIC system was not able to measure strain or displacement from both sides of a single coupon during loading).

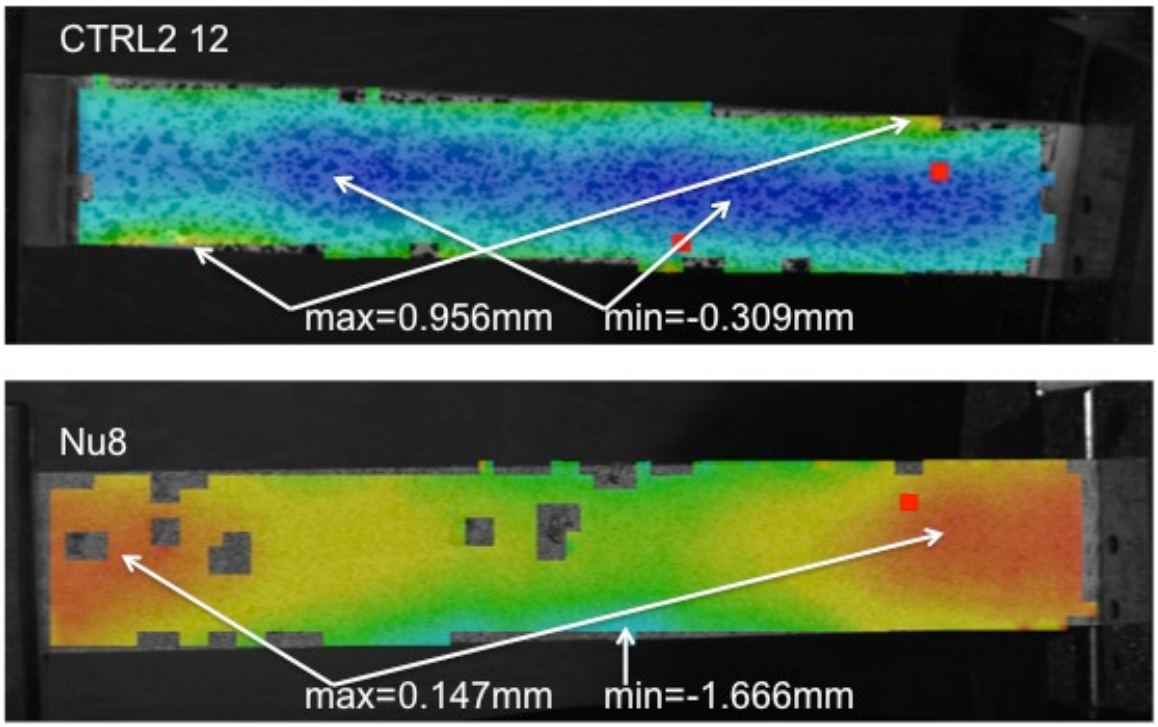


Figure 4.7 Coupon Displacement in Z Direction During Loading

The displacement seen on the carbon side (top) appears to cup away from the DIC system cameras, where the darker areas are a negative displacement; while the displacement seen on the E-glass side (bottom) appears to cup towards the DIC system cameras, where the darker areas have a positive displacement and the edges have a negative displacement. While some cupping is observed in the coupons, this may not completely explain the difference in Poisson's ratio and it should be studied further to determine what causes the difference and if it has any effect on the measured strength or stiffness of the coupons.

### 4.3.4. Water

Water and moisture exposure is one of the more typical environmental conditions experienced by composites, particularly those used outdoors. The arches used for bridges can be exposed to moisture in numerous ways such as from stream flow, rain, or humidity in the atmosphere. Overall it is expected that the majority of the arch material will be exposed to moisture many times throughout its lifespan so it is important to evaluate the composite's ability to resist water.

#### 4.3.4.1 Literature Review for Water Exposure

Moisture exposure can affect the integrity of a composite in multiple ways. Moisture has been observed to travel along the bond line between the matrix and fibers and can degrade the overall fiber-matrix bond. Moisture can also affect the matrix and fiber components individually. Glass fibers can be degraded by moisture

extracting ions from the fiber which alters its structure and properties (Karbhari et al. 2003). The chemical bonds in the matrix can also be degraded by moisture exposure, however an uncracked resin rich surface can help protect the fibers and maintain the tensile properties of the composite.

Moisture exposure can be done through immersion in water or through exposure to high humidity. Moisture exposure tests performed by Steckel were done using 100% humidity at a temperature of 38°C. Exposing the samples to humidity was chosen because that type of exposure is considered more severe than immersion at 23°C because the high humidity exposure allows for atmospheric reactions that would not occur in an immersion test (Steckel et al. 1999). The higher temperature can also lead to greater water absorption and chemical reactions rates. Steckel found that after testing various environmental conditions, the "most severe" degradation in tensile strength was experienced by a E-glass composite when exposed to 100% relative humidity at 38°C. Overall Steckel concluded that moisture absorption seen by the epoxy matrix was the "most important characteristic dictating composite environmental durability."

#### 4.3.4.2 Water Testing

Water testing was performed according to the test matrix through exposure to100% humidity at a temperature of 38°C. This exposure was done using a QUV weathering machine set for condensation at 38°C. Sheets were set into the window of the QUV weathering machine with the carbon side of the composite exposed to condensation; the sheets were positioned in this manner since it is expected that the

carbon side of the composite used in the arches is likely to have greater exposure to water than the E-glass side. Figure 4.8 shows the test set up with one sheet undergoing moisture exposure and a glass plate over the other exposure window.


Figure 4.8 QUV Weathering Machine

For three different exposure durations, 7.5 sheets were used, with 2.5 per duration. This number of sheets was used because 2.5 sheets was the smallest amount of material needed to produce 36 coupons (24 rectangular coupons and 12 notched coupons). The QUV weathering machine was only able to hold four sheets at a time so sheets were rotated in when others had finished their test duration.

When the sheets had finished their conditioning time they were removed from the QUV weathering machine, wiped down with a cloth and left to dry at room

temperature of 23°C. Upon visual inspection it was observed that the edges that had been sealed with resin had turned white in some places, this can be seen in Figure 4.9 where the picture on the right shows a close up of the color change. Other than the color change at the edges no other visual changes were observed. Since no coupons were cut less than an inch from the edge of the sheet, the effects observed around the edges of the sheet were not a concern.

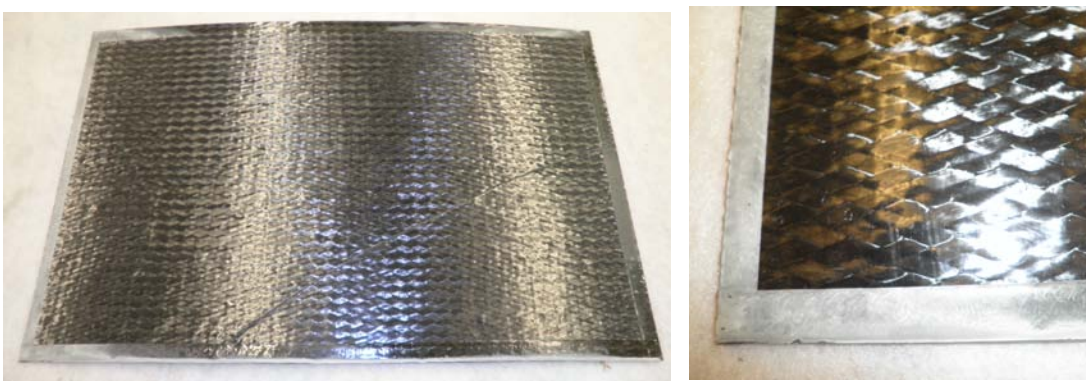

Figure 4.9 Water Exposed Sheets After Conditioning

Samples were conditioned for 500, 788, and 1000 hours to determine if there was a noticeable trend in the change of material properties. The samples that were put in to the QUV to be conditioned for 750 hours were actually conditioned for 788 hours due to equipment accessibility constraints. Table 4.8 shows the results from the three different exposure times, the coefficient of variation is reported as a percentage next to the mean value in parenthesis.

Table 4.8 Water Exposure Test Results

| Test Duration (hr) | $E_x$ kN/mm | $E_y$ kN/mm | $\nu_{xy}$ | $F_{xt}$ kN/mm | $F_{yt}$ kN/mm | $\tau_{20}$ kN/mm |
|---|---|---|---|---|---|---|
| 500 | 64.4 (6) | 40.0 (6) | 1.28 (4) | 1.35 (6) | 0.62 (7) | 0.15 (4) |
| 788 | 66.5 (5) | 39.0 (4) | 1.15 (6) | 1.43 (6) | 0.60 (6) | 0.15 (3) |
| 1000 | 67.8 (8) | 40.6 (7) | 1.20 (6) | 1.37 (9) | 0.57 (14) | 0.14 (5) |

A t-test showed that there was no significant change in elastic modulus in the longitudinal or transverse direction over time. The transverse tensile strength declined over time while the longitudinal tensile strength and ultimate shear stress showed no significant trend. In general the data was not pooled since each batch represents different exposure times. Although only one batch of samples were tested for each time period B-Basis values were calculated based on a normal distribution and can be seen in Table 4.9. B-Basis values were calculated for all batches that underwent environmental conditioning at different times; they are used for comparison purposes and are not considered acceptable to be published in the Composite Materials Handbook since the data does not meet the criteria of coming from three separate batches.

Table 4.9 B-Basis Values for Water Exposure Tests

| Test Duration (hr) | $E_x$ kN/mm | $E_y$ kN/mm | $F_{xt}$ kN/mm | $F_{yt}$ kN/mm | $\tau_{20}$ kN/mm |
|---|---|---|---|---|---|
| 500 | 55.3 | 34.6 | 1.17 | 0.53 | 0.13 |
| 788 | 57.5 | 35.2 | 1.24 | 0.51 | 0.14 |
| 1000 | 60.1 | 34.4 | 1.09 | 0.40 | 0.12 |

The sheets exposed to water for a duration of 1000 hours were weighed before and after exposure to determine if there was a noticeable weight change due to moisture absorption. Table 4.10 shows the recorded weights and percent change. The change in weight was not consistent and didn't appear to be a significant amount. It should also be noted that the coupons tested are cut from the larger sheets and would most likely have even a smaller weight change than what was observed.

Table 4.10 Sheet Weight After 1000 Hour Water Exposure

| Sheet | Start Weight (kg) | End Weight (kg) | Difference (kg) | Difference (%) |
|---|---|---|---|---|
| A | 0.230 | 0.228 | -0.002 | -0.87 |
| B | 0.586 | 0.588 | 0.002 | 0.34 |
| C | 0.604 | 0.604 | 0 | 0 |

### 4.3.5. Salt Water

Saltwater exposure, particularly in costal states, can occur quite regularly. If the arches are located in a costal area they may be exposed to salt water spray or have brackish water running below the bridge, which could cause the base of the arches to salt water immersion. The ability of FRP to resist degradation caused by saltwater would make FRP a more viable option in marine environments since steel is likely to corrode without additional protection (Waldron et al. 2001).

Another type of salt exposure that bridges commonly experience is from deicing salts used in the winter. Deicing salts are only used on the road surface however there is a chance that the salts could leach down to the arches. Commonly used deicing salts include sodium chloride (NaCl), anhydrous calcium chloride ($CaCl_2$) and magnesium chloride ($MgCl_2$) (Tannous and Saadatmanesh 1998).

#### 4.3.5.1 Literature Review for Saltwater Exposure

In a study by Tannous and Saadatmanesh E-glass FRP rebar was exposed to numerous solutions to observe the moisture absorption. It was found that the recorded diffusivities were generally higher from saltwater exposure than exposure to alkaline and acidic solutions due to the ions in saltwater that were able to penetrate the FRP more easily (Tannous and Saadatmanesh 1998). In another study on E-glass FRP rebar in concrete performed by Sen et al. it was proposed that the moisture of the saltwater solution used was the cause of degradation rather than the salts, since "plastics are unaffected by salt" (Sen et al. 1993). He believed that the moisture combined with alkalis present in the concrete is what caused the most damage to the glass fibers.

In a review article written by Waldron et al. (2001) it was discussed that saltwater exposure results can vary and it is difficult to determine if degradation is due to salts or due to moisture and alkali attack. There have been some indications that a saline solution is a slightly more severe environment than fresh water (Waldron et al. 2001). In general carbon FRP bars exposed to saltwater have shown very little degradation while E-glass FRP bars are more susceptible to a loss in strength and stiffness of up to 50% (Waldron et al. 2001).

#### 4.3.5.2 Saltwater Testing

Saltwater exposure was performed through immersion in a saltwater solution at 23°C. The saltwater solution used conformed to ASTM D1141 Standard Practice for the Preparation of Substitute Ocean Water (ASTM 2008a). The saltwater was contained in a polyethylene storage bin that was covered by a lid throughout the conditioning time. To circulate the saltwater a small aquarium pump was used that had the ability to pump 1000L/hr. To regulate the temperature at 23°C a small aquarium heater was used, also a thermometer was kept in the solution and monitored daily to make sure the temperature was 23±3°C.

All of the sheets were added to the solution at the same time and removed as their respective exposure durations were completed, sheets were removed after 500, 1000, and 2000 hours of exposure. The sheets were positioned parallel to the bottom of the container and spaced at least .6 mm apart. Spacers were made from notched blocks of high-density polyethylene, a spacer was used at each end of the sheets and each sheet was slid into a separate notch.

After sheets were removed from the solution they were rinsed with tap water, wiped with a dry cloth, and left to air dry at room temperature of 23°C. Similar to the water exposure, there was some discoloration of the edges after conditioning, however the discoloration was not as prominent and can be seen in Figure 4.10. The sheets were also very flat after being removed from conditioning. Since the sheets are only supported on the ends during conditioning it is possible for the sheets to loose their initial curvature through relaxation under their own

weight. Relaxation of carbon FRP and glass FRP tendons has been observed and after 1000 hours was estimated to be 0.5-1.0% and 1.8-2% respectively (Balazs and Borosnyoi 2001).

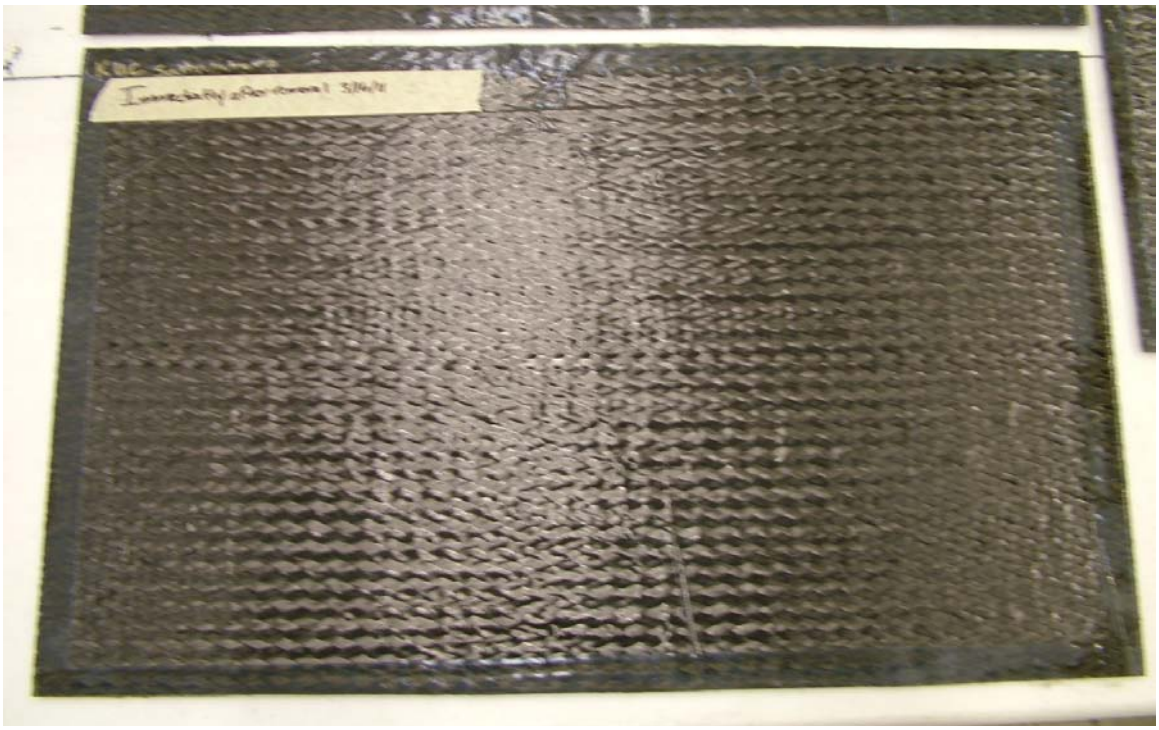

Figure 4.10 Sheet After Saltwater Exposure

Samples were conditioned for 500, 1000, and 2000 hours to determine if there was a noticeable trend in the change of material properties. Table 4.11 shows the results from the three different exposure times, the coefficient of variation is reported as a percentage next to the mean value in parenthesis. Similar to the water exposure results, the change in material properties over time appeared to have no trend that was statistically significant.

Table 4.11 Saltwater Exposure Test Results

| Test Duration (hr) | $E_x$ kN/mm | $E_y$ kN/mm | $\nu_{xy}$ | $F_{xt}$ kN/mm | $F_{yt}$ kN/mm | $\tau_{20}$ kN/mm |
|---|---|---|---|---|---|---|
| 500 | 64.1 (4) | 39.7 (5) | 1.21 (4) | 1.30 (8) | 0.59 (6) | 0.14 (6) |
| 1000 | 62.6 (5) | 36.6 (7) | 1.37 (3) | 1.34 (9) | 0.55 (9) | 0.13 (7) |
| 2000 | 64.0 (5) | 37.7 (4) | 1.22 (4) | 1.33 (7) | 0.55 (10) | 0.13 (7) |

A t-test showed that there was no significant change in the longitudinal elastic modulus or longitudinal tensile strength over time. The transverse tensile strength declined from the first duration then seemed to stabilize over time. The transverse elastic modulus and ultimate shear stress showed no significant trend. In general the data was not pooled since each batch represents different exposure times. Although only one batch of samples was tested for each time period, B-Basis values were calculated based on a normal distribution and can be seen in Table 4.12.

Table 4.12 B-Basis Values for Saltwater Exposure Tests

| Test Duration (hr) | $E_x$ kN/mm | $E_y$ kN/mm | $F_{xt}$ kN/mm | $F_{yt}$ kN/mm | $\tau_{20}$ kN/mm |
|---|---|---|---|---|---|
| 500 | 58.0 | 35.6 | 1.07 | 0.51 | 0.12 |
| 1000 | 55.5 | 30.4 | 1.06 | 0.43 | 0.11 |
| 2000 | 56.6 | 34.1 | 1.12 | 0.43 | 0.11 |

### 4.3.6. Alkali Solution

The alkali resistance of the composite is important to consider because the composite arches are filled with concrete. Concrete has a high content of calcium hydroxide and hardened cement stone, which leads it to be highly alkaline. When setting the arches up in the field the ends of the arches are surrounded by concrete

in the footings, exposing both the carbon side and E-glass side of the composite to an alkaline environment. After filling the arches the E-glass layer of the composite arch is exposed to concrete and susceptible to degradation from the alkali along the entire length of the arch.

#### 4.3.6.1 Literature Review for Alkali Exposure

Carbon fibers are generally resistant to alkali since they do not easily absorb liquids, however E-glass fibers are known to deteriorate in alkaline environments, with a decrease in capacity that can range from 30 to 100 percent (Balazs and Borosnyoi 2001). The use of resin can help decrease the deterioration of E-glass fibers. Vinyl ester resin has been shown to have the best resistance to alkaline environments, though the alkaline solution still can deteriorate the links between the molecules in the resin (Balazs and Borosnyoi 2001). Karbahari et al have noted that degradation due to alkali exposure is typically seen as a loss in tensile strength, but it is also possible for the stiffness to increase over longer time periods (Karbhari et al. 2002).

The rate of deterioration is also highly dependent on the type of fiber, resin, alkali solution and exposure time. Several different alkali solutions used for durability testing were found in the literature, Table 4.13 lists some those solutions.

Table 4.13 Common Solutions used for Alkali Exposure

| Authors | Solution Description and pH |
|---|---|
| Steckel et al. (1999) | $CaCO_3$ (pH 9.5) |
| Chu et al. (2004) | $CaCO_3$ and $Ca(OH)_2$ (pH 11.5) |
| Micelli and Nanni (2004) | $Ca(OH)_2$ Na(OH) and K(OH) (pH 12.6) |
| Conrad (1998) | Saturated solution of $Ca(OH)_2$ |
| Rostasy (1997) | Saturated solution of $Ca(OH)_2$ and K(OH) (pH 13) |
| Uomoto Nishisura (1997) | NaOH |

One of the difficulties in characterizing the degradation of E-glass due to alkali exposure is the inconsistency of solutions cited in the literature. As previously mentioned, the most common exposure to alkalis is through FRP being in contact with concrete so it is important to try to develop an alkali solution that would be similar to that found in concrete pore water. The pH of concrete pore water can be as high as 14, however a solution with a high pH doesn't automatically mean that it is also highly alkaline. One trend discussed by Karbhari et al (2005) is that a number of researchers have used solutions that had high pH levels but may not have a high presence of alkali salts; or have used alkali salts but not in a solution that would mimic exposure to alkaline pore water. Another issue observed was some solutions that need to be renewed over the conditioning period could be exposing samples to higher concentrations of alkalinity than would be typically seen in the field.

The solution suggested in the durability test matrix was a solution used by Steckel of calcium carbonate ($CaCO_3$) in water, resulting in a pH of 9.5 (Steckel et al. 1999). In another paper Karbhari goes on to discuss that while calcium carbonate solutions are typically used to represent concrete pore water the pH level of the

solution can vary dramatically overtime, a saturated solution can begin with a pH of 12.5 and rapidly drop to a pH of 8.5 (Karbhari et al. 2002). This change in pH is attributed to carbon dioxide in the air reacting with the salt in the solution and forming calcium bicarbonate that has a lower pH. Some researches have tried to mitigate the rapid drop in pH by adding calcium hydroxide to the solution. The addition of calcium hydroxide will bring up the pH of the solution, but at the cost of adding additional chemical compounds that could possibly affect the degradation of the composite in a way that is not representative of concrete pore water.

#### 4.3.6.2 Alkali Testing

Alkali exposure was performed through immersion in a solution of calcium carbonate, $CaCO_3$, at a pH of 9.5 at 23°C. The solution was created using deionized water and powdered $CaCO_3$. The powered $CaCO_3$ was added to deionized water until the solution reached a pH of 9.5. As mentioned in the previous section, solutions made with $CaCO_3$ tend to experience a rapid drop in pH. Some researchers have added other compounds such as calcium hydroxide to maintain pH levels, however since the effect of calcium hydroxide is unknown it was not added to the solution. After the initial amount of $CaCO_3$ was mixed no additional $CaCO_3$ or other compounds were added throughout the conditioning period. A drop in pH was observed and monitored with a pH meter over time, the pH rapidly dropped to 8.1 and remained at that level throughout the conditioning period.

The test set up for alkali conditioning was similar to the saltwater conditioning. The solution was contained in a polyethylene storage bin that was covered by a lid throughout the conditioning time. To circulate the $CaCO_3$ a small

aquarium pump was used that had the ability to pump 1000L/hr. To regulate the temperature at 23°C a small aquarium heater was used, also a thermometer was kept in the solution and monitored daily to make sure the temperature was 23±3°C.

All of the sheets were added to the solution at the same time and removed as their respective exposure durations were completed, sheets were removed after 500, 1000, and 2000 hours of exposure. The sheets were positioned parallel to the bottom of the container and spaced at least .6mm apart. Spacers were made from notched blocks of high-density polyethylene, a spacer was used at each end of the sheets and each sheet was able to slide into a separate notch.

After sheets were removed from the solution they were rinsed with tap water, wiped with a dry cloth, and left to air dry at room temperature of 23°C. Again it was observed that there was discoloration of the edges after conditioning. The edges appeared chalky white, it appeared as though the resin used on the edges absorbed or attracted some of the $CaCO_3$ used in the solution. Since the resin used for sealing the edges was not post cured it is possible that $CaCO_3$ particles may have stuck to the resin. Figure 4.11 shows a sheet after being exposed to the alkali solution. Similar to the saltwater exposed sheets, the alkali exposed sheets were also very flat after being removed from conditioning. Again, since the sheets are only supported on the ends during conditioning it is possible for the sheets to loose their initial curvature through relaxation under their own weight.

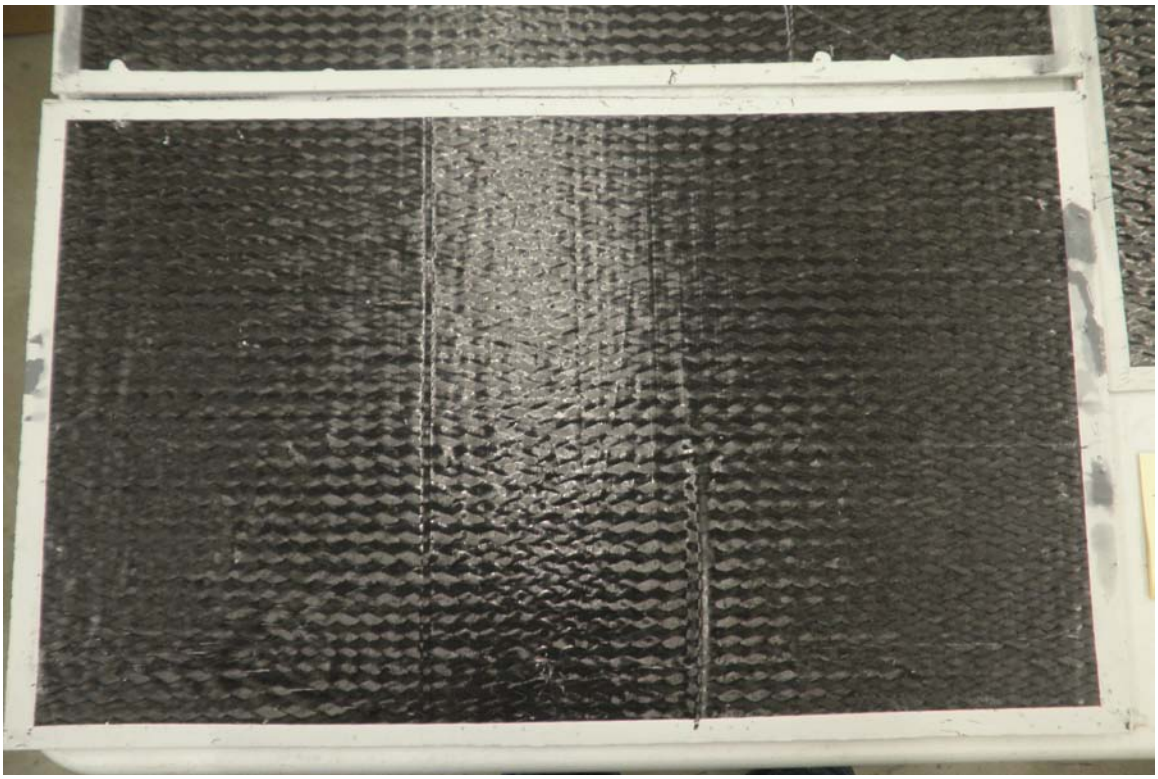

Figure 4.11 Alkali Exposed Sheet

Samples were conditioned for 500, 1000, and 2000 hours to determine if there was a noticeable trend in the change of material properties. Table 4.14 shows the results from the three different exposure times, the coefficient of variation is reported as a percentage next to the mean value in parenthesis. The change in material properties over time appeared to have no trend that was statistically significant.

Table 4.14 Alkali Exposure Test Results

| **Test Duration (hr)** | **$E_x$ kN/mm** | **$E_y$ kN/mm** | **$\nu_{xy}$** | **$F_{xt}$ kN/mm** | **$F_{yt}$ kN/mm** | **$\tau_{20}$ kN/mm** |
|---|---|---|---|---|---|---|
| 500 | 64.5 (7) | 40.2 (2) | 1.22 (12) | 1.31 (8) | 0.57 (5) | 0.13 (6) |
| 1000 | 63.7 (7) | 38.6 (7) | 1.31 (4) | 1.27 (7) | 0.55 (8) | 0.13 (9) |
| 2000 | 64.1 (6) | 38.9 (7) | 1.27 (4) | 1.37 (7) | 0.56 (11) | 0.13 (5) |

A t-test showed that there was no significant change in the longitudinal elastic modulus or longitudinal tensile strength over time. In general the data was not pooled since each batch represents different exposure times. Although only one batch of samples were tested for each time period, B-Basis values were calculated based on a normal distribution and can be seen in Table 4.15.

Table 4.15 B-Basis Values for Alkali Exposure Tests

| Test Duration (hr) | $E_x$ kN/mm | $E_y$ kN/mm | $F_{xt}$ kN/mm | $F_{yt}$ kN/mm | $\tau_{20}$ kN/mm |
|---|---|---|---|---|---|
| 500 | 59.4 | 38.0 | 1.08 | 0.51 | 0.12 |
| 1000 | 53.9 | 32.2 | 1.06 | 0.45 | 0.10 |
| 2000 | 55.4 | 32.9 | 1.14 | 0.41 | 0.12 |

### 4.3.7. Dry Heat

The composite FRP arches can be exposed to dry heat from an elevated temperature of the atmosphere, exposure to sunlight or other sources of heat or from a flame or fire. Typically the composite arches will experience dry heat from an elevated temperature of the atmosphere, while other exposures are unlikely to regularly occur. Exposure to direct sunlight is not common since the arches are below the soil.

#### 4.3.7.1 Literature Review for Dry Heat Exposure

High temperatures do not typically affect the fibers in a composite. In general the fiber used in composites is "temperature-resistant and can retain a majority of its strength and stiffness at high temperatures" (Cao et al. 2009). Carbon fiber can resist temperatures up to 800-1000°C, while E-glass can resist temperatures up to

300-500°C. Resins however typically soften, melt or ignite around temperatures of 150-200°C. Some studies show that a large reduction in tensile strength and stiffness only occurred when the surrounding temperatures exceeded the glass transition temperature, Tg, of the composite matrix (Cao et al. 2009). The durability of the vinyl ester resin can be enhanced by postcuring the part. In addition, the Tg of the polymer will increase, and this will result in a higher maximal end-use temperature (Herzog et al. 2005).

While the temperatures mentioned above are not normally experienced by a bridge structure, temperature as high as 60°C are also considered; this temperature was selected based on other studies that determined 60°C would be the "maximum exposure temperature anticipated in service" for FRP wrapped bridge columns (Steckel et al. 1999). In a study done by Cao (2009), carbon epoxy FRP samples tested at temperatures up to 55°C experienced significant reductions in tensile strength. The test results are explained through the epoxy resin softening after reaching the glass transition temperature of the epoxy, at 38°C, which lead to uneven loading of the carbon fibers and a lower composite tensile strength. In the same study, hybrid carbon and E-glass epoxy composite samples were tested and it was found that the results were similar and more consistent. The hybrid composite samples were "more stable" but did not show an improvement in tensile strength during loading under high temperatures (Cao et al. 2009).

#### 4.3.7.2 Dry Heat Testing

For dry heat conditioning, sheets were placed in an oven heated to 60° C. The Tg of DERAKANE 610C is unreported, but is expected to be similar to that of DERAKANE 8084. Ashland reports the Tg of DERAKANE 8084 after postcure as 115°C (Ashland 2006), however the samples used for all durability tested did not undergo a postcure. Experimental work done by Herzog found that the resin DERAKANE 8084 had a Tg of 107°C when postcured, and a Tg of only 60°C when cured at room temperature, approximately 23°C. However when comparing FRP samples made from E-glass fibers and DERAKANE 8084 resin it was found that the Tg "showed virtually no difference in Tg between room temperature cured and postcured samples" (Herzog et al. 2005). This study suggests that even though the oven temperature is the same as the experimental Tg of resin samples of DERAKANE 8084, there may not be a significant loss in material properties due to the matrix, since the fibers in the composite may raise the overall Tg.

All of the sheets were placed in the oven at the same time and removed after 500, 1000, and 2000 hours of exposure. The sheets were placed on racks and spaced apart from each other using 6mm thick blocks of foam at the ends of the sheets. Figure 4.12 shows the sheets and their arrangement in the oven. The oven had an internal thermometer and an external temperature display that was monitored daily to make sure the temperature was within ±1°C.

Figure 4.12 Dry Heat Test Setup

After the sheets were removed from the oven they were allowed to cool to the room temperature of around 23°C. Sheets in the oven remained flat, as observed in Figure 4.12, throughout the conditioning period, however after cooling, the sheets developed a significant curvature. Figure 4.13 shows the curvature of the sheets after conditioning. The curvature of the sheets, $\kappa$, after 1000 and 2000 hours of exposure was recorded and is shown in Table 4.16. From the three sheets measured at each exposure time, it appears the curvature increases over time while the temperature is kept constant.

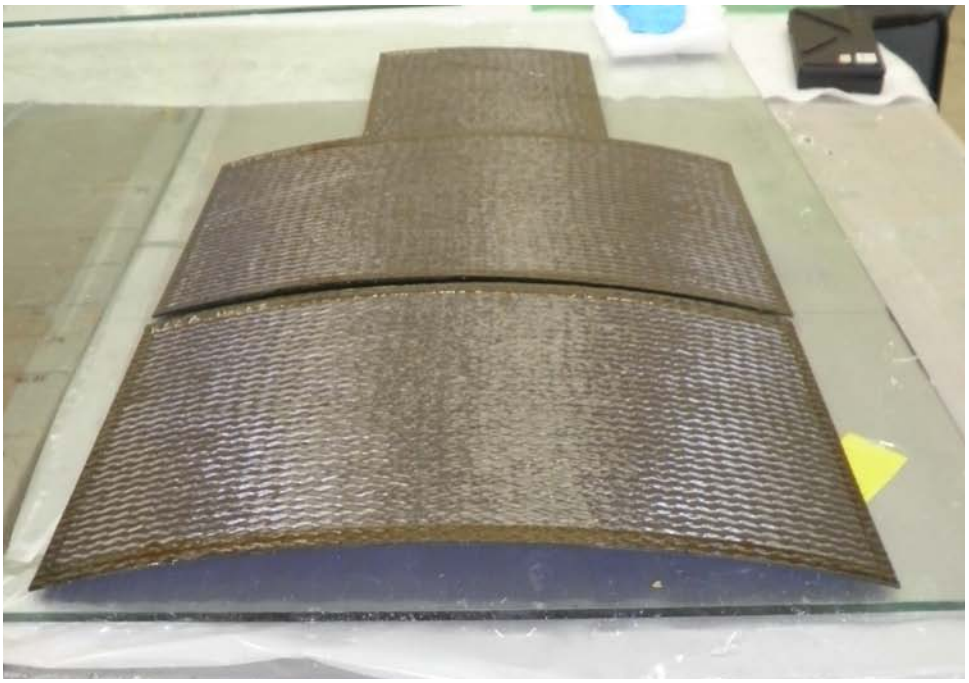

Figure 4.13 Dry Heat Conditioned Sheets After Exposure

Table 4.16 Curvature of Heat Exposed Sheets

| **Sheet ID** | **κ (1/mm)** |
|---|---|
| Heat 1000A | 0.72 |
| Heat1000B | 0.70 |
| Heat1000C | 0.69 |
| Heat 2000A | 0.70 |
| Heat 2000B | 0.90 |
| Heat 2000C | 1.03 |

Another visual observation made was the resin on edges of the sheet and the elastics in the glass material appeared to become slightly orange in color.

Samples were conditioned for 500, 1000, and 2000 hours to determine if there was a noticeable trend in the change of material properties. Table 4.17 shows the results from the three different exposure times, the coefficient of variation is reported as a percentage next to the mean value in parenthesis.

Table 4.17 Dry Heat Exposure Test Results

| Test Duration (hr) | $E_x$ kN/mm | $E_y$ kN/mm | $\nu_{xy}$ | $F_{xt}$ kN/mm | $F_{yt}$ kN/mm | $\tau_{20}$ kN/mm |
|---|---|---|---|---|---|---|
| 500 | 65.7 (3) | 42.0 (5) | 1.12 (6) | 1.32 (11) | 0.66 (8) | 0.17 (7) |
| 1000 | 64.0 (6) | 41.3 (8) | 1.09 (3) | 1.36 (7) | 0.57 (15) | 0.16 (5) |
| 2000 | 66.3 (6) | 43.9 (4) | 1.11 (4) | 1.32 (8) | 0.55 (15) | 0.17 (6) |

A t-test showed that there was no significant change in the longitudinal elastic modulus or longitudinal tensile strength over time. The transverse elastic modulus and ultimate shear stress showed no significant trend. The transverse tensile strength appeared to decline over time, however the coefficient of variation for the 1000 and 2000 hour samples were at the upper limit of the target coefficient of variation. In general the data was not pooled since each batch represents different exposure times. Although only one batch of samples was tested for each time period, B-Basis values were calculated based on a normal distribution and can be seen in Table 4.18.

Table 4.18 B-Basis Values for Dry Heat Exposure Tests

| Test Duration (hr) | $E_x$ kN/mm | $E_y$ kN/mm | $F_{xt}$ kN/mm | $F_{yt}$ kN/mm | $\tau_{20}$ kN/mm |
|---|---|---|---|---|---|
| 500 | 60.8 | 37.4 | 0.99 | 0.55 | 0.15 |
| 1000 | 55.8 | 34.2 | 1.13 | 0.38 | 0.15 |
| 2000 | 57.4 | 40.1 | 1.03 | 0.36 | 0.15 |

#### 4.3.7.3 Ignition Testing

While extensive fire testing was beyond the scope of this research, a small ignition test was conducted to assess the flammability of the material. The motivation behind this experiment was to determine if a person holding a typical lighter to the arch material could significantly damage the structure. The test was conducted by holding a small flame, generated by a Bunsen burner, to a sample of the composite material and recording how long to takes to ignite. This experiment was adapted from the Aircraft Materials Fire Test Handbook (U.S Deapartment of Transportation and Federal Aviation Administration 2000). The test method outlined in the Aircraft Materials Fire Test Handbook is intended for determining the resistance of materials to flame when tested according to the 60-second and 12-second vertical Bunsen burner Tests. The composite sample used was a concrete filled 75mm wide composite ring that was representative of the arch. The composite ring consisted of one layer of E-glass braided fibers and one layer of carbon braided fibers infused with the DERAKANE 8084 resin. It is important to note that the concrete in the sample tested may help dissipate the heat from the flame, therefore increasing the ignition temperature as opposed to testing only the thin composite laminate.

The flame was held against the outside of the sample for 10 min. After 10 min there was no ignition and the test was stopped. Since the material did not ignite it appeared that the composite would not be significantly damaged by a short-term exposure to a typical lighter. After the test, the sample was visually inspected and

very little change in the composite was observed. The ignition test setup can be seen in Figure 4.14 while a close up of the exposed area after testing can be seen in Figure 4.15.

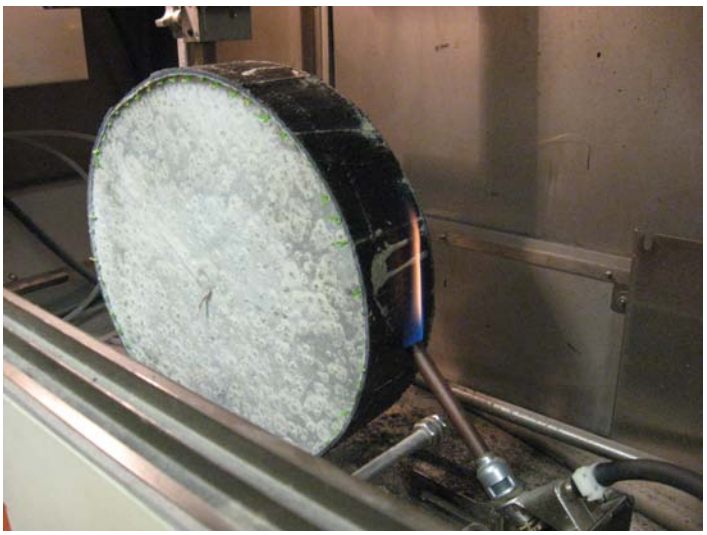

Figure 4.14 Ignition Test Setup

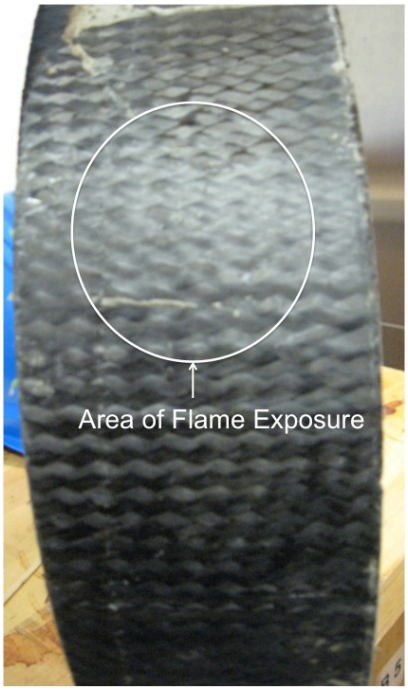


Figure 4.15 Area Exposed to Flame

### 4.3.8. Ultraviolet Light

While the arches are practically a buried structure, UV exposure still needs to be considered. The end arches may be exposed to direct sunlight as seen in Figure 4.16. Also, typical locations for the composite arch bridges have been over streams, which can reflect UV light on to the underside of the arches.

Figure 4.16 Bridge Demonstrating End Arch Exposure to Sunlight

#### 4.3.8.1 Literature Review for UV Exposure

Most polymers are greatly affected by the amount of solar ultraviolet exposure that reaches the Earth's surface (Karbhari et al. 2003). UV degradation typically affects only the surface of the composite, but even that small amount can affect the material properties of the composite by creating stress concentrations. UV exposure can lead to surface oxidation from the chemical reactions in the resin

(Micelli and Nanni 2004). Bond dissociation can also be caused by UV radiation, leading to chain scission or cross linking within the resin (Chin et al. 2001). UV exposure is also typically combined with moisture exposure, to mimic the sun during the day and dew at night, which can accelerate composite degradation.

When exposing samples to UV light and moisture, the majority of degradation may not be caused by UV exposure, since UV typically only affects the surface, but may be caused by the increase of moisture absorption due to surface cracking. One way to protect against UV degradation is by using a protective gel coat or resin rich layer. This does not prevent UV degradation but acts as a sacrificial layer to protect the integrity of the main composite.

One of the difficulties of UV testing is comparing results, whether it be to actual real time outdoor exposure or from indoor accelerated testing through the use of weathering machines. Repeatability of results from a laboratory testing device have been found acceptable, however it is more difficult to reproduce test results using nominally identical test devices (Chin et al. 2001). Outdoor testing is even more difficult to reproduce because test results from different outdoor exposure sites taken at different time periods are not comparable. The variability in test conditions makes it very difficult to correlate a particular laboratory test to a specific time period of outdoor exposure. Due to these issues Chin et al. (2001) feel that "current UV weathering methodology is not recommended for the prediction of service life."

While laboratory test results may not be comparable to real time outdoor exposure they are useful to compare to other materials and to observe the effects of UV over a period of time. Standards such as ASTM G 154 Standard Practice for Operating Fluorescent Light Apparatus for UV Exposure of Nonmetallic Materials (ASTM 2006) provide a guideline for UV exposure. By following such guidelines criteria can be established to determine if a particular composite is more durable than other materials under UV exposure.

#### 4.3.8.2 UV Testing

UV exposure was conducted using a QUV machine that has the capability to provide UV and moisture exposure, through either a spray or humidity. UV conditioning was performed through cycles of 4 hours of UV at 60°C and 4 hours of condensate (100% humidity). This cycle was used to "simulate the deterioration caused by water as rain or dew and the ultraviolet energy in sunlight" (Steckel et al. 1999). An additional step of a 5 min water spray before the 4 hours of condensate was added to each cycle to provide moisture for condensation that may evaporate during the UV period. The sheets were conditioned for 100 cycles before being removed from conditioning and allowed to air dry at a room temperature of 23°C.

After conditioning the sheets exhibited a curvature greater than unexposed samples, this curvature can be observed in Figure 4.17. The curvature could be a result of the thermal cycling and exposure to high temperatures. Other possible explanations include creep effects of softening of the material when exposed to high temperatures. Table 4.19 shows the curvature of the sheets after being conditioned.

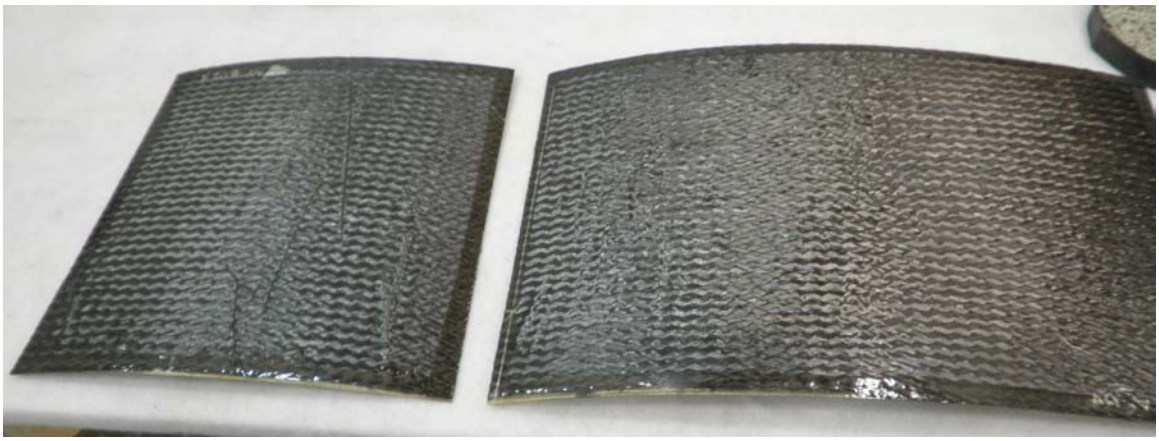

Figure 4.17 Sheets after UV Exposure

Table 4.19 Curvature of UV Exposed Sheets

| Sheet ID | κ (1/mm) |
|---|---|
| UV A | 0.76 |
| UV B | 0.80 |
| UV C | 0.53 |

The sheets did not appear to have any visual changes; in some material UV exposure can cause fading, whitening, or cracking of the surface of the material however none of these effects were observed. The test results from UV exposure can be seen in Table 4.20 along with calculated B-Basis values based on a normal distribution. The tensile strength in the transverse direction had a higher coefficient of variation than the target value of 15%, this could possibly be due to the effects of the sheet curvature or premature matrix cracking during the test.

Table 4.20 UV Exposure Test Results

| | $E_x$ (kN/mm) | $E_y$ (kN/mm) | $\nu_{xy}$ | $F_{xt}$ (kN/mm) | $F_{yt}$ (kN/mm) | $\tau_{20}$ (kN/mm) |
|---|---|---|---|---|---|---|
| Mean | 62.7 | 41.8 | 1.15 | 1.25 | 0.53 | 0.14 |
| STD | 4.56 | 5.27 | 0.06 | 0.09 | 0.09 | 0.02 |
| COV (%) | 7.28 | 12.59 | 4.84 | 7.46 | 17.37 | 10.89 |
| B-Basis | 52.3 | 29.9 | NA | 1.04 | 0.32 | 0.11 |

### 4.3.9. Freeze Thaw

Freeze thaw is an environmental condition that many bridges undergo, especially in northern states such as Maine. Concrete itself is very susceptible to damage from freeze thaw cycling due to pore water freezing and creating cracks in the concrete. Each time concrete undergoes a period of freezing more cracks can occur; the thaw period that follows can cause surface ice to melt and seep into the newly formed cracks which will cause them to spread even more during the next freeze period. As more freeze thaw cycles occur the cracks and damaged area will continue to spread. The freeze thaw damage that is easily observed in concrete is also present in composites, where the matrix is at risk of forming micro cracks and degrading the material properties of the composite.

#### 4.3.9.1 Literature review for Freeze Thaw Exposure

Thermal effects, such as those experienced through freeze thaw cycling, can cause micro cracks between the resin matrix and the fibers due to a difference in thermal expansion coefficients. When additional moisture is introduced during freeze thaw cycling the degradation effects are intensified due to water's ability to

penetrate the composite through the micro cracks (Micelli and Nanni 2004). The resin itself can undergo an initial post cure during the first high thermal period, but then begin to degrade after thermal cycling. The resin can also experience matrix hardening during the freeze period which leads to micro cracking and fiber-matrix bond degradation (Karbhari et al. 2003).

In a study performed by Rivera and Karbhari (Rivera and Karbhari 2001), sheets made of unidirectional carbon fiber and vinyl ester resin were exposed to aqueous freeze thaw cycles, with temperatures ranging from -10°C to 22.5°C. After testing samples in tension they found that the tensile strength and modulus decreased as a result of fiber-matrix debonding and matrix micro cracking (Rivera and Karbhari 2001). They also noted that the freeze thaw cycling effects on modulus were "significantly smaller than those on strength." Freeze thaw cycling also magnifies the problem of an asymmetric layup made from carbon fibers, E-glass fibers, and a vinyl ester resin, all of which have different coefficients of thermal expansion as discussed in 2.5.

#### 4.3.9.2 Freeze Thaw Testing

Freeze thaw testing was conducted in an ESPEC environmental chamber. The sheets were placed in the chamber on small 6 mm thick foam blocks at the corners to raise them from the surface of the conditioning chamber. The foam blocks were also placed in between the sheets to act as spacers. The chamber was set to run a program of 20 freeze thaw cycles. Each cycle consisted of 12 hours where the temperature was 38°C with 98% relative humidity followed by 12 hours

where the temperature was -18°C. In between each 12 hour cycle was a 1 hour ramp time to allow time for the temperature to adjust; Figure 4.18 shows a diagram of a typical cycle.

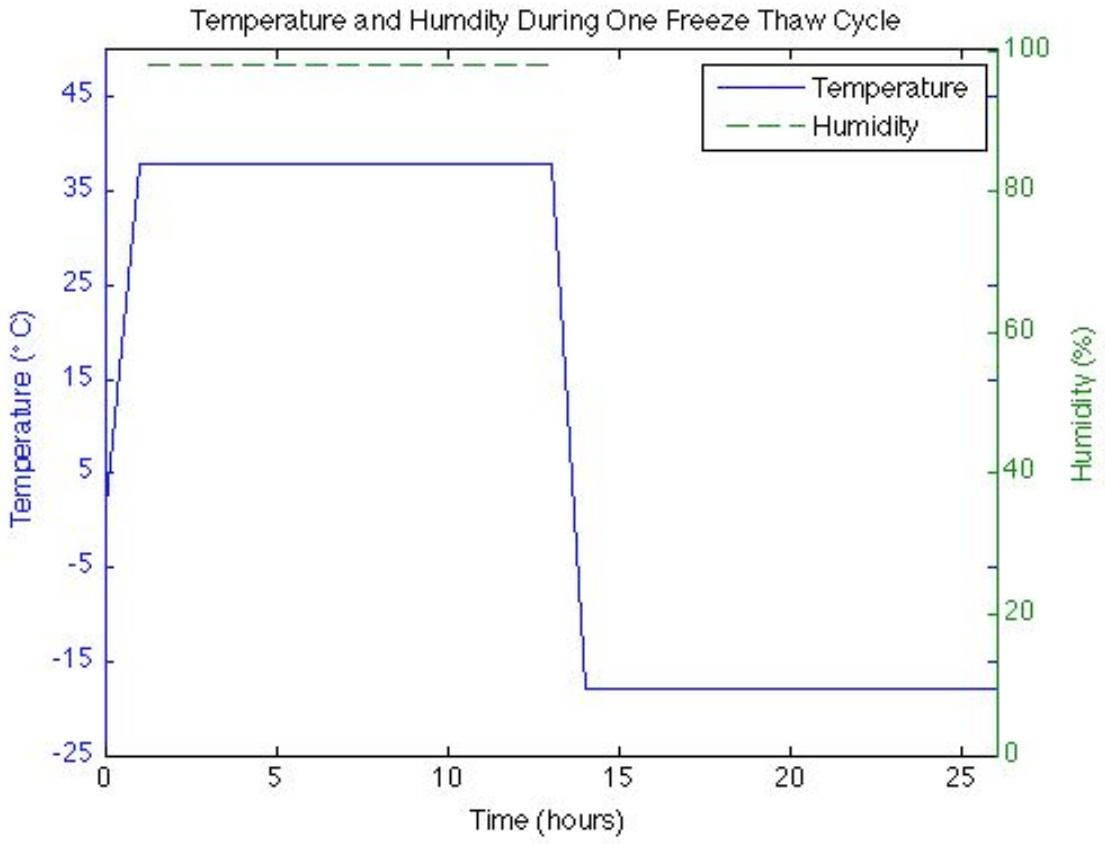


Figure 4.18 Temperature During One Freeze Thaw Cycle

It is important to note that the environmental chamber malfunctioned and stopped the program twice during the 20 cycles time period. Both times the machine malfunctioned it took 4 days before conditioning was resumed. During the time that the program was not running samples were left in the chamber and remained at room temperature.

During the freeze thaw testing the sheets were observed to curve and relax throughout the cycle. The sheets would typically exhibit a greater curvature than

normal during the freezing portion of exposure, then relax and start to flatten out again during the thaw cycle. Figure 4.19 shows the sheets in the conditioning chamber after conditioning was finished. Since the cycling ended after a frozen period the curvature in the sheet can be observed. The observed curvature was in the same direction as seen in the heated sheets. The sheets remained curved after being removed from the chamber, but relaxed a small amount while adjusting to the room temperature, 23°C, of where they were stored before coupons were cut. Table 4.21 shows the curvature of the sheets after conditioning and adjusting to the room temperature.


Figure 4.19 Freeze Thaw Sheets at End of Exposure

Table 4.21 Curvature of Freeze Thaw Exposed Sheets

| Sheet ID | κ (1/mm) |
|---|---|
| FT A | 0.25 |
| FT B | 0.36 |

Samples could not be tested within four days after conditioning due to a malfunction with the in house water jet cutting machine. The sheets were sent out to be cut by another water jet cutting machine and were tested 13 days after conditioning. The results from testing can be seen in Table 4.22 along with calculated B-Basis values based on a normal distribution.

Table 4.22 Freeze Thaw Exposure Test Results

| | $E_x$ (kN/mm) | $E_y$ (kN/mm) | $\nu_{xy}$ | $F_{xt}$ (kN/mm) | $F_{yt}$ (kN/mm) | $\tau_{20}$ (kN/mm) |
|---|---|---|---|---|---|---|
| Mean | 65.5 | 42.2 | 1.23 | 1.20 | 0.51 | 0.14 |
| STD | 4.88 | 2.32 | 0.10 | 0.07 | 0.06 | 0.01 |
| COV (%) | 7.45 | 5.51 | 8.13 | 5.89 | 12.02 | 7.78 |
| B-Basis | 54.4 | 36.5 | NA | 1.04 | 0.36 | 0.11 |

### 4.3.10. Fuel

Fuel exposure is one condition that may not be seen on a regular basis. The object of exposing the composite to fuel is to evaluate the effects fuel exposure may have on the arches in the case of a spill or a vehicular accident. In the case of a large spill, diesel fuel may be released onto the bridge deck; the other type of fuel to consider would be regular gasoline that may leak from cars in small amounts every day, or in larger amounts during an accident. In either case it is not likely the buried composite arches will ever be directly exposed to fuel, but since it can be corrosive, its effects should still be investigated.

#### 4.3.10.1 Literature Review for Fuel Exposure

In a test study performed by Steckel several combinations of carbon/epoxy systems and E-glass systems with epoxy, polyester, or vinyl ester resins were exposed to diesel fuel and tested in tension. Overall the samples performed well and only one E-glass/polyester system and one carbon/epoxy system had any reduction in tensile strength; even so the reductions, which were about 10% were speculated to be due to "panel to panel variations" (Steckel et al. 1999).

One application where composites are exposed to gasoline for long periods of time is underground fuel storage tanks that are made out of composite material. Beginning in 1965 some underground storage tanks were manufactured using glass reinforced plastics instead of steel (McConnell 2007). These tanks used resins that were formulated to contain aggressive fuels such as those containing ethanol. According to Ashland, the manufactures of DERAKANE epoxy vinyl ester resins, the DERAKANE line of resins are "well suited for corrosion liner upgrades" in steel underground storage tanks (McConnell 2007).

#### 4.3.10.2 Fuel Testing

For fuel testing samples were immersed in regular gasoline containing approximately 10% ethanol for 4 hours. Gasoline was selected over using a diesel reagent since it is considered to be more corrosive to composites (Stevens 2011). Gasoline was taken directly from the local gas station and poured into a polyethylene storage bin until all samples were covered by at least 25mm (1in) of gasoline; the total amount of gasoline used was about 3.8l liters (5 gal) a lid was

then placed on the bin throughout the exposure time. Four sheets were separated by at least 6mm using polyethylene slotted panels on both ends of the sheets. The test setup can be seen in Figure 4.20.

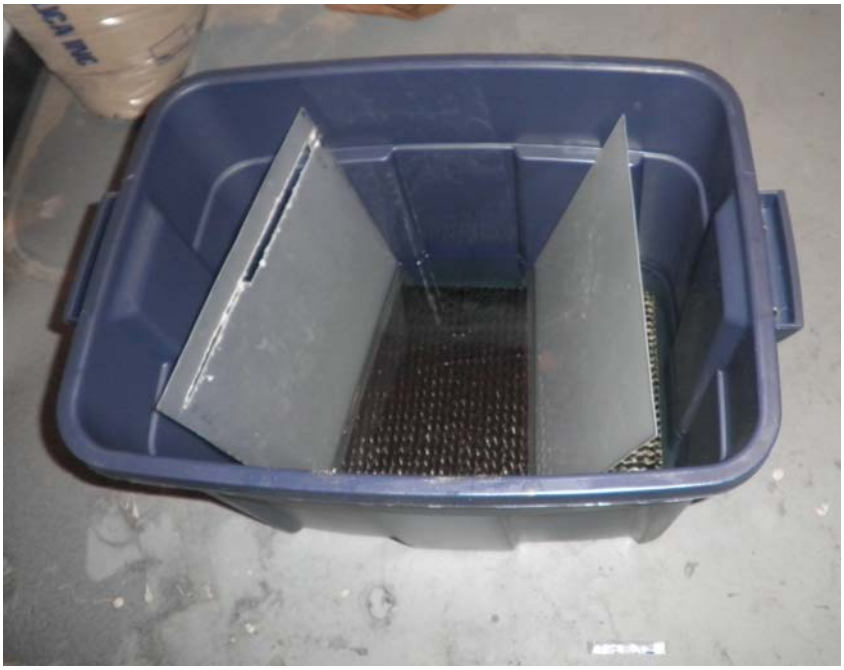

Figure 4.20 Fuel Exposure Test Setup

After being immersed in gasoline for 4 hours the sheets were removed and set on a plastic surface in a well ventilated room for an hour to allow the any gasoline residue to evaporate. After an hour the sheets were cleaned with a damp cloth before individual coupons were cut. Aside from a residual smell there were no visual changes in the coupons due to the fuel exposure. The results from testing can be seen in Table 4.23 along with calculated B-Basis values based on a normal distribution.

Table 4.23 Fuel Exposure Test Results

| | $E_x$ (kN/mm) | $E_y$ (kN/mm) | $\nu_{xy}$ | $F_{xt}$ (kN/mm) | $F_{yt}$ (kN/mm) | $\tau_{20}$ (kN/mm) |
|---|---|---|---|---|---|---|
| Mean | 65.5 | 42.7 | 1.20 | 1.33 | 0.49 | 0.13 |
| STD | 3.46 | 1.28 | 0.06 | 0.16 | 0.05 | 0.01 |
| COV (%) | 5.28 | 2.99 | 4.92 | 11.89 | 10.41 | 6.39 |
| B-Basis | 57.6 | 39.7 | NA | 0.96 | 0.37 | 0.12 |

### 4.3.11. Environmental Durability Test Matrix Results

After all of the conditions were investigated, data was gathered to be compared with the initial control samples tested. Table 4.24 summarizes the mean tensile properties of each of the environmental conditions; the percent of material properties retained is shown to the right of the mean value in italics. Those conditions that did not retain 90% of the original material properties are in bold. The data was pooled for the environmental conditions that had samples tested for multiple exposure times for comparison purposes. A t-test was used to compare each mean value to the control values, it was found that the majority of mean values were statistically different from the control samples; however samples exposed to water were found to be statistically the same as the control samples for properties other than ultimate shear stress.

Table 4.24 Mean Tensile Properties After Durability Testing

| **Environmental Condition** | **$E_x$ (kN/mm)** | | **$E_y$ (kN/mm)** | | **$F_{xt}$ (kN/mm)** | | **$F_{yt}$ (kN/mm)** | | **$\tau_{20}$ (kN/mm)** | |
|---|---|---|---|---|---|---|---|---|---|---|
| Control | 67.7 | | 40.2 | | 1.38 | | 0.55 | | 0.15 | |
| Water | 66.1 | *98* | 39.9 | *99* | 1.38 | *100* | 0.60 | *109* | 0.14 | *93* |
| Saltwater | 63.6 | *94* | 38.1 | *95* | 1.32 | *96* | 0.56 | *102* | 0.13 | ***87*** |
| Alkali | 64.1 | *95* | 39.2 | *98* | 1.32 | *96* | 0.56 | *102* | 0.13 | ***87*** |
| Dry Heat | 65.3 | *97* | 42.3 | *105* | 1.33 | *96* | 0.60 | *109* | 0.17 | *113* |
| UV | 62.7 | *93* | 41.8 | *104* | 1.25 | *91* | 0.53 | *96* | 0.14 | *93* |
| Freeze Thaw | 65.5 | *97* | 42.2 | *105* | 1.20 | ***87*** | 0.51 | *93* | 0.13 | ***87*** |
| Fuel | 65.5 | *97* | 42.7 | *106* | 1.33 | *96* | 0.49 | ***89*** | 0.14 | *93* |
| Italics= Percent of material properties retained Bold= Less than 90% retained | | | | | | | | | | |

After comparing the mean values of all the five measured tensile properties for each condition it was found that most conditions retained above 90% of the material properties. Those that did not retain above 90% material properties include the longitudinal tensile strength after freeze thaw exposure, the transverse tensile strength after fuel exposure, and the ultimate shear stress after saltwater, alkali and freeze thaw exposure. All of those conditions that did not retain above 90% material properties did retain above 85% of the material properties.

In addition to comparing the mean tensile properties, B-Basis values were also calculated for comparison. Table 4.25 summarizes the B-Basis values for the tensile properties of each of the environmental conditions; the percent of material properties retained is shown to the right of the mean value in italics. Those conditions that did not retain 90% of the original material properties are in bold. Again, the data was pooled for the environmental conditions that had samples tested for multiple exposure times for comparison purposes.

Table 4.25 B-Basis Tensile Properties After Durability Testing

| **Environmental Condition** | **$E_x$ (kN/mm)** | | **$E_y$ (kN/mm)** | | **$F_{xt}$ (kN/mm)** | | **$F_{yt}$ (kN/mm)** | | **$\tau_{20}$ (kN/mm)** | |
|---|---|---|---|---|---|---|---|---|---|---|
| Control | 61.6 | | 35.1 | | 1.01 | | 0.45 | | 0.13 | |
| Water | 58.6 | *95* | 35.8 | *102* | 1.20 | *119* | 0.52 | *116* | 0.13 | *100* |
| Saltwater | 58.6 | *95* | 34.1 | *97* | 1.14 | *113* | 0.48 | *107* | 0.12 | *92* |
| Alkali | 59.4 | *96* | 35.1 | *100* | 1.15 | *114* | 0.48 | *107* | 0.12 | *92* |
| Dry Heat | 59.4 | *96* | 37.8 | *108* | 1.13 | *112* | 0.45 | *100* | 0.15 | *115* |
| UV | 52.3 | ***85*** | 29.9 | ***85*** | 1.04 | *103* | 0.32 | ***71*** | 0.11 | ***85*** |
| Freeze Thaw | 54.4 | ***88*** | 36.5 | *104* | 1.04 | *103* | 0.36 | ***80*** | 0.11 | ***85*** |
| Fuel | 57.6 | *94* | 39.7 | *113* | 0.96 | *95* | 0.37 | ***82*** | 0.12 | *92* |
| Italics= Percent of material properties retained Bold= Less than 90% retained | | | | | | | | | | |

The calculated B-Basis values show a larger range of environmental conditions that showed less than 90% retention of material properties. Some of the conditions such as UV, freeze thaw, and fuel had less samples included in the calculation of B-Basis values, which could lead to a lower overall value and the appearance of a greater loss in material properties. The other four environmental conditions, which had a larger samples size, all showed at least 90% retention of material properties.

One of the common observations of the sheets after exposure was that the sheets which were exposed elevated temperatures exhibited a larger curvature than the control sheets. The mean curvature of the sheets after exposed to different conditions is compared in Table 4.26, also included in the table is the maximum temperature experienced by the sheets during conditioning.

Table 4.26 Mean Curvature of Exposed Sheets

| Condition | Max Temp. (°C) | κ (1/mm) |
|---|---|---|
| Heat 1000 hr | 60 | 0.70 |
| Heat 2000 hr | 60 | 0.88 |
| UV | 60 | 0.70 |
| Freeze Thaw | 38 | 0.30 |

From this table it appears that the maximum temperature and exposure duration may both effect the curvature of the sheet. The samples that had a longer heat exposure time of 2000 hours had a greater curvature than those that had been exposed for 1000 hours. The UV exposed samples saw the same maximum temperature as the heat exposed sheets during cycling, and a corresponding similar curvature, while the freeze thaw samples had a lower maximum temperature and a lower curvature.

#### 4.3.11.1 Acceptance Criteria for Durability of Composite Materials

The acceptance criteria, AC125, requires that samples retain at least 90% of the tensile properties (tensile strength, longitudinal elastic modulus, and transverse elastic modulus) after 1000 hours of exposure. Samples exposed to water, saltwater, alkali, and dry heat were all tested after 1000 hours of conditioning. Table 4.27 summarizes the mean tensile properties after 1000 hours of conditioning and the percent of material properties retained, which are shown to the right of the mean value in italics. The control values used are based off of a mean value of the pooled control data. Figure 4.21 and Figure 4.22 are bar charts, which show the comparison of elastic modulus and tensile strength of each conditioned sample set, the error bars represent one standard deviation.

Table 4.27 Mean Tensile Properties after 1000 Hours of Conditioning

| **Environmental Condition** | **$E_x$ (kN/mm)** | | **$E_y$ (kN/mm)** | | **$F_{xt}$ (kN/mm)** | |
|---|---|---|---|---|---|---|
| Control | 67.7 | | 40.2 | | 1.38 | |
| Water | 67.79 | *100.1* | 40.56 | *100.9* | 1.37 | *99.3* |
| Saltwater | 62.59 | *92.5* | 36.56 | *91.0* | 1.34 | *97.1* |
| Alkali | 63.73 | *94.1* | 38.55 | *96.9* | 1.27 | *92.0* |
| Dry Heat | 60.47 | ***89.3*** | 37.66 | *93.7* | 1.36 | *98.6* |
| Italics= Percent of material properties retained Bold= Less than 90% retained | | | | | | |

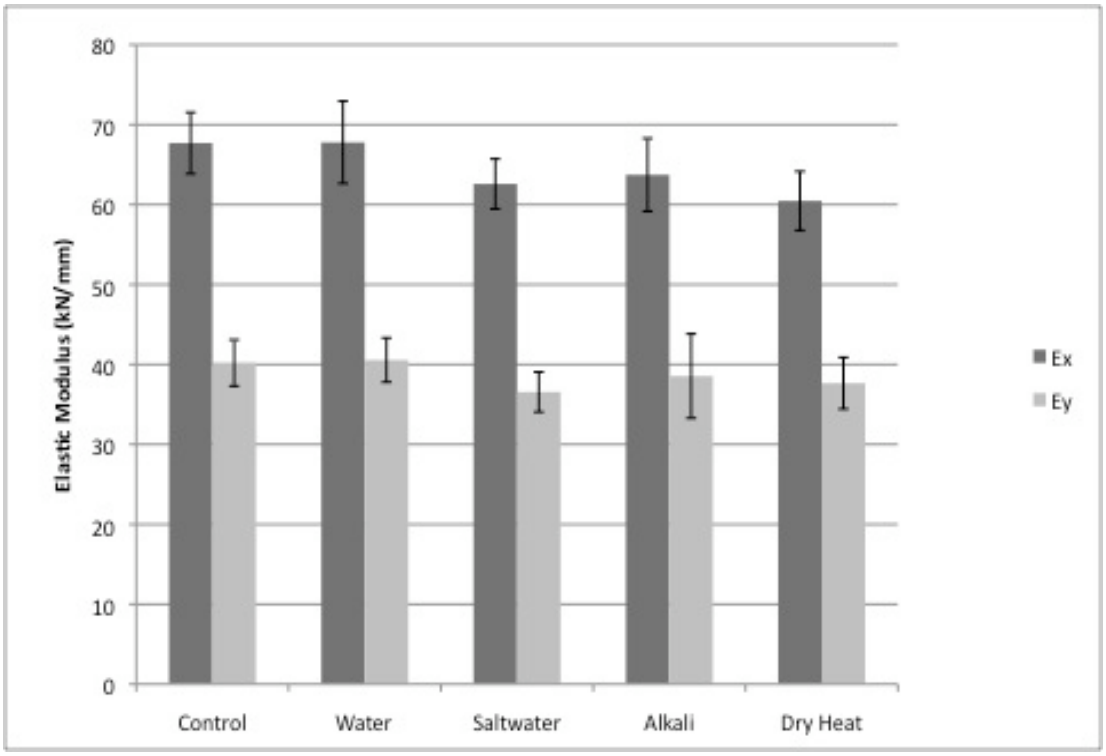


Figure 4.21 Comparison of Mean Elastic Modulus After 1000 Hours of Exposure

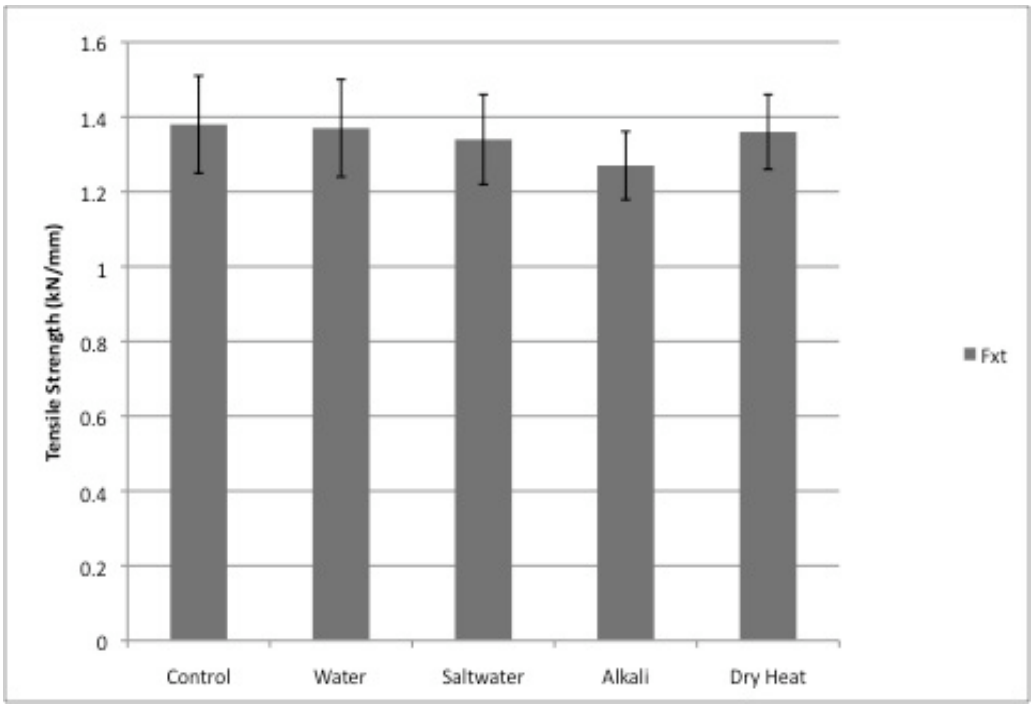


Figure 4.22 Comparison of Mean Tensile Strength After 1000 Hours of Exposure

When comparing the mean values only one condition, the longitudinal elastic modulus for dry heat exposed samples, does not meet the acceptance criteria of retaining 90% of the control property. While the heat exposure did not meet the acceptance criteria in this round of testing it is recommended that further testing be done to minimize the variability seen throughout all of the environmental testing before determining that the composite would not be acceptable for heat exposure. Furthermore, the sample retained 89.3% of the elastic modulus which is only 0.7% below the 90% retention. The effect of testing variability can be seen by comparing B-Basis values; if a B-Basis comparison is used the longitudinal elastic modulus after heat exposure would pass the acceptance criteria.

Table 4.28 summarizes the calculated B-Basis values for the tensile properties after 1000 hours of conditioning and the percent of material properties retained. The control values used are the B-Basis values of the pooled control data. Figure 4.23 and Figure 4.24 are bar charts, which show the comparison of calculated B-Basis values for elastic modulus and tensile strength of each conditioned sample set.

Table 4.28 B-Basis Tensile Properties after 1000 Hours of Conditioning

| **Environmental Condition** | **$E_x$ (kN/mm)** | | **$E_y$ (kN/mm)** | | **$F_{xt}$ (kN/mm)** | |
|---|---|---|---|---|---|---|
| Control | 61.6 | | 35.1 | | 1.01 | |
| Water | 60.1 | *97.6* | 34.4 | *98.0* | 1.09 | *107.9* |
| Saltwater | 55.5 | *90.1* | 30.4 | ***86.6*** | 1.06 | *105.0* |
| Alkali | 53.9 | ***87.5*** | 32.2 | *91.7* | 1.06 | *105.0* |
| Dry Heat | 55.8 | *90.6* | 34.2 | *97.4* | 1.03 | *102.0* |
| Italics= Percent of material properties retained Bold= Less than 90% retained | | | | | | |

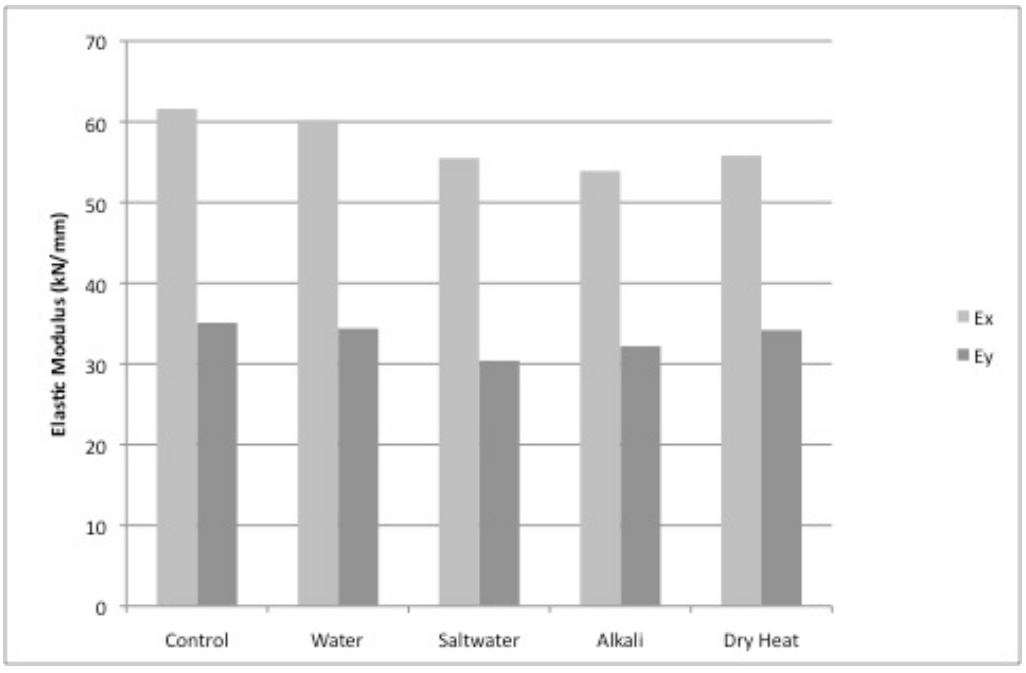


Figure 4.23 Comparison of B-Basis Elastic Modulus After 1000 Hours of Exposure

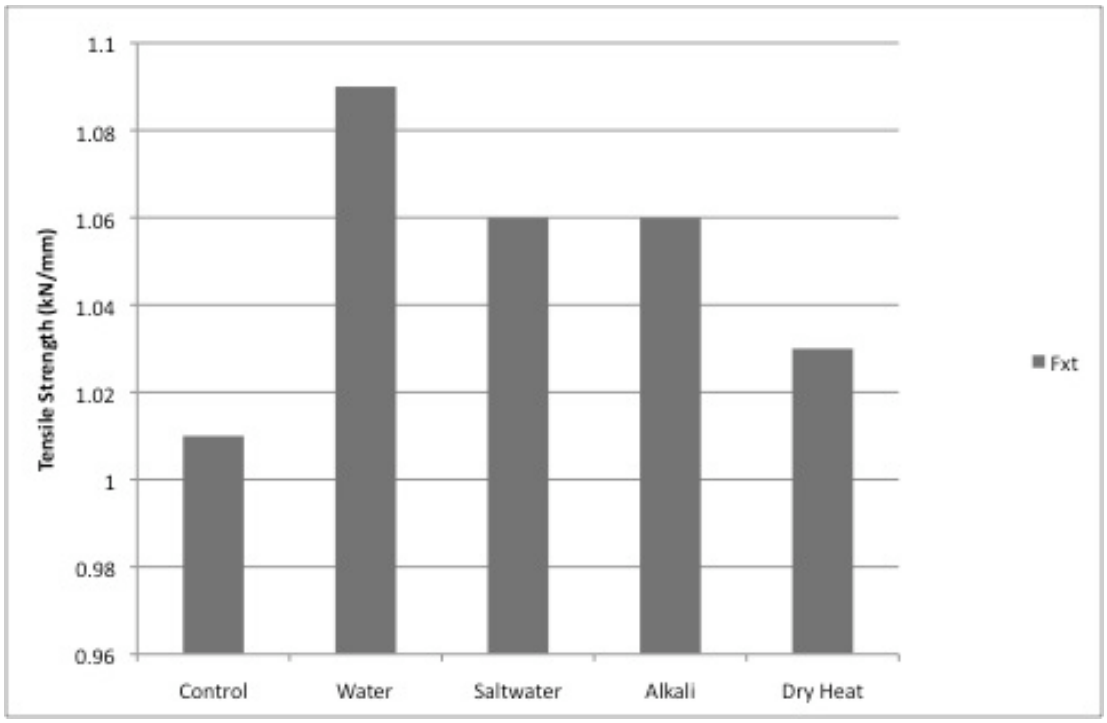


Figure 4.24 Comparison of B-Basis Tensile Strength After 1000 Hours of Exposure

If the acceptance criteria is determined using B-Basis values, all conditions pass except for the longitudinal elastic modulus for the alkali exposed sample and the transverse elastic modulus for the saltwater exposed samples. Both of these conditions retain above 85% of the material properties, but do not have the 90% retention that the acceptance criteria specifies. Again, it is recommended that further testing be done to minimize the variability seen throughout all of the environmental testing before determining that the composite would not be acceptable for alkali or saltwater exposure, especially since the mean value comparison shows that both conditions would pass.

In addition, it should be noted that both the carbon and E-glass layers of the composite were exposed to the alkali and saltwater solution. In the arch structure only the E-glass layer would see significant alkali exposure and only the carbon

layer would see significant saltwater exposure. Since the longitudinal elastic modulus is dominated by the carbon layer, the 87.5% retention after alkali exposure is likely lower than what could be expected in a real structure. Also since the transverse elastic modulus is dominated by the E-glass layer, the 86.6% retention after saltwater exposure is likely lower than what could be expected in a real structure.

### 4.3.12. Abrasion

While abrasion resistance is not addressed in the durability test matrix, a brief study was conducted to determine ways to mitigate damage from abrasion to the arch surface. Abrasion can be expected from sand particles and other debris being rubbed against the arches. These particles and debris can be carried by the wind or by water during high stream flows. The objective of this study is to see what improvements could be easily made to the existing system to provide additional abrasion protection. Additional abrasion protection may be useful for arches that are on the ends of the bridge and are more exposed to the wind and first impact of material carried downstream. Arches can also be abraded during transportation, particularly from straps used to tie down arches to the truck bed.

#### 4.3.12.1 Literature review for Abrasion Resistance

Abrasion can wear away the surface resin on a composite and create micro cracks, which make it more susceptible to moisture and other harmful environmental conditions. If abrasion continues to wear away at the composite past the surface layer of resin the fibers can also become damaged or cut which

would decrease the elastic properties and strength of the composite. A study done by Suresha et al. (2010) found that the wear rate of a carbon fiber vinyl ester composite was 184% higher than the wear rate of a glass fiber vinyl ester composite. In the case of the arches the carbon layer is on the outside and more likely to be exposed to abrasion than the E-glass fibers, so the carbon fibers may protect the glass fibers.

One of the easiest ways to protect the outer carbon fibers is by adding an additional sacrificial surface layer that would at least slow the detrimental effects of abrasion. An example of this would be increasing the amount of resin on the surface of the arch. While extra resin alone provides some more protection of the fibers, a study done by Suresha and Chandramohan (2008) concluded that the abrasive wear rate is higher in unfilled glass fiber-reinforced vinyl ester composites than it is in composites where an extra filler was added to the resin.

#### 4.3.12.2 Abrasion Testing

Knowing that fillers added to the surface resin can slow the abrasive wear rate down, it was proposed to add a lightweight layer on top of the carbon during infusion. A polyester batting was selected as a filler because of its low cost, light weight, and porous structure that would create a resin rich layer. The batting was also easy to apply as an additional layer around an arch tube or on a sheet. To compare the effectiveness of the additional abrasion layer sample coupons were manufactured and tested according to ASTM D 4060 Standard Test Method for Abrasion Resistance of Organic Coatings by the Taber Abraser (ASTM 2007).

Samples were manufactured as infused sheets of braided E-glass and braided carbon, with half of the samples infused with the additional layer of batting on top of the carbon layer. From the infused sheet, coupons were cut to be 102mm (4in) by 102mm (4in) squares that would fit on the Taber Abraser. All samples were labeled and weighed before testing. The coupons were mounted to the rotating turntable on the Taber Abraser and subjected to two abrasive wheels covered with 200 grit sandpaper and applied with a load of 250g each. The two wheels abrade the coupon in different directions, one rubs out towards the edge of the samples while the other rubs inward towards the center, this creates a crisscrossed circular strip covering approximately 30 $cm^2$ of the sample. Figure 4.25 shows a coupon with the additional abrasion layer in the test setup. The Taber Abraser also has a vacuum that clears any abraded material from the surface.


Figure 4.25 Abrasion Test Setup

Four control samples were abraded for 100, 200, 400 and 600 cycles. At 600 cycles the carbon braid had been completely worn away in several spots, therefore no additional tests were performed. Six samples with the additional abrasion layer were tested for 100, 200, 400, 600, 1000, and 3000 cycles. The additional samples with the highest cycle count were tested to determine the number of cycles it would take to wear away the carbon in multiple spots, similar to what was seen in with the 600 cycle control sample. After all samples were tested they were cleaned, weighed, and visually inspected.

The effect of the additional abrasion layer was evaluated based on sample weight loss over the number of cycles and through visual inspections of the abraded surface. Figure 4.26 shows the percent of weight loss for both types of samples verses the number of cycles the sample was subjected to. The control samples had a much steeper reduction in weight loss per number of cycles and had lost over 5% of the sample weight after 600 cycles while the samples with the additional abrasion layer did not see a comparable percent change in weight loss until 3000 cycles. The percent change in weight loss shows that the additional abrasion layer provides approximately 5 times more abrasion resistance than the control samples.

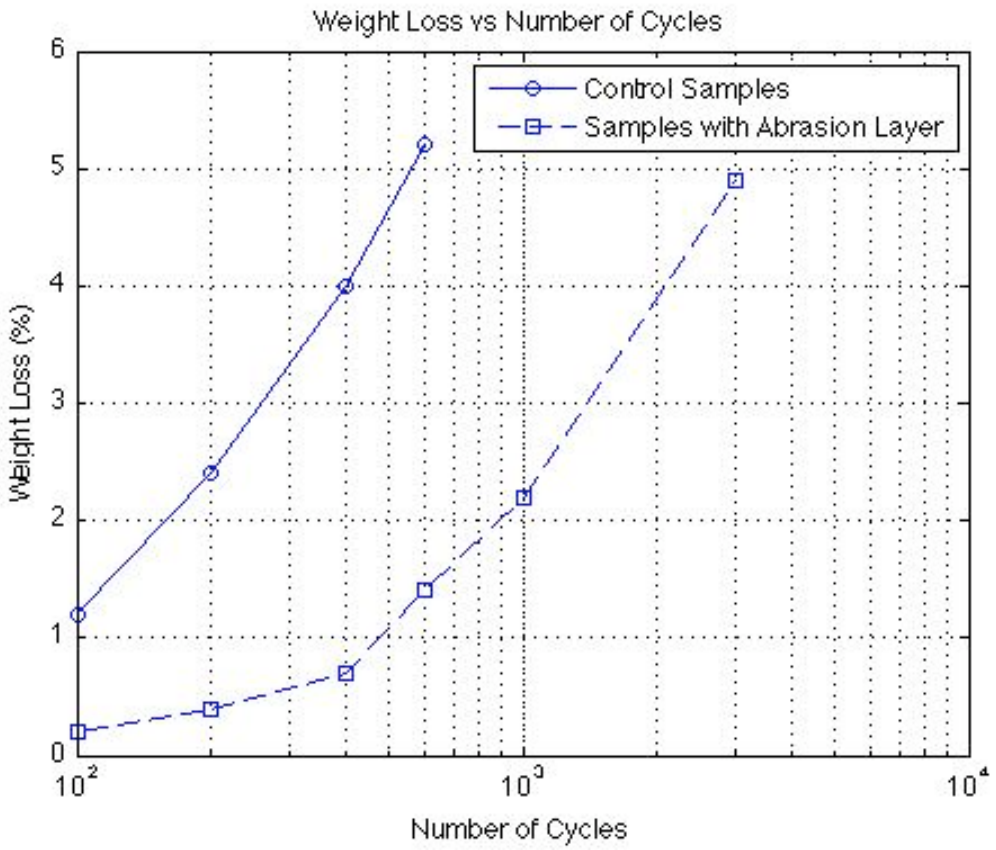


Figure 4.26 Percent Weight Loss due to Abrasion

In addition to a comparison in percentage of weight lost, a visual inspection was conducted; Figure 4.27 shows some of the samples after abrasion testing where the sample with the abrasion layer are the bottom set. In as little as 100 cycles the control samples had visible damaged carbon fibers and worn away spots, and at 100 cycles the carbon fibers had been completely worn away in several locations. The samples with the additional abrasion layer did not show damaged carbon fibers until 600 cycles, and not until 3000 cycles had the carbon fibers been completely worn away similar to the control sample at 100 cycles.

Figure 4.27 Visual Comparison of Abraded Samples

Through the visual comparison of the control samples at 100 cycles and the samples with the additional abrasion layer at 3000 cycles it appears that the abrasion layer provides significantly more abrasion resistance than the control samples. The visual comparison can be seen in Figure 4.28. Overall it was shown that the addition of an abrasion layer could provide a significant amount of protection to the fiber reinforcement of the composite.

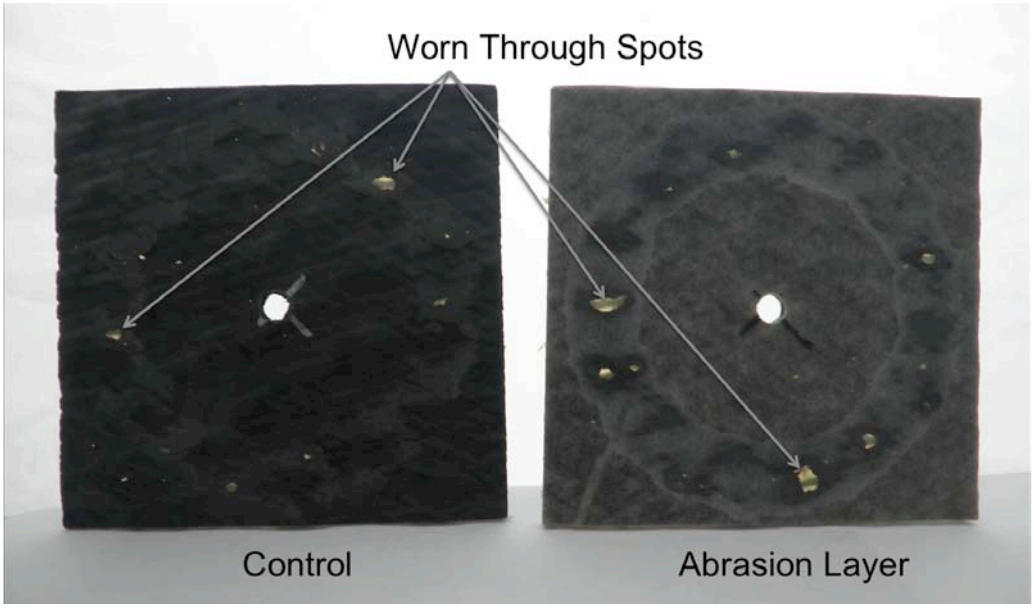


Figure 4.28 Visual Comparison of Control Samples at 100 cycles and Samples with an Abrasion Layer at 3000 cycles

## 4.4 Conclusions and Recommendations for Future Work

Seven environmental conditions outlined in the original durability test matrix were investigated to determine their effects on the tensile properties of the composite arch material. Samples exposed to water, saltwater, alkali, and heat were tested after 3 different exposure durations to determine if there was a trend in the change of material properties over time. There was no apparent trend in the change of material properties over time and most of the changes seen were believed to be from variability between batches of coupons. The three other environmental conditions, UV, freeze thaw, and fuel exposure were conditioned for only one exposure duration.

The control samples were pooled after determining if they were from the same population using the k-sample Anderson Darling statistic. In addition B-Basis values, meaning that 90% of the population will be above the value with a 95% confidence level, were calculated and used to compare conditioned sample groups to the pooled control properties. The mean values of the conditioned samples were also compared to the pooled control properties.

When comparing the material properties mean values of the samples that had been exposed to different environmental conditions, most samples retained above 90% of the control material properties. Those that did not retain 90% did retaine greater than 85% of the control material properties. Comparing the B-Basis, again most samples retained greater than 90% of the control material properties.

The environmental conditions that had fewer samples tested, UV, freeze thaw, and fuel, had lower B-Basis values, and the B-Basis value may increase if more samples are tested.

Water, saltwater, alkali, and dry heat exposure was evaluated following AC 125, where after 1000 hours of testing, samples must retain at least 90% of the material properties. Using a comparison of mean values only the longitudinal elastic modulus after dry heat exposure did not pass the criteria. When comparing B-Basis values only the longitudinal elastic modulus after alkali exposure and transverse elastic modulus after saltwater exposure did not pass the criteria. While those conditions did not pass during this round of testing, additional testing should be performed before determining that the composite would not be acceptable.

Recommendations for future work include additional testing for four different purposes. The first purpose would be to study the variability in unconditioned samples over time, specifically for tensile strength. The tensile strength varied from batch to batch over time with no obvious trend, testing additional control samples can help determine the reason for the variability.

The second round of additional testing would be for conditioned samples in order to generate acceptable B-Basis values as specified by the Composite Materials Handbook. For each environmental condition and specified exposure duration, approximately one batch of 12 samples was tested for each material property. To generate B-Basis values deemed acceptable by the Composite Material Handbook, a minimum of 3 batches containing at least 18 samples overall must be tested.

Additional durability testing should also be conducted for longer exposure times outlined by the durability test matrix and AC 125. Samples should be exposed to water, saltwater, alkali solution and dry heat for an additional 3000 and 10000 hours. Samples should then be tested to determine the percent material properties retained and compared to the acceptance criteria of retaining 85% of the material properties after 3000 hours of exposure.

Lastly, additional testing should be performed to investigate the effects of combined environmental conditions. Balazs (2001) stated that the effect of water and alkali absorption is accelerated by an elevated temperature; also UV exposure may be accelerated by cycles of saltwater exposure. Another combination that should be explored is freeze thaw cycling followed by saltwater exposure. It was observed that the composite sheets curved and relaxed during freeze thaw cycling, this could cause cracking in the matrix making the material more susceptible to moisture exposure after the freeze thaw cycles.

From the abrasion testing it was found that the additional abrasion layer made out of a polyester batting appeared to increase the abrasion resistance by at least 5 times when determined by percent weight loss and about 30 times when compared visually. Future recommendations would be to experiment with other types of abrasion layers, such as painting on an extra layer of resin. It would also be beneficial if samples could be abraded and then tested in tension to see the effect on tensile strength and modulus for a better measurement of degradation.

## REFERENCES


A&P Technology. (2009a). "Data Sheet for Product Code: UM6447." Cincinnati, Ohio.

A&P Technology. (2009b). "Data Sheet for Product Code: UM6448." Cincinnati, Ohio.

A&P Technology. (2010). "Invoice." AEWC, ed.

A&P Technology. (2011). "Data Sheet for AIT2011."

AASHTO. (2009). "AASHTO LRFD Guide Specifications for Design of Externally Bonded FRP Systems for Strengthening Concrete Bridges." Section 3: Material Specifications.

Ashland. (2005). "Material Safety Data Sheet Pliogrip 7779 Prepolymer." 8.

Ashland. (2006). "DERAKANE 8084 Epoxy Vinyl Ester Resin."

Ashland. (2010). "DERAKANE 610C Epoxy Vinyl Ester Resin."

ASTM, A. S. f. T. M. (2004). "ASTM E 132 Standard Test Method for Poisson's Ratio at Room Temperature." ASTM International, West Conshohocken, PA.

ASTM, A. S. f. T. M. (2006). "ASTM G 154 Stand Practice for Operating Fluorescent Light Apparatus for UV Exposure of Nonmetallic Materials." ASTM International, West Conshohocken, PA.

ASTM, A. S. f. T. M. (2007). "ASTM D 4060 Standard Test Method for Abrasion Resistance of Organic Coatings by the Taber Abraser." ASTM International, West Conshohocken, PA.

ASTM, A. S. f. T. M. (2008a). "ASTM D1141 Standard Practice for the Preparation of Substitute Ocean Water." ASTM International, West Conshohocken, PA.

ASTM, A. S. f. T. M. (2008b). "ASTM D 3039: Standard Test Method for Tensile Properties of Polymer Matrix Composite Materials." ASTM International, West Conshohocken, PA, 13.

Ayranci, C., and Carey, J. (2008). "2D braided composites: A Review for Stiffness Critical Applications." *Composite Structures*, 85, 43-58.

Balazs, G. L., and Borosnyoi, A. "Long-term behavior of FRP." *ASCE International Workshop*, 84-91.

Bannon, D. J. (2009). "Characterization of Concrete-Filled Fiber Reinforced Polymer Arch Memebers," University of Maine, Orono.

Betts, D. N., Salo, A. I. T., and Bowen, C. R. (2010). "Charcterisation and modelling of the cured shapes of arbitrary layup bistable composite laminates." *Composite Structures*, 92, 1694-1700.

Bowman, C. L., Roberts, G. D., Braley, M. S., Xie, M., and Booker, M. J. (2003). "Mechanical Properties of Triaxial Braided Carbon/Epoxy Composites." NASA Glenn Research Center, Cleveland OH.

Byun, J.-H. (2000). "The analytical characterization of 2-D Braided Textile Composites." *Composite Science and Technology*, 60, 705-716.

Cao, S., WU, Z., and Wang, X. (2009). "Tensile Properties of CFRP and Hybrid FRP Composites at Elevated Temperatures." *Journal of Composite Materials*, 43(No. 04/2009), 315-329.

Chin, J. W., Martin, J., and Nguyen, T. (2001). "Effects of Ultraviolet (UV) Radiation." Gap Analysis for Durability of Fiver Reinforced Polymer Composites in Civil Infrastructure, 80-99.

Chu, W., Wu, L., and Karbhari, V. M. (2004). "Durability evaluation of moderate temperature cured E-glass/vinylester systems." *Composite Structures*, 2004(66), 367-376.

Conrad, J. O., Bakis, C. E., Boothby, T. E., and Nanni, A. (1998). "Durability of Bond of Various FRP Rods in Concrete." Proceedings of CDCC '98, Sherbrooke, Canada, 299-310.

Cox, B. N., and Flanagan, G. (1997). "Handbook of Analytical Methods for Textile COmposites." NASA National Aeronautics and Space Administration, Hampton, Virginia Langley Research Center.

Daniel, I. M., and Ishai, O. (2006). *Engineering Mechanics of Composite Materials*, Oxford University Press, New York, NY.

Dano, M.-L., Gendron, G., and Picard, A. (2000). "Mechanical Behavior of a Triaxial Woven Fabric Composite." *Mechancis of Advanced Materials and Structures*, 7(2), 207-224.

Department of Defense. (2002). "Composite Materials Handbook."

DESS Machine. (2007). DESS Machine & Mfg Inc., Dover, DE.

Donadon, M. V., Falzon, B. G., Iannucci, L., and Hodgkinson, J. M. (2007). "A 3-D Micromechanical Model for Predicting the Elastic Behaviour of Woven Laminates." *Composites Science and Technology*, 67, 2467-2477.

El-Chiti, I. (2004). "FRP-Concrete Arch," University of Maine, Orono, Maine.

Goslin, K., Parent, L., and Nagy, E. (2009). "Temperature Effects of Rigidified Inflatable FRP Tubes Filled with Expansive SCC DRAFT." AEWC Advanced Structures and Composites Center, Orono, ME.

Grafil Inc. (2008). "PYROFIL TR50S 15K." Sacramento, CA.

Herzog, B., Gardner, D., Lopez-Anido, R., and Goodell, B. (2005). "Glass-Transition Temperature Based on Dynamic Mechanical Thermal Analysis Techniques as an Indicator of the Adhesive Performance of Vinyl Ester Resin." *Journal of Applied Polymer Science*, 97(6), 2221-2229.

Huang, Z.-M., and Ramakrishna, S. (2003). "Modeling Inelastic and Strength Properties of Textile Laminates: A Unified Approach." *Composite Science and Technology*, 63, 445-466.

ICC Evaluation Service. (2007). "Acceptance Criteria for Concrete and Reinforced and Unreinforced Masonry Strenghtening using Externally Bonded Fiber-Reinforced Polymer (FRP) Composite Systems." AC125, Whittier, CA.

Karbhari, V. M. (2005). "Using Composites in Seismic Retrofit Applications." State of Califonia Department of Transporation, El Segundo, California.

Karbhari, V. M., Chin, J. W., Hunston, D., Benmokrane, B., Juska, T., Morgan, R., Lesko, J. J., Sorathia, U., and Reynaud, D. (2003). "Durability Gap Analysis for Fiber-Reinfored Polymer Composites in Civil Infrastructure." *Journal of Composites for Construction*, 7(3), 238-247.

Karbhari, V. M., Murphy, K., and Zhang, S. (2002). "Effect of Concrete Based Alkali Solutions on Short-Term Durability of E-Glass/Vinylester Composites." *Journal of Composite Materials*, 36(17), 2101-2121.

Kshirsagar, S., Lopez-Anido, R., and Gupta, R. (2000). "Environmental Aging of Fiber-Reinforced Polymer-Wrapped Concrete Cylinders." *ACI Materials Journal*, 97(6), 703-712.

Masters, J. E. (1996). "Strain Gage Selection Criteria for Textile Composite Materials." National Aeronautics and Space Administration
Lockheed Martin Engineering & Sciences, Hampton, VA.

Masters, J. E., Foye, R. L., Pastore, C. M., and Gowayed, Y. A. (1993). "Mechanical Properties of Triaxially Braided Composites: Experimental and Analytical Results." *Journal of Composites Technology & Research*, 15(2), 112-122.

McConnell, V. P. (2007). "Global Underground: The State of composite Storage Tanks." *Reinforced Plastics*, 51(6), 26-27,29-31.

Micelli, F., and Nanni, A. (2004). "Durability of FRP rods for concrete structures." *Construction and Building Materials*, 2004(18), 491-503.

Pando, M. A., Lesko, J. J., Fam, A. Z., and Rizkalla, S. H. "Durability of Concrete-Filled Tubular FRP Piles." *Proceedings of the 3rd International Conference on Composites in Infrastructures*, San Francisco.

Pantelides, C. P., Reay, J. T., and Reaveley, L. D. (2006). "Time Dependent Effects from Monitoring of State Street Bridge FRP Composite Retrofit." *UT-07.01*, University of Utah Department of Civil & Environmental Engineering, Salt Lake City, Utah.

PPG Fiber Glass. (2008). "Technical Data Sheet: Hybon 2022 Roving." Pittsburgh, PA.

Rivera, J., and Karbhari, V. M. (2001). "Cold-temperature and Simultaneous Aqueous Environment Related Degreadation of Carbon/Vinylester Composites." *Composites: Part B*, 33, 17-24.

Rostasy, F. (1997). "Durability of FRP in Aggressive Environments." Proceedings of the 3rd International Symposium on Non-Metallic (FRP) Reinforcement for Concrete Structures, Sapporo, Japan, 107-114.

Scholz, F. W., and Stephens, M. A. (1986). "K-Sample Anderson-Darling Tests of Fit, For Continous and Discrete Cases ", University of Washington Department of Statistics, Seattle, Washington.

Sen, R., Mariscal, D., and Shahawy, M. (1993). "Durability of Fiberglass Predtensioned Beams." *ACI Structural Journal*, 90(5), 525-533.

Steckel, G. L., Hawkins, G. F., and Bauer, J., Jerome L. (1999). "Durability Issues for Composites in Ifrastructure." 44th International SAMPE Symposium, Center for Adcanced Structural Applications: The Aerospace Corporation.

Stevens, M. (2011). "Fuel Corrosion." M. Demkowicz, ed.

Suresha, B., Kumar, K. S., Seetharamu, S., and Kumaran, P. S. (2010). "Friction and Dry Sliding Wear Behavior of Carbon and Glass Fabric Reinforced Vinyl Ester Composites." *Tribology Interational*, 43, 602-609.

Tan, P., Tong, L., and Steven, G. P. (1997). "Modelling for Predicting the Mechanical Properties of Textile composites-A Review." *Composties Part A*, 28A.

Tannous, F. E., and Saadatmanesh, H. (1998). "Environmental Effects on the Mechanical Properties of E-Glass FRP Rebars." *ACI Materials Journal*, 95(2), 14.

Tate, J. S., Kelkar, A. D., and Kelkar, V. A. "Failure Analysis of Biaxial Braided composites Under Fatigue Loading." *The 15th European conference of Fracture*, Stockholm, Sweden.

Tomblin. (2006). "Buried FRP-Concrete Arches," University of Maine, Orono, ME.

Torayca. (2009). "Torayca T700S Data Sheet." Santa Ana, CA.

U.S Deapartment of Transportation, and Federal Aviation Administration. (2000). "Aircraft Materials Fire Test Handbook." National Technical Information Service, Washington, D.C.

Uomoto, T., and Nishisura, T. (1997). "Development of New Alkali Resistant Hybrid AGFRP Rod." Proceedings of the 3rd International Symposium on Non-Metallic (FRP) Reinforcement for Concrete Structures, Sapporo, Japan, 67-74.

Waldron, P., Byars, D. E. A., and Dejke, V. "Durability of FRP in Concrete: A Start of the Art." *Proceedings of the International Workshop on: Composites in Construction: A Reality*, Capri, Italy, 92-101.

Walton, H. (2011). "Response of FRP Arches to Concrete Filling Loads," University of Maine, Orono, ME.

Wu, Z., Wang, X., Iwashita, K., Sasaki, T., and Hamaquchi, Y. (2010). "Tensile Fatigue Behavior of FRP and Hybrid FRP Sheets." *Composites: Part B*, 41, 396-402.

## BIOGRAPHY OF THE AUTHOR

Mackenzie Demkowicz was born in Waterville, Maine on July 21, 1987 to Roberto and Michele Demkowicz. She was raised in Winthrop, Maine and graduated from Winthrop High School in 2005. She attended the University of Maine and graduated with a Bachelor's degree in Civil engineering, Summa Cum Laude, in 2009. She continued her education at the University of Maine in the Civil Engineering graduate program in the summer of 2009 at the AEWC Advanced Structures and Composites Center.

After receiving her degree, Mackenzie plans to purse a career in structural engineering. Mackenzie is a candidate for the Master of Science degree in Civil Engineering from the University of Maine in August, 2011.